1
Bulk Metal and Ceramics Nanocomposites

Pulickel Ajayan

1.1
Introduction

The field of nanocomposite materials has had the attention, imagination, and close scrutiny of scientists and engineers in recent years. This scrutiny results from the simple premise that using building blocks with dimensions in the nanosize range makes it possible to design and create new materials with unprecedented flexibility and improvements in their physical properties. This ability to tailor composites by using nanosize building blocks of heterogeneous chemical species has been demonstrated in several interdisciplinary fields. The most convincing examples of such designs are naturally occurring structures such as bone, which is a hierarchical nanocomposite built from ceramic tablets and organic binders. Because the constituents of a nanocomposite have different structures and compositions and hence properties, they serve various functions. Thus, the materials built from them can be multifunctional. Taking some clues from nature and based on the demands that emerging technologies put on building new materials that can satisfy several functions at the same time for many applications, scientists have been devising synthetic strategies for producing nanocomposites. These strategies have clear advantages over those used to produce homogeneous large-grained materials. Behind the push for nanocomposites is the fact that they offer useful new properties compared to conventional materials.

The concept of enhancing properties and improving characteristics of materials through the creation of multiple-phase nanocomposites is not recent. The idea has been practiced ever since civilization started and humanity began producing more efficient materials for functional purposes. In addition to the large variety of nanocomposites found in nature and in living beings (such as bone), which is the focus of chapter 3 of this book, an excellent example of the use of synthetic nanocomposites in antiquity is the recent discovery of the constitution of Mayan paintings developed in the Mesoamericas. State-of-the-art characterization of these painting samples reveals that the structure of the paints consisted of a matrix of clay mixed with organic colorant (indigo) molecules. They also contained inclusions of metal nanoparticles encapsulated in an amorphous silicate substrate, with oxide nanoparticles on the substrate

Nanocomposite Science and Technology. Edited by P.M. Ajayan, L.S. Schadler, P.V. Braun

ISBN: 3-527-30359-6

[1]. The nanoparticles were formed during heat treatment from impurities (Fe, Mn, Cr) present in the raw materials such as clays, but their content and size influenced the optical properties of the final paint. The combination of intercalated clay forming a superlattice in conjunction with metallic and oxide nanoparticles supported on the amorphous substrate made this paint one of the earliest synthetic materials resembling modern functional nanocomposites.

Nanocomposites can be considered solid structures with nanometer-scale dimensional repeat distances between the different phases that constitute the structure. These materials typically consist of an inorganic (host) solid containing an organic component or vice versa. Or they can consist of two or more inorganic/organic phases in some combinatorial form with the constraint that at least one of the phases or features be in the nanosize. Extreme examples of nanocomposites can be porous media, colloids, gels, and copolymers. In this book, however, we focus on the core concept of nanocomposite materials, i.e., a combination of nano-dimensional phases with distinct differences in structure, chemistry, and properties. One could think of the nanostructured phases present in nanocomposites as zero-dimensional (e.g., embedded clusters), 1D (one-dimensional; e.g., nanotubes), 2D (nanoscale coatings), and 3D (embedded networks). In general, nanocomposite materials can demonstrate different mechanical, electrical, optical, electrochemical, catalytic, and structural properties than those of each individual component. The multifunctional behavior for any specific property of the material is often more than the sum of the individual components.

Both simple and complex approaches to creating nanocomposite structures exist. A practical dual-phase nanocomposite system, such as supported catalysts used in heterogeneous catalysis (metal nanoparticles placed on ceramic supports), can be prepared simply by evaporation of metal onto chosen substrates or dispersal through solvent chemistry. On the other hand, material such as bone, which has a complex hierarchical structure with coexisting ceramic and polymeric phases, is difficult to duplicate entirely by existing synthesis techniques. The methods used in the preparation of nanocomposites range from chemical means to vapor phase deposition.

Apart from the properties of individual components in a nanocomposite, *interfaces* play an important role in enhancing or limiting the overall properties of the system. Due to the high surface area of nanostructures, nanocomposites present many interfaces between the constituent intermixed phases. Special properties of nanocomposite materials often arise from interaction of its phases at the interfaces. An excellent example of this phenomenon is the mechanical behavior of nanotube-filled polymer composites. Although adding nanotubes could conceivably improve the strength of polymers (due to the superior mechanical properties of the nanotubes), a noninteracting interface serves only to create weak regions in the composite, resulting in no enhancement of its mechanical properties (detailed in chapter 2). In contrast to nanocomposite materials, the interfaces in conventional composites constitute a much smaller volume fraction of the bulk material.

In the following sections of this chapter, we describe some examples of metal/ceramic nanocomposite systems that have become subjects of intense study in recent years. The various physical properties that can be tailored in these systems for specific

applications is also considered, along with different approaches to synthesizing these nanocomposites.

1.2 Ceramic/Metal Nanocomposites

Many efforts are under way to develop high-performance ceramics that have promise for engineering applications such as highly efficient gas turbines, aerospace materials, automobiles, etc. Even the best processed ceramic materials used in applications pose many unsolved problems; among them, relatively low fracture toughness and strength, degradation of mechanical properties at high temperatures, and poor resistance to creep, fatigue, and thermal shock. Attempts to solve these problems have involved incorporating second phases such as particulates, platelets, whiskers, and fibers in the micron-size range at the matrix grain boundaries. However, results have been generally disappointing when micron-size fillers are used to achieve these goals. Recently the concept of nanocomposites has been considered, which is based on passive control of the microstructures by incorporating nanometer-size second-phase dispersions into ceramic matrices [2]. The dispersions can be characterized as either

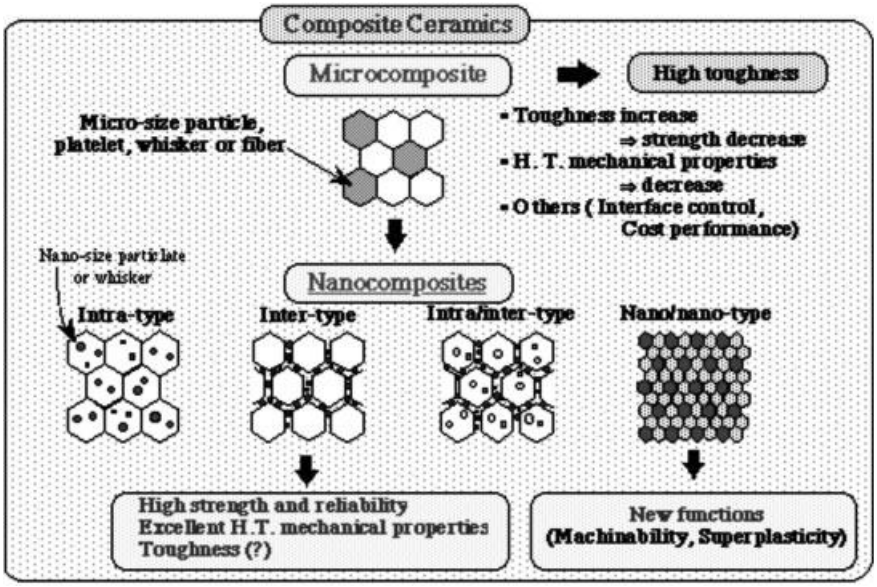

Fig. 1.1 New concept of ceramic metal nanocomposites with inter- and intra-granular designs: properties of ceramic materials can be improved by nanocomposite technology. This technique is based on passive control of the microstructures by incorporating nanometer-sized second dispersions into ceramic materials. This is a completely new method to fabricate materials with excellent mechanical properties (such as high strength and toughness), due to the desirable microstructure of ceramics (Source:[228] Reprinted with permission)

intragranular or intergranular (Figure 1.1). These materials can be produced by incorporating a very small amount of additive into a ceramic matrix. The additive segregates at the grain boundary with a gradient concentration or precipitates as molecular or cluster sized particles within the grains or at the grain boundaries. Optimized processing can lead to excellent structural control at the molecular level in most nanocomposite materials. Intragranular dispersions aim to generate and fix dislocations during the processing, annealing, cooling, and/or the in-situ control of size and shape of matrix grains. This role of dispersoids, especially on the nano scale, is important in oxide ceramics, some of which become ductile at high temperatures. The intergranular nanodispersoids must play important roles in control of the grain boundary structure of oxide (Al_2O_3, MgO) and nonoxide (Si_3N_4, SiC) ceramics, which improves their high-temperature mechanical properties [3–6]. The design concept of nanocomposites can be applied to ceramic/metal, metal/ceramic, and polymer/ceramic composite systems.

Dispersing metallic second-phase particles into ceramics improves their mechanical properties (e.g., fracture toughness). A wide variety of properties, including magnetic, electric, and optical properties, can also be, tailored in the composites due to the size effect of nanosized metal dispersions, as described later in the chapter. Conventional powder metallurgical methods and solution chemical processes like sol–gel and coprecipitation methods have been used to prepare composite powders for ceramic/metal nanocomposites such as Al_2O_3/W, Mo, Ni, Cu, Co, Fe; ZrO_2/Ni, Mo; MgO/Fe, Co, Ni; and so on. The powders are sintered in a reductive atmosphere to give homogeneous dispersions of metallic particles within the ceramic matrices. Fracture strength, toughness, and/or hardness are enhanced due to microstructural refinement by the nanodispersions and their plasticity. For transition metal particle dispersed oxide ceramic composites, ferromagnetism is a value-added supplement to the excellent mechanical properties of the composites [7,8]. In addition, good magnetic response to applied stress was found in these ceramic/ferromagnetic-metal nanocomposites, allowing the possibility of remote sensing of initiation of fractures or deformations in ceramic materials.

Nanocomposite technology is also applicable to functional ceramics such as ferroelectric, piezoelectric, varistor, and ion-conducting materials. Incorporating a small amount of ceramic or metallic nanoparticles into $BaTiO_3$, ZnO, or cubic ZrO_2 can significantly improve their mechanical strength, hardness, and toughness, which are very important in creating highly reliable electric devices operating in severe environmental conditions [9]. In addition, dispersing conducting metallic nanoparticles or nanowires can enhance the electrical properties, as described later. Dispersion of soft materials into a hard ceramic generally decreases its mechanical properties (e.g., hardness). However, in nanocomposites, soft materials added to several kinds of ceramics can improve their mechanical properties. For example, adding hexagonal boron nitride to silicon nitride ceramic can enhance its fracture strength not only at room temperature but also at very high temperatures up to 1500 °C. In addition, some of these nanocomposite materials exhibit superior thermal shock resistance and machinability because of the characteristic plasticity of one of the phases and the interface regions between that phase and the hard ceramic matrices.

Advanced bulk ceramic materials that can withstand high temperatures (>1500 °C) without degradation or oxidation are needed for applications such as structural parts of motor engines, gas turbines, catalytic heat exchangers, and combustion systems. Such hard, high-temperature stable, oxidation-resistant ceramic composites and coatings are also in demand for aircraft and spacecraft applications. Silicon nitride (Si_3N_4) and silicon carbide/silicon nitride (SiC/Si_3N_4) composites perform best in adverse high-temperature oxidizing conditions. Commercial Si_3N_4 can be used up to ~1200 °C, but the composites can withstand much higher temperatures. Such Nanocomposites are optimally produced from amorphous silicon carbonitride (obtained by the pyrolysis of compacted polyhydridomethylsilazane $[CH_3SiH\text{-}NH]_m[(CH_3)_2Si\text{-}NH]_n$ at about 1000 °C), which produces crystallites of microcrystals of Si_3N_4 and nanocrystals of SiC [10] (Figure 1.2). The oxidation resistance, determined by TGA analysis, arises from the formation of a thin (few microns) silicon oxide layer.

Processing is key to the fabrication of nanocomposites with optimized properties. Some examples of commonly used processes for creating nanocomposites are discussed below.

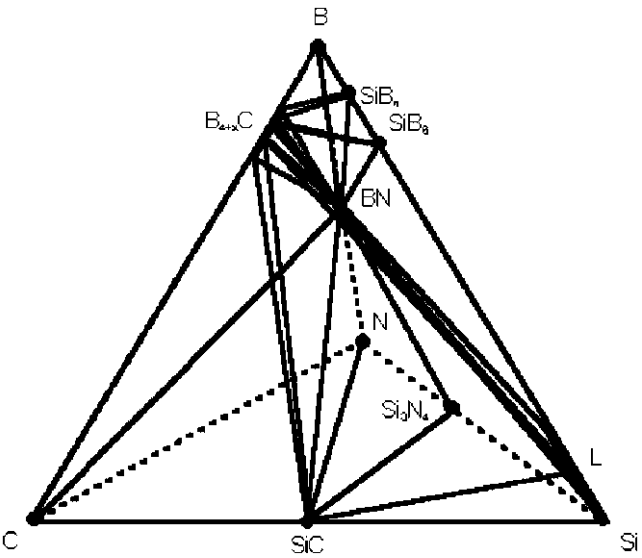

Fig. 1.2 Calculated phase diagrams of the system Si/B/C/N allows for the creation of high-temperature ceramic nanocomposites. The system Si/B/C/N is being investigated with respect to processing new covalent materials. Based on this system, several nanocomposites (SiC/Si_3N_4) have been developed that can, for example, withstand high temperatures (~1500 °C) without degradation or oxidation [10]. (Source [229] used with permission) alternative web site: http://aldix.mpi-stuttgart.mpg.de/E_head.html, used with permission

1.2.1 Nanocomposites by Mechanical Alloying

Mechanical alloying was originally invented to form small-particle (oxide, carbide, etc.) dispersion-strengthened metallic alloys (Figure 1.3) [11]. In this high-energy ball milling process, alloying occurs as a result of repeated breaking up and joining (welding) of the component particles. The process can prepare highly metastable structures such as amorphous alloys and nanocomposite structures with high flexibility. Scaling up of synthesized materials to industrial quantities is easily achieved in this process, but purity and homogeneity of the structures produced remains a challenge. In addition to erosion and agglomeration, high-energy milling can provoke chemical reactions that are induced by the transfer of mechanical energy, which can influence the milling process and the properties of the product. This idea is used to prepare magnetic oxide-metal nanocomposites via mechanically induced displacement reactions between a metal oxide and a more reactive metal [12,13]. High-energy ball milling can also induce chemical changes in nonmetallurgical systems, including silicates, minerals, ferrites, ceramics, and organic compounds. The interest in mechanical alloying as a method to produce nanocrystalline materials is due to the simplicity of the method and the possibility for scaled-up manufacturing.

Displacement reactions between a metal oxide and a more reactive metal can be induced by ball milling [14]. The reaction may progress gradually, producing a nanocomposite powder. In some cases, the reaction progresses gradually, and a metal/metal-oxide nanocomposite is formed. Milling may also initiate a self-propagating com-

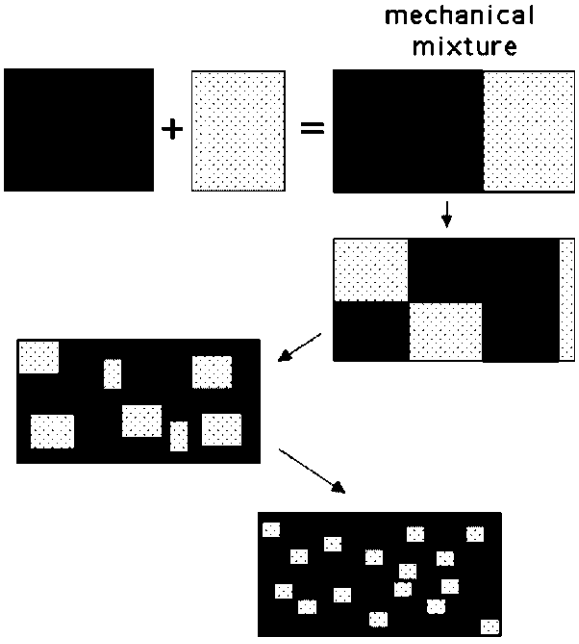

Fig. 1.3 Schematic of the formation process of typical nanocomposite microstructures by the mechanical alloying method. (Source [230, 11] used with permission)

bustive reaction [15]. The nature of such reactions depends on thermodynamic parameters, the microstructure of the reaction mixture, and the way the microstructure develops during the milling process. The mechanical stresses developed during high impact hits can also initiate combustion in highly exothermic systems, melting the reaction mixture and destroying the ultrafine (nanocrystalline) microstructure. Milling mixtures of ceramic and metal powders can induce mechanochemical reactions, and this process is an efficient way of producing nanocermets [16]. Depending on the thermodynamics of the metal/metal-oxide systems and the kinetics of the exchange (displacement) reactions during processing, various nanocomposite systems could evolve. As an example, the reduction of metal oxides with aluminum during reactive ball milling can result in nanocomposites of Al_2O_3 and metallic alloys (Fe, Ni, Cr; particularly binary alloy systems), and such ceramics with ductile metal inclusions produce toughened materials with superior mechanical properties [17]. These nanocomposite materials also have better thermomechanical properties, such as higher thermal shock resistance, due to better metal–ceramic interfacial strength.

Ball milling by direct milling of a mixture of iron and alumina powders has been used to prepare nanocomposites with magnetic phases, such as nanoparticles of iron embedded in an insulating alumina matrix [18]. The average particle size can be reduced to the 10-nm range, as indicated by x-ray diffraction linewidths and electron microscopy. The magnetic properties of this system (e.g., saturation magnetization and coercivity) can be tailored by changing the phase composition, particle size, and the internal stresses accumulated during milling. In this system, the iron nanoparticles were formed with lattice strains of about 0.005; coercivities up to 400 Oe were achieved. The magnetization of the iron particles is 25 %–40 % less than that expected for bulk iron. Systems of smaller magnetic particles embedded in a nonmagnetic matrix can be prepared by high-energy ball milling [19]. For example, nanocomposites of Fe_3O_4 particles dispersed in Cu have been prepared by ball milling a mixture of Fe_3O_4 and Cu powders directly, as well as by enhanced ball milling-induced reaction between CuO and metallic iron [20]. Both processes result in magnetic semi-hard nanocomposites with a significant superparamagnetic fraction, due to the very small particle sizes of the dispersed magnetic phase. In situ chemical reactions provide a means to control the ball milling process and to influence the microstructure and magnetic properties of the product. Nanocomposite magnets (such as hard magnetic SmCoFe phases in soft magnetic Fe/Co systems), discussed in detail later in this chapter, are routinely prepared by mechanical milling and heat treatment. The metastable nanocrystalline/amorphous structures inherently obtained in mechanically alloyed powders result from repeated deformation and fracture events during collisions of powders with the balls. Plastic deformation in powders initially occurs through the formation of shear bands, and when high dislocation densities are reached, the shear bands degenerate into randomly oriented subgrains. The large surface area of the nanocrystalline grains often helps in the transformation of crystalline into amorphous structures [21]. Deformation-induced defect density and the local changes in temperature due to impacts affect the diffusion coefficients of the several species involved during the milling process. In fact, the final microstructure and stoichiometry of mechanically milled samples often reflects the competing processes of milling-induced disorder and

diffusion-limited recovery, rather than being solely dependent on the starting material (e.g., depending on whether the starting mixtures are pre-alloyed or in their elemental forms).

1.2.2 Nanocomposites from Sol–Gel Synthesis

Aerogels, due to their high-porosity structure, are clearly an ideal starting material for use in nanocomposites. Aerogels are made by sol–gel [22,23] polymerization of selected silica, alumina, or resorcinol-formaldehyde monomers in solution and are extremely light (densities $\sim 0.5 - 0.001$ g cc^{-1}) but highly porous, having nanosize pores. In nanocomposites derived from aerogels, the product consists of a 'substrate' (e.g., silica aerogel) and one or more additional phases (of any composition or scale). In the composites, there is always at least one phase whose physical structures have dimensions on the order of nanometers (the particles and pores of the aerogel). The additional phases may also have nanoscale dimensions or may be larger. The systems most commonly made are silica-based nanocomposite systems [24], but this approach can be extended to other aerogel (alumina, etc.) precursors.

Aerogel nanocomposites can be fabricated in various ways, depending on when the second phase is introduced into the aerogel material. The second component can be added during the sol–gel processing of the material (before supercritical drying). It can also be added through the vapor phase (after supercritical drying), or chemical modification of the aerogel backbone may be effected through reactive gas treatment. These general approaches can produce many varieties of composites. A non-silica material is added to the silica sol before gelation. The added material may be a soluble organic or inorganic compound, insoluble powder, polymer, biomaterial, etc. The additional components must withstand the subsequent processing steps used to form the aerogel (alcohol soaking and supercritical drying). The conditions encountered in the CO_2 drying process are milder than in the alcohol drying process and are more amenable to forming composites. If the added components are bulk insoluble materials, steps must be taken to prevent its settling before gelation. The addition of soluble inorganic or organic compounds to the sol provides a virtually unlimited number of possible composites. Two criteria must be met to prepare a composite by this route. First, the added component must not interfere with the gelation chemistry of the aerogel precursor. Possible interference is difficult to predict in advance, but it is rarely a problem if the added component is reasonably inert. The second problem is the leaching out of the added phases during the alcohol soak or supercritical drying steps. This problem can be a significant impediment if a high loading of the second phase is desired in the final composite. When the added component is a metal complex, it is often useful to use a chemical binding agent that can bind to the silica backbone and chelate the metal complex. Many use this method to prepare nanocomposites of silica aerogels or xerogels. After the gel is dried, the resulting nanocomposite consists of an aerogel with metal atoms or ions uniformly (atomically) dispersed throughout the material. Thermal post-processing creates nanosize metal par-

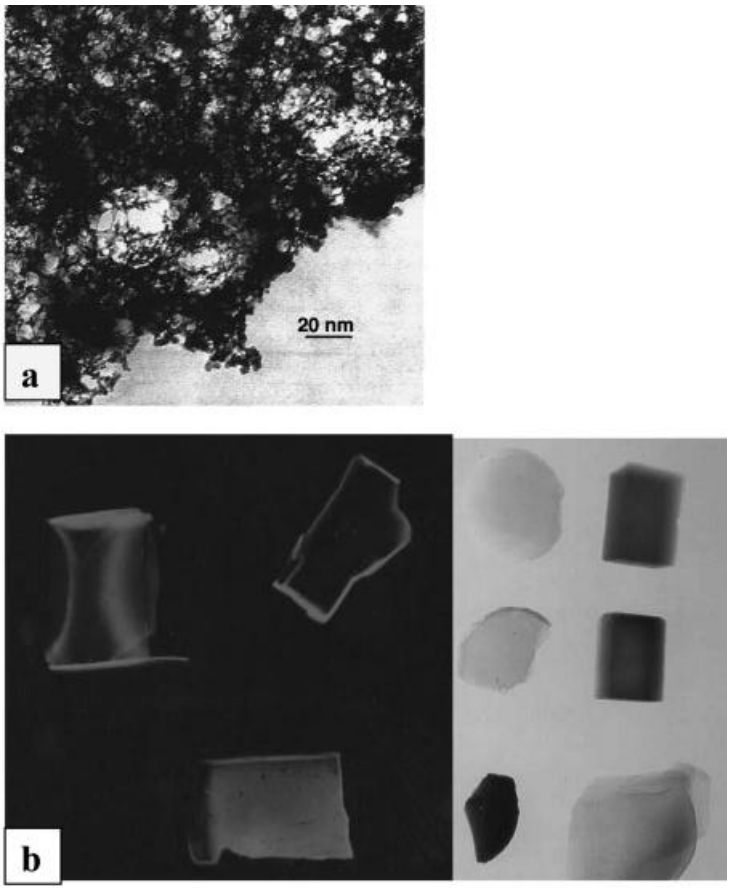

Fig. 1.4 (a) Microstructure of aerogel-encapsulated phase nanocomposite. (b) Left image of three pieces of nanocomposites shows silica aerogel samples that have been coated with silicon nanoparticles by chemical vapor methods. The composites emit red light when excited with ultraviolet light. Right image of six pieces of nanocomposites prepared by adding metal salts or other compounds to a sol before gelation; they show different colors depending on the metal species present. The deep blue aerogel contains nickel; the pale green, copper; the black, carbon and iron; the orange, iron oxide. (Source, the silica aerogel photo gallery [231] used with permission)

ticles within the aerogel matrix. Such composites can have many applications. An example is their use as catalysts for gas-phase reactions or for catalyzed growth of nanostructures.

Vapor phase infiltration through the open pore network of aerogels provides another route [25] to creating various forms of aerogel-based nanocomposites; almost any compound can be deposited uniformly throughout an aerogel. In fact, adsorbed materials in silica aerogels can be modified into solid phases by thermal or chemical decomposition. The same is true for materials that have a porous interior structure, such

as zeolites. The nanosize pores within these porous hosts can be utilized for depositing a second phase by chemical or vapor phase infiltration and thermal decomposition. Recently, single-walled carbon nanotubes have been deposited within pores of zeolites to create nanocomposite materials that have unique properties, such as superconductivity [26].

Some examples of nanocomposites (Figure 1.4) that have been created out of silica-based aerogel matrices are the following:

Silica aerogel/carbon composites [27]: These can be made by the decomposition of hydrocarbon gases at high temperatures. The fine structure of aerogels allows the decomposition to take place at a low temperatures (200–450 °C). Carbon loadings of 1%–800% have been observed. The carbon deposition is uniform throughout the substrate at lower loadings, but at higher loadings, the carbon begins to localize at the exterior surface of the composite. These nanocomposites have interesting properties, such as electrical conductivity (above certain loadings) and higher mechanical strength relative to the aerogel.

Silica aerogel/silicon composites [28]: Thermal decomposition of various organosilanes on a silica aerogel forms deposits of elemental silicon. In this case, rapid decomposition of the silane precursor leads to deposits localized near the exterior surface of the aerogel substrate. The nanocomposite, with 20–30-nm diameter silicon particles, exhibits strong visible photoluminescence at 600 nm.

Silica aerogel/transition-metal composites [29]: Organo/transition-metal complexes can be used to deposit metal compounds uniformly through the aerogel volumes. The compounds can be thermally decomposed to their base metals. These intermediate composites, due to the disperse nature of the metallic phase and hence their high reactivity, can be converted to metal oxides, sulfides, or halides. The loading of the metallic phase can be changed by repeated deposition steps. The nanocomposites contain crystals of the desired metal species with sizes in the range of 5–100 nm in diameter.

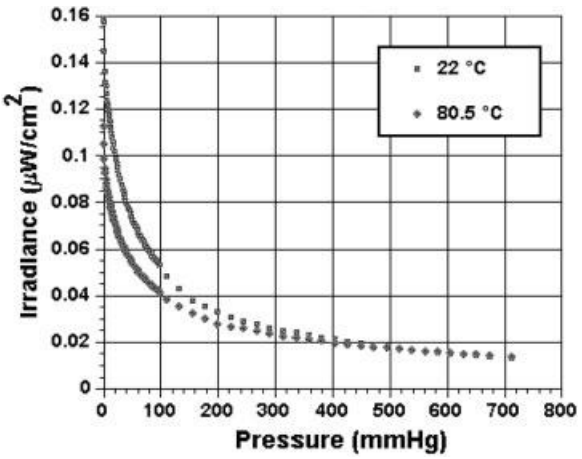

Fig. 1.5 Photoluminescence intensity (irradiance) vs. oxygen pressure (concentration gives a similar plot) at two temperatures measured with a prototype sensor made of silica aerogels. The photoluminescence intensity is indirectly proportional to the amount of gaseous oxygen within the aerogel. The quenching of photoluminescence by oxygen is observed in many luminescent materials. Source [232] used with permission)

The chemical structure of the silica (or other oxide) backbone of an aerogel can also be easily modified. For example, silica aerogel surfaces can be partially reduced by hydrogen. The resulting composite consists of thin interior surface layers of oxygen-deficient silica (SiO_x). This material exhibits strong visible photoluminescence at 490 – 500 nm when excited by ultraviolet (330 nm) light. The chemical process used to change the surface characteristics of the aerogel does not alter the physical shape or optical transparency of the original structure. This composite is the foundation for the aerogel optical oxygen sensor [30] (Figure 1.5), which is based on the fact that the intensity of photoluminescence is indirectly related to the oxygen concentration in the nanocomposite.

1.2.3 Nanocomposites by Thermal Spray Synthesis

Thermal spray processing is a commercially relevant, proven technique for processing nanostructured coatings [31]. Thermal spray techniques are effective because agglomerated nanocrystalline powders are melted, accelerated against a substrate, and quenched very rapidly in a single step. This rapid melting and solidification promotes the retention of a nanocrystalline phase and even amorphous structure. Retention of the nanocrystalline structure leads to enhanced wear behavior, greater hardness, and sometimes a reduced coefficient of friction compared to conventional coatings.

Figure 1.6 shows a generalized thermal spray process [32]. To form the starting powders, conventional powders can be cryomilled to achieve a nanocrystalline structure [33 – 35]. Under the right conditions, for example, Fe alloyed with Al, precipitates form, and these precipitates stabilize the nanoscale grain structure to 75 % of the melting temperature of the pure metal. Pure metals (except for aluminum) require some alloying before the nanocrystalline structure is stable at elevated temperatures [36]. For WC/Co and Cr_3Cr_2/NiCr, the hard particles are broken into nanometer-size grains, and they are embedded in the binder [37, 38]. Other systems have also been milled for thermal spraying, such as steel [39] and NiCr/Cr_3C_2. In all cases, there appears to be some nitrogen or oxygen contamination.

The nanoscale powders, prepared by various techniques, must be agglomerated so that grains on the order of 50 nm can be introduced into the thermal spray gun. Unlike sintering of ceramics, this agglomeration does not prevent full densification. A reasonably narrow particle size distribution ensures uniform heating. Nanocrystalline feedstock is generally injected internally (inside the torch), but powders can be injected externally. The type of flame or jet produced depends on the thermal spray technique, and within each technique, gas heating and gas flow parameters can control the velocity and temperature profile. The temperature and velocity profile, combined with the spray distance (the distance from the end of the nozzle to the substrate), control the temperature that the powders reach. Successive impact of particles in a molten or viscous state on the substrate or on previously deposited layers of material forms a coating.

The ability to maintain the nanocrystalline structure during processing and upon consolidation is critical to improving its properties because it is the nanoscale micro-

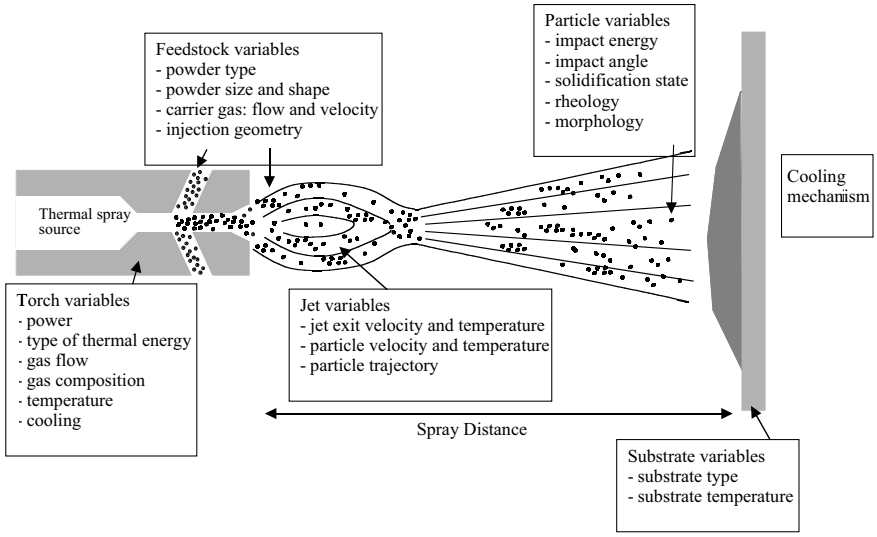

Fig. 1.6 Schematic for a generalized thermal spray process, showing the different variables used. The qualities of the coatings (bonding to the substrate, microstructure of the coating, hardness, wear resistance, etc.) are affected by a multidimensional parameter space

structure that leads to the unique properties. Several parameters are critical: (a) The thermal stability of the agglomerated powders: nanocrystalline materials can experience grain growth at temperatures well below the temperatures observed for conventional materials. The high surface area drives this growth. (b) The degree of melting that occurs in flight: this can be controlled by the spray distance, the temperature of the jet, and the velocity of the jet, and optimal parameters are determined primarily by experiment. (c) The cooling rate: a high cooling rate leads to high nucleation and slow grain growth, which promotes the formation of nanocrystalline grains. The systems that tend to maintain their nanocrystalline structure even at elevated temperature are apt to have impurities or a second phase that stabilize the grain structure [40]. For example, cryomilling often results in nanoscale particles (oxides, nitrides, or oxynitrides) [41] that fix the grain boundaries. In addition, significant impurities or excess solute atoms at the grain boundaries also limit grain growth [42, 43].

Plasma spraying and high velocity oxy fuel (HVOF) processes are the most widely used thermal spray methods for producing nanocrystalline and nanocomposite coatings. In plasma spraying, an electric arc is used to ionize an inert gas to produce a highly energetic thermal plasma jet with gas temperatures and velocities of approximately 11 000 K and 2000 ms^{-1}. Vacuum plasma spraying and low-pressure plasma spraying have been used to effectively process WC/Co nanocomposite coatings. Use of HVOF involves an internal combustion chamber in which fuel (hydrogen, propylene, acetylene, propane) is burned in the presence of oxygen or air (HVAF). This results in a hypersonic gas velocity. The particle velocities are higher than the 800 ms^{-1} achieved with plasma spray, and the thermal energy is lower (it may reach 3000 K), which reduces superheating and particle vaporization. The high speed and

low temperatures result in more strongly adhering and more homogeneous coatings with lower oxide content.

WC/Co coatings are of great interest because they already exhibit excellent wear properties. Nanostructuring further increases the wear resistance and decreases the coefficient of friction. Thermally sprayed WC/Co coatings, however, do not always exhibit improved properties. WC/Co coatings sprayed via HVOF exhibited decreased wear resistance due to decomposition of the carbide phase during spraying [44]. Nanostructured powders reach temperatures almost 500 ° higher than their conventional counterparts. Vacuum plasma spraying, however, resulted in coatings with significantly improved wear resistance and lower coefficient of friction, presumably because the Ar atmosphere prevented oxidation of the carbide phase [45].

Cr_3C_2/NiCr composites are also used in applications where wear resistance is required, but they have an added advantage over WC/Co, which has excellent corrosion resistance. Nanostructuring of these coatings has also resulted in improved hardness and scratch resistance, as well as reduced coefficient of friction. The improved homo-

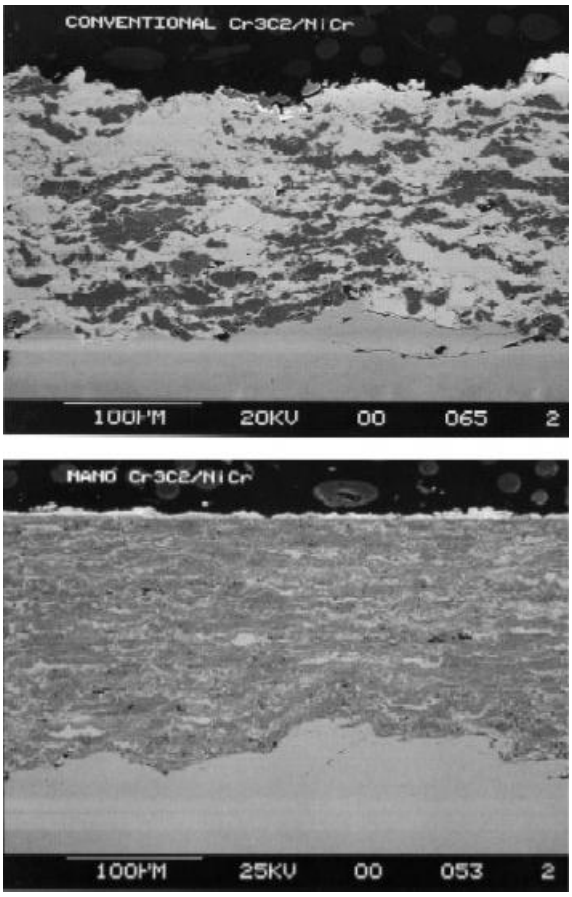

Fig. 1.7 Microstructures of thermal-sprayed Cr_3C_2/NiCr coatings. Top micrograph shows conventional coating and bottom micrograph shows nanocomposite microstructure. A uniform, dense microstructure is observed in the nanostructured coatings, compared to an inhomogeneous microstructure in the conventional coating. (Source [37] used with permission)

geneity of these structures, as well as a high density of Cr_2O_3 nanoparticles (formed by oxidation during the thermal spray process), compared to conventional materials, cause the improved properties. Figure 1.7 shows an example of the improved homogeneity of nanostructured coatings. Ceramics such as alumina/titania and zirconia have also been thermally sprayed, and the nanostructured powders have lead to submicron final grain sizes in the coatings. Key to achieving excellent properties is minimizing the degree of melting [46] so as to maintain the nanostructure in the final coating. On the other hand, significant deformation or splatting of the particles is required upon impact, to assure a large surface contact between the particles [47]. Thus, some melted particles lend well to continuous, good-quality coatings.

1.3 Metal Matrix Nanocomposites

During the past decade, considerable research effort has been directed towards the development of in situ metal-matrix composites (MMCs), in which the reinforcements are formed by exothermal reactions between elements or between elements and compounds [48]. With this approach, MMCs with a wide range of matrix materials (including aluminum, titanium, copper, nickel, and iron), and second-phase particles (including borides, carbides, nitrides, oxides, and their mixtures) have been produced. Because of the formation of stable nanosized ceramic reinforcements, in situ MMCs exhibit excellent mechanical properties.

MMCs are a kind of material in which rigid ceramic reinforcements are embedded in a ductile metal or alloy matrix. MMCs combine metallic properties (ductility and toughness) with ceramic characteristics (high strength and modulus), leading to greater strength to shear and compression and to higher service temperature capabilities. The attractive physical and mechanical properties that can be obtained with MMCs, such as high specific modulus, strength, and thermal stability, have been documented extensively. Interest in MMCs for use in the aerospace and automotive industries and other structural applications has increased over the past 20 years. This increase results from the availability of relatively inexpensive reinforcements and the development of various processing routes that result in reproducible microstructure and properties.

The family of discontinuously reinforced MMCs includes both particulates and whiskers or short fibers. More recently, this class of MMCs has attracted considerable attention as a result of (a) availability of various types of reinforcement at competitive costs, (b) the successful development of manufacturing processes to produce MMCs with reproducible structure and properties, and (c) the availability of standard or near-standard metal working methods, which can be utilized to fabricate these composites. The particulate-reinforced MMCs are of particular interest due to their ease of fabrication, lower costs, and isotropic properties. Traditionally, discontinuously reinforced MMCs have been produced by several processing routes such as powder metallurgy, spray deposition, mechanical alloying (MA), and various casting techniques. All these techniques are based on the addition of ceramic reinforcements to the matrix materials, which may be in molten or powder form. For conventional MMCs, the

reinforcing phases are prepared separately prior to the composite fabrication. Thus, conventional MMCs can be viewed as ex situ MMCs. In this case, the scale of the reinforcing phase is limited by the starting powder size, which is typically on the order of micrometers to tens of micrometers and rarely below 1 μm. Other main drawbacks that must be overcome are interfacial reactions between the reinforcements and the matrix and poor wettability between the reinforcements and the matrix due to the surface structure of the reinforcements as well as to contamination.

The properties of MMCs are widely recognized to be controlled by the size and volume fraction of the reinforcements as well as by the nature of the matrix/reinforcement interfaces. An optimum set of mechanical properties can be obtained when fine, thermally stable ceramic particulates are dispersed uniformly in the metal matrix. Efforts have been made to meet such requirements and have led to the development of novel composites – in situ MMCs in which the reinforcements are synthesized in a metallic matrix by chemical reactions between elements or between element and compound during fabrication of the composite. Compared with conventional MMCs produced by ex situ methods, in situ MMCs exhibit the following advantages: (a) formation of reinforcements that are thermodynamically stable in the matrix, leading to less degradation in elevated-temperature services; (b) reinforcement/matrix interfaces that are clean, resulting in strong interfacial bonding; (c) the formation of reinforcing particles of a finer size with a more uniform distribution in the matrix, which yields better mechanical properties.

The great potential that in situ metal matrix nanocomposites offer for widespread applications has resulted in the development of a variety of processing techniques for production during the past decade. Using these routes, in situ composites with a wide range of matrix materials (including aluminum, titanium, copper, nickel, and iron) and second-phase particles (including borides, carbides, nitrides, oxides, and their mixtures) have been produced. Particularly attractive among the several techniques available for synthesizing MMCs are the solidification processes in which the reinforcing particles are formed in situ in the molten metallic phase prior to its solidification. What makes them so attractive is their simplicity, economy, and flexibility. The judicious selection of solidification processing techniques, matrix alloy compositions, and dispersoids can produce new structures and affect a unique set of useful engineering properties that are difficult to reach in conventional monolithic materials. Specifically, the solidification conditions that are present during processing play an important role in dictating the microstructure and the mechanical and physical characteristics of these structures. Microstructure refinement arising from rapid solidification processing (RSP) offers a potential avenue for alleviating solute segregation and enhancing dispersion hardening by substantially reducing the size of the reinforcing phases and modifying their distribution in the matrix. As example, RSP of Ti/B or Ti/Si alloys accompanied by large undercoolings and high cooling rates is very effective in producing in situ Ti-based nanocomposites containing large volume fractions of reinforcing particles [49]. These particles are formed in situ in Ti/B or Ti/Si alloys either upon solidification or, subsequently, by controlled decomposition of the resulting supersaturated solid solutions.

More recently, several workers have used the RSP route [50] to fabricate in situ TiC particulate-reinforced Al-based composites. In their work, master material ingots were prepared by melting a mixture of Al, Ti, and graphite powder in a graphite-lined induction furnace under an argon atmosphere, followed by direct chill cast. Chill block melt spinning was used to prepare rapidly solidified samples in ribbon form. These ribbons were further milled into powders ($100 \pm 250\ \mu$m), which were subsequently canned and degassed and then extruded into rods. In situ formed TiC particles of 40 ± 80 nm were reported to be distributed uniformly in the aluminum matrix with a grain size of $0.3 \pm 0.85\ \mu$m. The authors reported that RSP can significantly refine the microstructure of the composites. For TiC/Al composites, the microstructure is often characterized by the presence of agglomerated TiC particles. These particles, with a size of $0.2 \pm 1.0\ \mu$m, accumulate at the Al subgrain or the grain boundaries. The larger particles have polyhedral morphology, and the smaller ones are round or globular. In comparison, typical rapidly solidified microstructures consist of a uniform, fine-scale dispersion of TiC particles with a size of 40 ± 80 nm in an Al supersaturated matrix of $0.30 \pm 0.85\ \mu$m grain size. One main advantage of RSP is its ability to produce alloy compositions not obtainable by conventional processing methods. Furthermore, RSP materials have excellent compositional homogeneity, small grain sizes, and homogeneously distributed fine precipitates or dispersoids.

The homogeneity of composite materials is crucially important to high-performance engineering applications such as in the automotive and aircraft industries. A uniform reinforcement distribution in MMCs is essential to achieving effective load-bearing capacity of the reinforcement. Nonuniform distribution of reinforcement can lead to lower ductility, strength, and toughness of the composites. Nanoscale ceramic particles synthesized in situ are dispersed more uniformly in the matrices of MMCs, leading to significant improvements in the yield strength, stiffness, and resistance to creep and wear of the materials. For example, in situ fabrication of TiC-reinforced Al, Al/Si, and Al/Fe/V/Si matrix composites by the RSP route is far more effective in

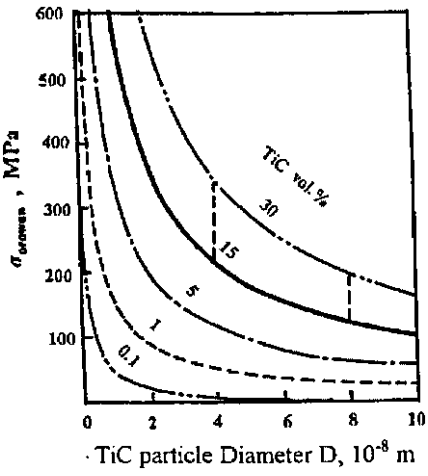

Fig. 1.8 Increase in strength (σ) of in-situ fabricated TiC-reinforced Al nanocomposites with increasing volume fractions or decreasing diameters of dispersed-phase (TiC) particles. (Source [50] used with permission)

Tab. 1.1 Typical magnetic properties of nanocrystal/amorphous composites and amorphous alloys. Alloy 1: $Fe_{73.5}$ Cu_1 Nb_3 $Si_{13.5}$ B_9 (at. %). Alloy 2: $Fe_{73.5}$ Cu_1 Nb_3 $Si_{16.5}$ B_6 (at. %). Core loss: 100 kHz, 0.2 T [52].

Alloy	t (μm)	B_s (T)	B_r/B_s (%)	H_c (A m^{-1})	μ_c (1 kHz)	Core loss (kW/m^{-3})	λ_s ($\times 10^{-6}$)	Curie temp. (K)
Alloy 1	18	1.24	54	0.53	100000	280	+2.1	843
Alloy 2	18	1.18	58	1.1	75000	280	~ 0	833
Fe/Si/B/M	20	1.41	16	6.9	6000	460	+20	631
Co/Fe/Si/B/M	18	0.53	50	0.32	80000	300	~ 0	453

improving the tensile properties of these composites, due to the formation of a refined microstructure. The in situ composites exhibit excellent strength at room temperature and elevated temperatures. The values of strength (σ) increased with increasing volume fractions or decreasing diameters of dispersed-phase (TiC) particles (Figure 1.8). When the volume fraction of dispersed particles is about 15 – 30 vol % and the particle diameters 40 – 80 nm, the values of σ are 120 – 270 MPa and 200 – 350 MPa, respectively (Figure 1.8).

Nanocrystalline materials in general are single- or multi-phase polycrystals with grain sizes in the nanometer range. Owing to the extremely small dimensions, many properties of nanocrystalline samples are fundamentally different from, and often superior to, those of conventional polycrystals and amorphous solids. For example, nanocrystalline materials exhibit increased strength or hardness, improved ductility or toughness, reduced elastic modulus, enhanced diffusivity, higher specific heat, enhanced thermal expansion coefficient, and superior soft magnetic properties in comparison with conventional polycrystalline materials [51]. Crystallizing completely amorphous solids under proper heat treatment conditions can result in formation of nanocrystalline materials. However, controlled crystallization of amorphous alloys can

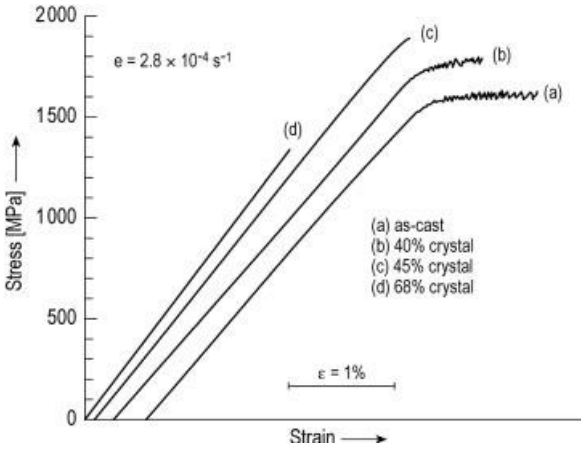

Fig. 1.9 Compressive stress–strain curves of amorphous and partly crystallized $Zr_{57}Al_{10}Cu_{20}Ni_8Ti_5$ alloy nanocomposite (a) as-cast, (b) 40 vol. % nanocrystals, (c) 45 vol. % nanocrystals and (d) 68 vol. % nanocrystals. The sample containing a volume fraction of 40 % nanocrystals (b) seems to provide the best compromise between strength and ductility. (Source [53] used with permission)

be used to obtain partially crystallized materials with nanosized crystallites embedded in the residual amorphous matrix. This special nanocrystal/amorphous nanocomposite structure allows the materials to exhibit excellent mechanical or magnetic properties. The Fe/Cu/Nb/Si/B alloys are a good example of this type of material. The Fe/Si/B/*M* (*M*: additives) alloys properly prepared by annealing amorphous alloys and having bcc Fe solid solution and 10-nm-diameter nanostructures embedded in the residual amorphous matrix, show excellent soft magnetic properties (Table 1.1). The nanocrystal/amorphous composite shows high saturation flux density, low magnetostriction, and excellent soft magnetic properties. This nanocomposite, therefore, is expected to find use in many kinds of magnetic devices such as choke coils and transformers.

Production of bulk nanostructured composites with amorphous matrices has been carried out by die casting and mechanical alloying and subsequent consolidation at elevated temperatures in Zr-based alloys [53]. The distribution of finely dispersed nanocrystals increases the flow stress significantly. For example, a $Zr_{57}Al_{10}Cu_{20}Ni_8Ti_5$ sample containing a volume fraction of 40% nanocrystals (Figure 1.9, curve b) seems to provide the best compromise between strength and ductility.

1.4 Bulk Ceramic Nanocomposites for Desired Mechanical Properties

Over the past half century, ceramics have received significant attention as candidate materials for use as structural materials under conditions of high temperature, wear, and chemical attack that are too severe for metals. However, one characteristic of these ceramics that has prevented them from being widely used is their inherent brittleness. Thus, significant scientific effort has been directed towards making ceramics more flaw-tolerant through design of their microstructure. An important example of high-toughness structural ceramics is *self-reinforced* silicon nitrides, which were first developed during the 1970s [54]. These materials have high toughness and room-temperature strength, along with good resistance to corrosion and oxidation. However, their high-temperature ($>1000\,^{\circ}C$) strength is compromised by low creep resistance and the occurrence of subcritical crack growth. These phenomena are caused by the softening of a glassy phase that is located at the grain boundaries as the temperature is increased. A possible way to overcome this problem is the fabrication of Si_3N_4/SiC nanocomposites [55]. Also, several approaches have been used to improve the processability (the sinterability of these materials is rather poor) and high-temperature properties of monolithic silicon nitrides, with limited success.

Considerable attention has been devoted to 'functionally graded nanocomposite materials', for which gradually varying the dispersion (nanoparticles) to matrix ratio in chosen directions continuously changes the material. An example of such a material is SiC dispersions in a C (pyrolytic graphite) matrix, which has served well as thermal barriers on the space shuttle due to its excellent resistance to oxidation and thermal shock. One route to preparing these composite systems is by chemical vapor deposition using multicomponent gas reactions. For example, 10–100-nm sized SiC disper-

sions can be prepared with pyrographite using precursors of $SiCl_4/C_3H_8/H_2$ or $SiCl_4/CH_4$ in CVD. The entire range of compositions from carbon to SiC has been prepared by this method [56]. Changing the deposition conditions can control the morphologies of the second phase and hence the microstructure of the composites; this control influences the mechanical properties of the material. Nanocrystalline carbide-embedded composites, particularly those with amorphous or diamond-like carbon matrices, can be considered for tribological applications. The challenges here are to minimize formation of the sp^2 soft graphite-like phase during synthesis and to retain a high fraction of the hard a-C matrix. Pulsed laser deposition (in which laser-ablated plumes from graphite are intercepted by a low-energy metal plasma produced by magnetron sputtering) [57] at near room temperature has been used successfully to create ~10 nm TiC/TiCN nanocrystals embedded uniformly in a-C with diamond-like characteristics. Hardness values as high as 60 GPa, coefficient of friction values as low as 0.1, and high toughness values have been achieved in these films, which have high tribological value and possible applications in surface-protection coating technologies. The two-phase heterogeneous structure in the nanocomposites provides crack deflection mechanisms, reducing the tendency toward easy brittle failure in these hard composites.

Significant interest was generated in 1991 when Niihara [58] reported large improvements in both the fracture toughness and the strength of materials with a unique microstructure: ceramics with nanometer-range particles (20–300 nm) embedded within a matrix of larger grains and at their grain boundaries. These ceramics reportedly showed up to 200% improvement in both strength and fracture toughness, better retention of strength at high temperatures, and better creep properties. Materials like SiC, Al_2O_3, ZrO_2 and Si_3N_4 are excellent candidates for demanding structural applications due to their mechanical and thermomechanical properties (Figure 1.10) [59]. The incorporation of fine SiC and Si_3N_4 particles (smaller than 300 nm) in an alumina

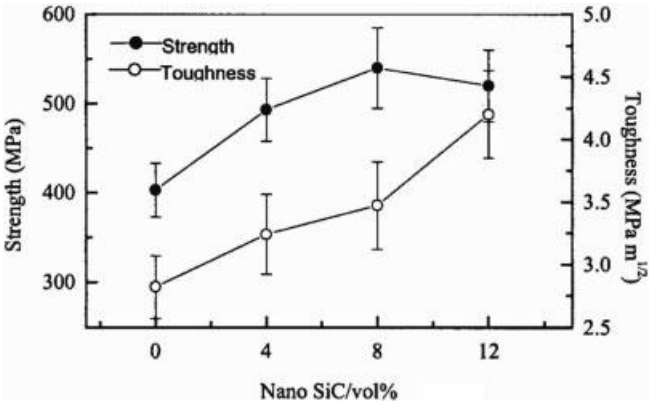

Fig. 1.10 Mechanical properties of a SiC/zirconia-toughened mullite nanocomposite as a function of nanosized SiC content. (Source [59] used with permission)

(Al_2O_3, a structural ceramic material) matrix first demonstrated the concept of structural nanocomposites. The dispersion of these particles improved the fracture toughness from 3 to 4.8 MPa $m^{1/2}$ and the strength from 350 to 1050 MPa at only 5 vol. % additions of SiC [60]. The bending strength of such composite was also measured to be $\sim$ 1 GPa. Further improvements in strength to about 1500 MPa were achieved by annealing the samples at 1300 °C. The high strengths were maintained to about 1000 °C. For Si_3N_4/SiC nanocomposites, several processing techniques have been used, including conventional powder processing, sol–gel processing, and polymer precursor processing; the SiC particles can originate from admixed commercial SiC powders, SiCN powders produced by plasma synthesis, in situ reaction pyrolysis of carbon-coated Si_3N_4 particles, and pyrolysis of a polycarbosilane based on SiCN precursor. An example of conventional processing is co-milling of the solid precursor powder materials followed by hot pressing, which produces nanocomposites possessing both inter- and intra- granular SiC particles [61]. Intragranular particles are most effective in toughening the material, because they are mainly responsible for crack deflection and crack impediment. Intergranular particles are often detrimental (initiating cracks), but they could provide some advantages by grain refinement during processing. The toughness of the composite depends on the volume fractions of these two types of dispersoids, and controlling these fractions precisely is challenging. In polymer-based processing, a mixture of Si_3N_4 powder, sintering additives, and polymethylphenylsilane is pyrolyzed at $\sim$1000 °C in Ar and sintered in nitrogen. Another possibility is preparing an amorphous Si/N/C powder by crosslinking and pyrolysis of polymethylsilazane [62]. Whereas the conventional process leads to a micronanostructure with nano-sized SiC dispersions mainly inside Si_3N_4 grains, the polymer-processing route results in atto (nano-nano) structures. Hybrid polymer/powder processing can also be applied to other composite microstructures such as Al_2O_3/SiC. Coating a silicon-containing polymer (polycarbosilane) onto alumina powder, followed by pyrolysis, can result in a finer SiC nanophase [63]. Novel, superior processing routes can be used to prepare well dispersed ceramic nanocomposites, for example Al_2O_3/SiC. Colloidal consolidation and reaction sintering is one such process [64]: micro-size particles of the two phases are colloidally dispersed and consolidated to form uniform compacts. The SiC phase particles are then oxidized to reduce them to nanometer-size cores. The interfacial reaction between the oxidized SiC particles and the alumina matrix produces mullite. The advantage of this process is that particle sizes need not be brought down to nanoscale by milling and can be controlled well by oxidation. Also, due to the volume increase that occurs during reaction sintering, shrinkages often seen during sintering are small.

Materials fabricated from polymer-derived powders made by hot pressing have yielded the best mechanical properties. These techniques are expensive and limit the shapes that can be fabricated. Gas-pressure sintering or pressure-less sintering are the most attractive processing techniques. However, to date, research on gas-pressure sintering has used mixed powders, which result in poor powder dispersion, agglomeration of SiC, and changes in the glass phase chemistry due to reaction with SiC. Thus, the focus for future processing rests on routes that produce commercially viable powders with uniform dispersion of SiC particles (with controlled size and volume

fraction) that can be fabricated into dense components by gas-pressure or pressure-less sintering. The effects of reinforcement on the mechanical properties of silicon nitride nanocomposites is not well understood. As with the Al_2O_3/SiC nanocomposites, the presence of the SiC at the grain boundaries restricts grain growth, resulting in the formation of a matrix of finer Si_3N_4 grains. In fact, at higher volume percent of reinforcements, grain growth is reported to be severely restricted, resulting in fine α-Si_3N_4 grains and a composite showing superplastic (large strain to failure) behavior. The 'nanosize' strengthening and toughening effect due to thermal expansion mismatch proposed for Al_2O_3/SiC composites needs to be critically examined for Si_3N_4/SiC composites: the difference between the thermal expansion coefficients of Si_3N_4 and SiC is small and in the opposite sense as in Al_2O_3/SiC. The presence of a liquid phase in Si_3N_4 and its composites further complicates matters: reactions between the reinforcements and the liquid phase could alter its composition and quantity, thus changing the sintering behavior and creep resistance. Thus, a more fundamental understanding of the effect of nanosized SiC reinforcements on the behavior of Si_3N_4 matrix composites is required. In particular, systematic studies of the effects of reinforcement size and volume fraction on the microstructure, processing, and properties of these nanocomposites are needed. Such studies exist for composites in which the reinforcement size is in the several-micron range, and in these studies, both the reinforcement size and volume fraction significantly affect the fracture toughness and strength [65].

For unreinforced Si_3N_4 ceramics, there is sufficient evidence that creep in the liquid phase-sintered materials is controlled by grain boundary transport and sliding. Thus, the incorporation of fine reinforcements at the grain boundaries may improve creep resistance [66]. The amount and viscosity of the intergranular phase due to chemical reactions and accelerated crystallization, the hindrance of grain-boundary sliding due to fixing by SiC particles, and the obstruction of easy diffusion paths by the SiC particles explain the better creep resistance of the nanocomposites [67]. For Al_2O_3/SiC nanocomposites, the better creep resistance (5 vol. % SiC nanoparticles reduces the tensile creep of Al_2O_3 by 2 – 3 orders of magnitude) is explained by SiC nanoparticles fixing the grain boundaries, resulting in less grain-boundary sliding, a small viscoelastic contribution to creep, and enhanced grain-boundary strength, allowing plastic deformation of grains through dislocation motion [68]. The presence of nonbridged grain boundaries causes a rearrangement of the microstructure due to initial grain sliding. But this initial sliding process is stopped easily as boundaries fixed by the SiC nanoparticles are encountered; hence, only lattice mechanisms based on dislocation motion or, to a lesser extent, viscoelastic mechanism, contribute to creep. However, in general, the studies on nanocomposites and the exact mechanisms of creep resistance have not been entirely conclusive, and systematically investigating the effects of various microstructural parameters as a functions of particle size, oxidation, and volume of the dispersed phase is desirable. An additional factor that needs careful control is the volume fraction of reinforcements on the grain boundary as opposed to within the grain. The erosion properties of such composites also deserve mention. The residual surface stress induced by grinding and polishing nanocomposites (e.g., Al_2O_3/SiC) and monolithic alumina are quite different, and studies show that the

residual surface stress in the nanocomposite is more sensitive to surface treatment than that in the corresponding monolithic structure. Direct observations by transmission electron microscopy suggest that deformation micromechanisms, from twinning in the alumina to dislocation generation in the nanocomposite, dominate the plastic deformation induced by the surface treatments.

Crack-tip bridging by particles is a primary mechanism of strengthening ceramic nanocomposites. Small brittle particles (for example, silicon carbide particles in Al_2O_3/SiC composites) cause crack tip bridging at small distances behind the cracks [69]. Residual stresses around the particles cause the strengthening mechanism to operate effectively even at small volume fraction loading of SiC. The increase in the nanocomposite strength due to the reduction in the critical flaw size is achieved by the fine dispersion of nanoparticles [70]. Intergranular fracture, which is responsible for fracture in monolithic alumina, is suppressed in the nanocomposite, because the crack extension along grain boundaries is suppressed by particles that strongly bond the matrix–matrix interfaces. Hence, transgranular fracture is a common mode of fracture in nanocomposites. Tensile stresses in the intragranular particles induce the cracks to extend to the particles, leading to particle bridge toughening.

Finally, dispersing metallic second-phase particles into ceramics is not only suitable for improving the mechanical properties of ceramics, but also presents a wide variety of advantages for addition of new functions such as magnetic, electric, and optical properties, due to the size effect of nanosized metal dispersion. Granular films can be made with a ceramic phase embedded with nanosize metal granules [71] (e.g., Fe/Al_2O_3, Fe/SiO_2). Such films display unusual and often enhanced transport, optical, and magnetic properties. An important parameter that affects the physical behavior of granular films is the percolation threshold of the embedded metal phase. Percolation effects in nanocomposites are discussed later in this chapter. A dramatic manifestation of this percolation effect is the change, by many orders of magnitude, of the electrical resistivity (insulator-to-metal transition) as the percolation threshold is passed. The percolation threshold is generally found to be in the range of 0.5 – 0.6 metal volume fractions for nanocomposite films [72]. The mechanical properties can also undergo changes near the percolation threshold. The obvious explanation for this is that a change occurs in deformation behavior as the embedded phase forms connected networks that spread through the matrix phase. Conventional powder metallurgical methods and solution chemical processes like sol–gel, and coprecipitation methods can also be used to prepare composite powders for ceramic/metal nanocomposites such as Al_2O_3/W, Mo, Ni, Cu, Co, Fe; ZrO_2/Ni, Mo; MgO/Fe, Co, Ni and so on. They are sintered in a reductive atmosphere that gives homogeneous dispersion of metallic particles within the ceramic matrices. The microstructural refinement by nanodispersion and the plasticity enhance the fracture strength, toughness, and/or hardness.

In summary, the advantage of ceramic nanocomposites lies not only in the mechanical strength of the composite material but also in other mechanical properties such as fracture toughness, hardness, and creep resistance. The degree of improvement in these properties depends on the composite systems involved. Although there are some generalities in the strengthening and toughening mechanisms in such composites, such as crack deflection and crack-tip bridging by the dispersed particles, the

actual size, location, and volume fraction of particles strongly influence the final outcome with respect to mechanical behavior.

1.5 Thin-Film Nanocomposites: Multilayer and Granular Films

Thin-film nanocomposites are films consisting of more than one phase, in which the dimensions of at least one of the phases is in the nanometer range. These nanocomposite films can be categorized as multilayer films, in which the phases are separated along the thickness of the film, or granular films, in which the different phases are distributed within each plane of the film (Figure 1.11). Multilayered thin-film nanocomposites consist of alternating layers of different phases and have a characteristic thickness on the order of nanometers. These films are usually used for their enhanced hardness, elastic moduli, and wear properties. The elastic moduli is higher in multilayered thin films than in homogeneous thin films of either component. The supermodulus effect [73] is observed in some metallic systems, by which, at certain characteristic thicknesses (typically ~2 nm, corresponding to a bilayer consisting of one layer of each phase) of the film, the elastic modulus increases by more than 200%. The most satisfactory explanation of this effect assumes an incoherent interface between the adjacent layers [74], suggesting that atoms are displaced from their equilibrium positions and that, during loading, all the layers undergo compression, which results in a higher resistance to deformation. The increase in hardness of the multilayer nanocomposites has been explained [75] by considering that, when ultrathin films of materials with different dislocation line lengths are stacked, the strength approaches the theoretical limit. The dislocations cannot move from layer to layer, due to the difference in dislocation line lengths, and the films are thin enough that independent dislocation sources do not become operative. Conventional thin-film deposition techniques (sputtering, physical vapor deposition, CVD, electrochemical deposition, etc.) can produce multilayer nanocomposites, and the excellent flexibility of these techniques creates extremely thin films of uniform compositions.

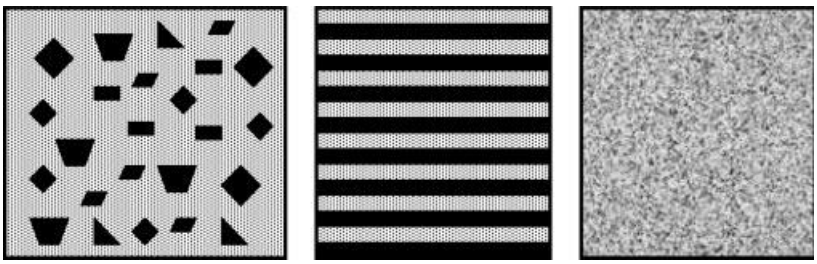

Fig. 1.11 Schematic of possible microstructures for nanocomposite and nanostructured coatings: isotropic dispersed multiphase microstructure (e.g., TiC/amorphous carbon), multilayered microstructure (e.g., TiN/TiC) for nanocomposite coatings, and homogeneous alloyed microstructure as possible homogeneous nanostructured coatings (e.g., NiCoCrAlY alloy)

Granular nanocomposite films are those that contain both phases (metal and ceramic) in the same layer of the film and have no abrupt interfaces across the film thickness as in multilayer films. Here, one phase can be in the nanosize range (similar to dispersions), or both phases can have nanocrystalline grains distributed contiguously and laterally in the film. Granular nanocomposite coatings are also common; in these, the matrix phase is a polymer and the dispersed phase is inorganic. Granular films in which at least one distributed phase has electrical/magnetic properties are mainly used in electrical and magnetic applications [76]. In certain systems consisting of metal and ceramic particles (such as iron oxide/silver and alumina/nickel), changing the fraction of the phases present can alter the magnetic properties. At small volume fractions of the metal component, the material exhibits ferromagnetic behavior. Beyond a certain volume fraction of the metal phase, the ferromagnetic ordering gives way to superparamagnetism, because, once the metal particles attain percolation, the film behaves essentially like the metallic phase. An important parameter that critically affects the properties of granular films is the percolation threshold of the metal, which typically corresponds to a metal volume fraction of 0.5 – 0.6. A dramatic observation at percolation is the large (several orders of magnitude) change in electrical resistivity of such films, going from an insulating ceramic-like behavior to a conducting-metal behavior. Similar techniques (such as CVD or electrochemical methods) as used in multilayer film growth can also be used to prepare homogeneous nanostructured composite films. As an example, nanostructured AlN/TiN composite films were made by CVD using high-speed deposition of gaseous precursors ($AlCl_3$, $TiCl_4$, NH_3) to form insoluble solid mixtures [77]. In the films so generated, the grain sizes corresponded to 8 nm (AlN) and 6 nm (TiN). The grain size range allows the films to have better ductility and greater toughness compared to bulk AlN/TiN composites.

1.6 Nanocomposites for Hard Coatings

Improved wear resistance, good high-temperature stability, and improved friction properties are important characteristics of good coatings for use in applications such as cutting tools. Most widely used coatings are made from TiN, TiC, TiAlN, CrN, diamond-like carbon (DLC), WC/C, MoS_2, Al_2O_3, etc. For improved coatings in which lower friction, increased life time, increased toughness, higher thermal stability, and in some cases, environmental (biomedical, for example) compatibility are needed, new types of materials are being considered, including nanocomposite materials [78]. Nanocomposite structures such as multilayers or even isotropic coatings can be made from nanoscale entities with properties superior to single-phase materials. This approach of using nanocomposites is an alternative to using specific alloying elements in single-phase coating materials (to improve properties such as hardness) and provides far better flexibility in tailoring multifunctional coatings.

Nanocomposite coatings usually consist of two or more phases combined as multiple layers [79] or as homogeneous isotropic multiphase mixtures. Classical multilayer (3 to many layers) coatings have total thicknesses of several micrometers, and the

many layers are typically used to provide toughness (by crack deflection at the many interfaces) and properties such as oxidation resistance (due to, e.g., TiAlN layers). Building multilayer structures also provides better tribological properties [80]. Gradient layers are also often introduced to counterbalance the vast differences in thermal expansion coefficients between multiple layers, which would cause internal stresses and delamination at the interfaces between layers. In nanoscale multilayer coatings, when the thickness of each layer is in the nanometer range, superlattice effects can increase the hardness and other properties of the coatings. The increased hardness of such coatings (e.g., TiN/VN), where the superlattice period is a few nanometers, can be orders of magnitude higher than that of the corresponding base materials [81, 82]. The hardness increase in these nanoscale multilayer films results mainly from hindering dislocation movements across the sharp interfaces between two materials having vastly different elastic (particularly shear modulus) properties and lattice mismatch (coherency strain) [83]. One interesting point to note is that, if the individual layers are very thin (less than 3–5 nm typically), the hardness increase can disappear, because the strain field around the dislocations falls mainly outside the particular layer. Also, the sharpness of the interface also affects the hardening mechanisms, because high-temperature interdiffusion between layers can decrease the sharp variation in shear modulus. Another possible reason for increased hardness and improved chemical stability is chemical differences intentionally inserted at the interfaces so as to induce strains and electronic interactions; for example, TiAlN/CrN multilayer structures are more efficient than TiAlN films [84]. The hardness effect resulting from lattice mismatch disappears at multilayer periods greater than 10 nm, due to lattice relaxation (Figure 1.12). Hence, for practical applications, the thickness of the layers in these coatings is designed based on the above considerations so as to obtain the optimum hardness values and wear properties with appropriate temperature stability. In fact, for many coating applications (e.g., coatings for cutting tools), toughness at high operating temperatures and chemical stability are more crucial than hardness alone [85]. Commercial multilayer coatings with multilayer periods in the nanoscale range do exist; for example, WC/C coatings used in the cutting tool industry. When the multilayer nanoscale coatings are deposited by periodic variation of the deposition (e.g., sputtering) conditions, a templating effect is often observed. In building superlattice structures from different materials of different structures, the layer first deposited can force the next layer (of the different material) to adopt the crystallographic structure of the first layer; this occurs, for example, in TiN/Cr_2N coatings in which Cr_2N is forced into the structure of the TiN (fcc) underlayer [86] and in TiN/AlN, in which the AlN (originally wurtzite) is forced into the NaCl structure of the TiN.

In addition to nanoscale multilayer coatings, it is also possible to fabricate isotropic nanocomposite coatings consisting of crystallites embedded in an amorphous matrix, with grain sizes in the nanometer range. These coatings generally have one phase that is hard (load bearing; e.g., transition metal carbides and nitrides) and a second phase that acts as a binder and provides structural flexibility (amorphous silicon nitride, amorphous carbon). The formation of these composite structures involves phase separation between two materials (which show complete immiscibility in solid solution),

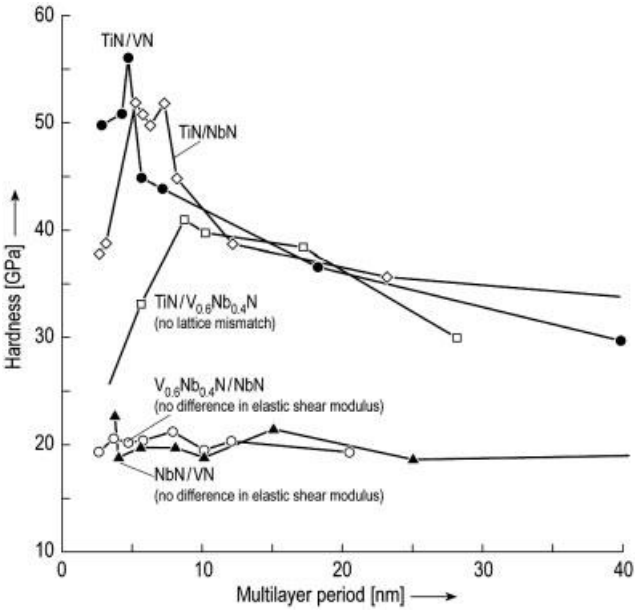

Fig. 1.12 Hardness of several multilayered nanocomposite coatings as a function of multilayer period in the coatings. The individual layers in these coatings can differ in inherent elastic properties (modulus) as well as in structure and lattice spacing. (Source [78] used with permission)

which are often codeposited, for example, by sputtering or plasma deposition. Unlike in multilayer composite systems, the possible material compositions and particle sizes in nanocomposite coatings are restricted by material properties and deposition conditions. Typically, these nanocomposite coatings are deposited by plasma-assisted chemical vapor deposition (PACVD) or physical vapor deposition (PVD). Very hard (~50–60 Gpa) coatings of nanocomposites have been made from a TiN/a-Si_3N_4 system, using PACVD from $TiCl_4$, $SiCl_4/SiH_4$, and H_2 at about 600 °C [87]. The nanocomposite contains nanocrystalline TiN (4–7 nm) in a matrix of amorphous Si_3N_4. The gas phase nucleation (uncontrollable rates), chlorinated precursors (unreacted species remain in the process, contaminating the films), and high processing temperatures are disadvantages in this process. PVD processing can be used to prepare the same coatings by sputtering Ti and Si targets in nitrogen gas at room temperatures. The disadvantage is that the films are of inferior quality, and the hardness is lower than the PACVD-deposited nanocomposite coatings. In addition to improved hardness, nanocomposite coatings also show better oxidation resistance in comparison to TiN coatings.

It is interesting to note and analyze the high hardness of these nanocrystalline particles/amorphous matrix coatings. Typically in single-phase nanocrystalline materials, the major increase in hardness comes from the lack of plastic deformation because the dislocations face far more barriers to mobility. However, hindered dislocation alone cannot explain the superior hardness properties of these nanocomposite coatings.

Since the nanocrystallites within the amorphous matrices are only a few nanometers large, dislocation formation simply does not occur, and hence, plastic deformation is largely quenched. Plastic deformation occurs through a pseudo-plastic deformation in which the nanocrystals move against each other. Since this process requires higher energy, resistance to plastic deformation in these materials is relatively high. Crystalline carbides in amorphous carbon matrices are a good example of this category of nanocomposites and can provide hard, low-friction coatings [88]. Ti/C systems are most promising in this regard. Advances in laser-assisted deposition techniques (e.g., magnetron sputtering-assisted pulsed-laser deposition) have aided the fabrication of hard composites with nanocrystalline and amorphous phases [89]. The volume fraction and particle size of the coatings can be adjusted to obtain optimum properties in terms of toughness and hardness. The design of appropriate particle size allows for the optimum generation of dislocations and micro- and nano-cracks, which result in a self-adjustment in composite deformation from hard elastic to plastic at loads exceeding the elastic limit. Thus, compliance of the coatings is improved and catastrophic brittle failure is avoided. Such load-adaptive nanocomposites based on optimal design of the composite microstructure are extremely useful in applications subject to wear.

Hard coatings such as TiN and Ti-C-N/DLC have significant advantages in aerospace systems. Apart from their hardness, toughness, and low friction properties, these coatings also resist attack by corrosive fluids that are used (as engine oils or lubricants) in aircraft engines and parts. Magnetron sputter-assisted pulsed-laser deposition is a good candidate technique for depositing such coatings in different configurations, such as functional-gradient, multilayer, and granular nanocomposites [90]. The tailoring of the different architectures in creating appropriate coatings that blend the various tribological properties is key to creating high-performance hard coatings. Nanostructured coatings provide several pathways for reducing stress in hard coatings and terminating cross-sectional dislocations, with possibilities for controlling dislocation movement by dispersion strengthening or lattice mismatching between alternate layers, as discussed above.

Other systems that create excellent nanocomposite-based, low friction, hard coatings are based on carbide particles (Ti, Ta, Nb, etc.) in DLC matrices [91–93] (Figure 1.13). Several techniques, such as PVD, pulsed-laser deposition, and reactive magnetron sputtering, are used to deposit these coatings. These typically contain larger crystalline particles (10–50 nm) surrounded by thick amorphous carbon coatings (5 nm). The particle sizes are large enough to allow dislocations but are too small for crack propagation. The larger grain separation allows incoherency strains to develop and, under loading, cracks to originate between crystallites, which allow pseudoplastic deformation. Thus, their hardness is also much higher ($\sim$30 Gpa) than that of single-crystalline carbide materials, and these coatings have, in addition, much higher toughness. These types of coatings can also be modified by introducing other elements; for example, W or Cr for creating optically absorptive coatings for solar energy converters [94] and materials such as MoS_2 (TiN/MoS_2, TiB_2/MoS_2) for lubricating coatings [95].

Metal carbide/ductile metal systems are considered for cutting tools, because the carbide phase provides hardness and the metal provides toughness. For example, composites such as WC/Co, WC/TiC/Co are commonly used in cutting and forming tool

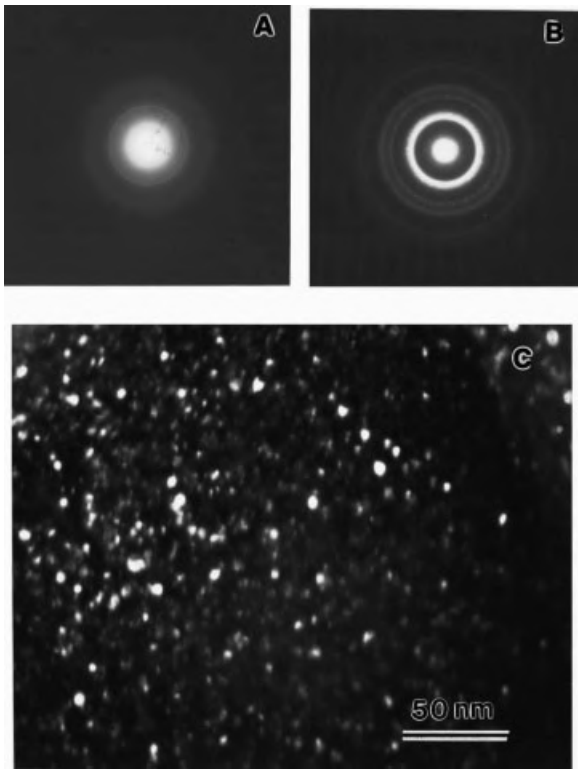

Fig. 1.13 Plan-view transmission electron microscope examinations of W-DLC layers: (a) electron diffraction pattern of a W-DLC with 9.7 at. % W, (b) electron diffraction pattern of a W-DLC with 32.0 at. % W, (c) dark-field micrograph of the W-DLC layer with 9.7 at. % W, taken with WC rings. (Source [93] used with permission)

applications, and these can be synthesized by various routes [96]. These nanocomposites, in which the particle or grain sizes of the component phases are in the nanometer range, have much better mechanical properties (strength, hardness, toughness). Typically, reductive decomposition of W- and Co-containing salts, followed by gas-phase carburization (with CO/CO_2) are used to prepare nanocomposites such as WC/Co. These processes produce carbon-deficient metastable carbide phases with inferior mechanical properties. Alternative approaches, in which a polymer precursor such as polyacrylonitrile is used as the carbon source during the chemical synthesis and subsequent heat treatment to obtain high-quality nanocomposites (particle sizes ~50–80 nm), have been developed [97]. TaC/Ni nanocomposites are interesting from two aspects: excellent thermal stability and outstanding mechanical properties [98]. They are used as surface coatings for protection against wear and corrosion. These nanocomposites can be prepared by devitrification of sputtered amorphous films of Na/Ta/C of nonstoichiometric composition. The grain size of the matrix Ni is about 10–30 nm, and the TaC particles (~10–15 nm) are uniformly distributed in the matrix. Even at 700 °C, no grain growth is observed, suggesting excellent thermal stability for these nanocrystalline duplex-phase composites. The measured hardness of the composite (12 GPa) matches that of conventional WC/Co nanocomposites at a much reduced volume fraction (35 %) of the composite.

Chemical and physical vapor deposition (CVD and PVD, respectively), and laser ablation have been used to prepare a variety of superhard nanocomposites made of nitrides, borides, and carbides. In these systems, the hardness of the nanocomposite significantly exceeds that given by the rule of mixtures in bulk. For example, the hardness of nanocrystalline $M_nN/a\text{-}Si_3N_4$ (M = Ti, W, V, etc.) nanocomposites with the optimum content of Si_3N_4 (close to the percolation threshold) reaches 50 GPa, although that of the individual nitrides does not exceed 21 GPa. For a binary solid solution, such as $TiN_{1-x}C_x$, the hardness increases monotonically with increasing x from that of TiN to the that of TiC, following the rule of mixtures. Recently, superhardness has been achieved in coatings consisting of a hard transition-metal nitride and a soft metal that does not form thermodynamically stable nitrides, such as nanocrystalline M_nN-M' (M = Ti, Cr, Zr, M' = Cu, Ni) [99]. However, these systems have low thermal stability and their hardness decreases upon annealing to $\geq 400\,^{\circ}C$.

The generic concept for the design of novel superhard nanocomposites that are stable up to high temperatures ($\sim 1000\,^{\circ}C$, which is very important in industrial applications) is based on thermodynamically driven segregation in binary (and ternary) systems. These systems display immiscibility and undergo spinodal decomposition even at such temperatures. In these systems, any small local fluctuation in the composition of the mixed phase decreases the free energy of the system, thus leading to spontaneous segregation and, as a result, a nanocomposite that remains stable against grain or particle coarsening develops. For many hard coatings (e.g., PVD deposited films, in which the compressive stress is typically 4 to 6 GPa or even greater than 10 GPa), the measured enhancement of the apparent hardness and elastic modulus is due to high biaxial compressive stress. It is important to perform annealing experiments in such systems to verify what the real, 'intrinsic' hardness of the film is. The observed high resistance of superhard nanocomposites to crack formation has been studied in terms of conventional fracture mechanics scaled down to dimensions of 1 – 2 nm. An analysis of indentation curves measured on superhard nanocomposites in terms of Hertzian elastic response shows that they are indeed strong materials. The stress concentration factor based on nanoscale flaws is low, and therefore, the stress needed to propagate such a small nanocrack is very high. The propagation of such nanocracks in 3D nanocomposites involves much deflection and branching of the plane of the cracks, which hinder growth of the nanocracks. However, the self-organization of these systems, due to thermodynamically driven spinodal segregation, results in a very low concentration of intrinsic flaws. Thus, the remarkably high resistance of these nanocomposites to crack formation can be understood in terms of a high threshold for the initiation of larger microcracks, which may lead to their catastrophic growth.

Carbon – carbon nanocomposites: Carbon – carbon composites have received much attention due to their tremendous potential for applications in the aerospace, automobile, and energy industries. This material's attractive properties include low specific weight, low thermal expansion, high thermal shock resistance, and high strength over large temperature ranges. They are usually made with carbon fiber reinforcement, with the matrix being disordered or partially graphitized carbon infiltrated from various resins, pitches, and gaseous (hydrocarbon) precursors. The main limitation of

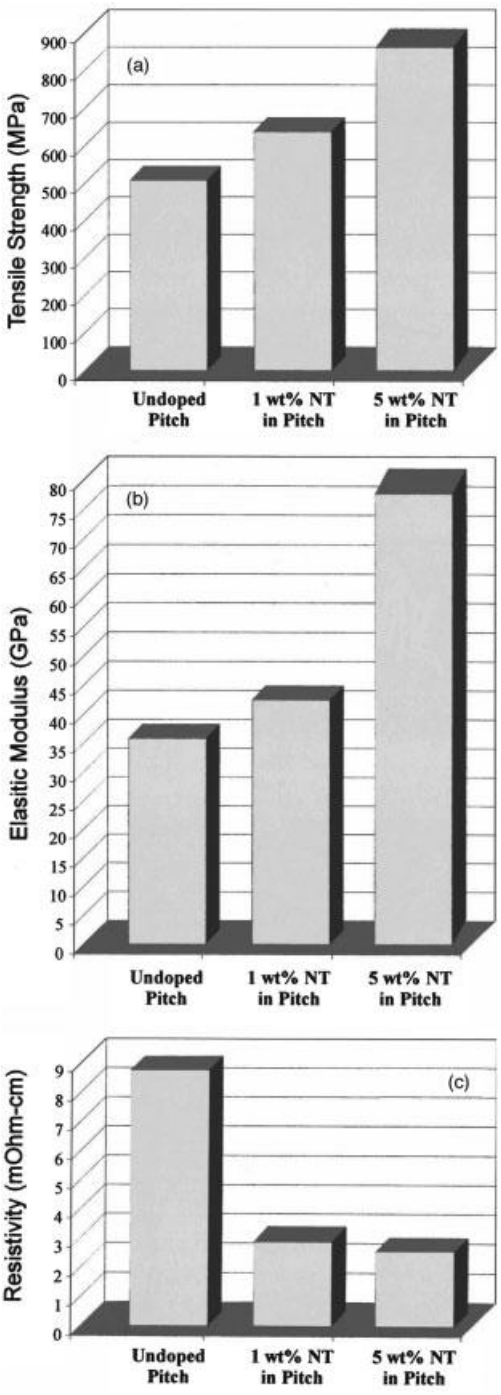

Fig. 1.14 Comparison of the tensile strength (a), modulus (b), and electrical resistivity (c) of composite carbon fibers with 1 and 5 wt. % nanotube loadings with the corresponding values in unmodified isotropic pitch fibers. Each data point represents an average value for strength, modulus, or resistivity obtained from 12 composite fibers. Standard deviations of experimental values are strength, 15 %; modulus, 15 %; and resistivity, 20 %. (Source [100] used with permission)

these composites is their susceptibility to oxidation, but surface modification or coating of the fibers or addition of appropriate ceramic refractory fillers that shield against oxygen attack at high temperatures alleviates this problem. The advent of several novel forms of nanocarbons has led to attempts to create nanocomposites with nanocarbon (e.g., nanotubes) components. In a recent experiment, single-walled carbon nanotubes (5% by weight) were uniformly dispersed in an isotropic petroleum pitch matrix to make nanotube-based carbon nanocomposite fibers (Figure 1.14), with better electrical and mechanical properties than isotropic pitch-based carbon fibers [100]. The tensile strength increased nearly 100%, and the electrical conductivity increased fourfold. The advent of the new carbon nanostructures suggests that novel carbon–carbon composites can be prepared with properties far superior to those of conventional carbon–carbon-fiber-based composites. The challenges lie in achieving proper dispersion of these nanostructures and tailoring the interfacial strength between the nanocarbons and the matrix.

1.7 Carbon Nanotube-Based Nanocomposites

The mechanical behavior of carbon nanotubes is exciting, since nanotubes are seen as the ultimate carbon fiber ever made [101]. The most important application of nanotubes, based on their mechanical properties, will be as reinforcements in composite materials. Chapter 2 includes a detailed discussion of nanotube-based polymer composites; here, we briefly discuss some developments regarding ceramic/metal-matrix-based nanotube composites. The nanotube reinforcements promise to increase the fracture toughness of the composites by absorbing energy through their highly flexible elastic behavior during deformation, which will be especially important for nanotube-based ceramic matrix composites. Possible applications are in lightweight armor or conductive durable ceramic coatings. An increase in fracture toughness on the order of 10% has been seen in nanotube/nanocrystalline SiC ceramic composite fabricated by a hot-pressing method at 2273 K (25 MPa in Ar for 1 h) [102].

Nanoscale ceramic powders with carbon nanotubes provide another opportunity for creating dense ceramic-matrix composites with enhanced mechanical properties. The strength and fracture toughness of hot-pressed α-alumina is typically much greater than that of conventional grain-size polycrystalline alumina. Addition of carbon nanotubes to the alumina results in lightweight composites with even greater strength and fracture toughness (Figure 1.15). The mechanical properties of such composites depend strongly on the processing method and surface treatment of the carbon nanotubes. Sintered alumina has high strength, hardness, and fracture toughness. An exciting possibility, as well as a processing challenge, is incorporating carbon nanotubes into an alumina-matrix composite to improve these properties. Alumina (γ-phase) matrix composites with 5–20 vol. % MWNT (multiwalled nanotubes) have been fabricated [103]. The γ-phase alumina powder was transformed to α-alumina (with mean particles sizes close to 60 nm) during sintering at 1300 °C. The MWNT were lightly oxidized at 640 °C in air, which removed the disordered carbonaceous material and

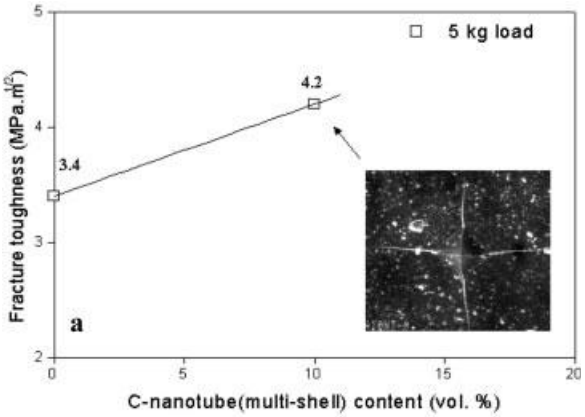

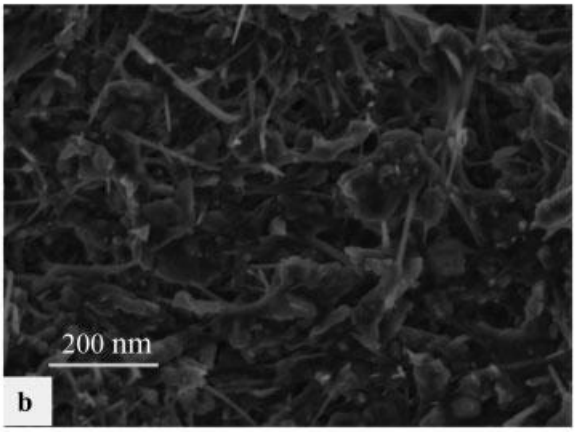

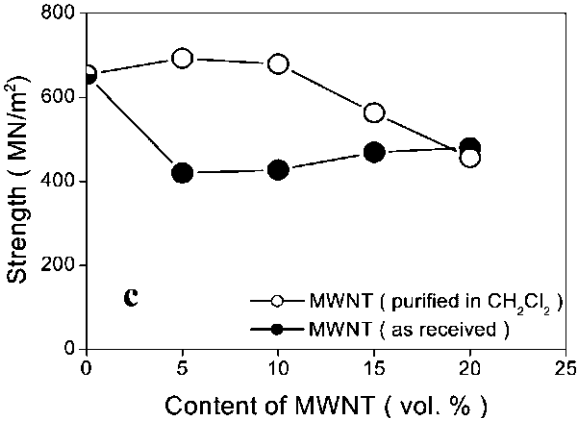

Fig. 1.15 (a) Fracture toughness of multiwalled nanotube (MWNT)/alumina nanocomposite compared with that of sintered nanophase alumina. The inset in (a) shows an indent and resulting cracks. The microstructure of the nanocomposite is shown in (b). (c) Diametral strengths of alumina-matrix nanotube composites hot-pressed in Ar at 1300 °C and 60 MPa for 1 h and containing various amounts of MWNT. (Source [103])

made it easier to disperse the nanotubes. The alumina- MWNT mixtures were dispersed in organic solvents via ultrasound, dried, and then sintered by hot pressing in a graphite die at 1300 °C and a pressure of 60 Mpa. The structures of the MWNT remained the same before and after processing, without any visible degradation. The density of the sintered composites was $> 97\%$ of the theoretical density.

The diametral strengths of alumina-MWNT composites with different MWNT contents indicate great improvements in fracture toughness with addition of nanotubes. The bulk alumina made from nanoparticles had a strength of 654 MPa, compared to typical strengths of 200 – 350 MPa for sintered bulk alumina, and was even comparable to strengths reported for single-crystal alumina (sapphire) of 350 – 1000 MPa. With the addition of purified, well-dispersed nanotubes, the strength first increased at 5 and 10 vol. % MWNT and then decreased for higher vol. percents of MWNT. The fracture toughness of bulk alumina and alumina/MWNT composites shows that, for 5 vol. % MWNT composites, the toughness increased by about 25% to about 5.1 MPa $\sqrt{m}$. The toughness values were higher than those reported for single-crystal alumina (sapphire) and polycrystalline alumina. The hardness of the composite depends on how well the nanotubes are dispersed in the matrix and how the nanotube surface is modified (with functional groups via oxidation) to produce anchors to the matrix; for the best value, the Vickers hardness is 20.4 GPa compared to 18.4 GPa for bulk alumina. From the general trends in the results of a few scattered reports in the literature, the strength and fracture toughness of bulk structures hot-pressed from nanophase ceramic powders is much higher than the typical strength and toughness of conventional polycrystalline ceramics. The addition of small amounts of nanotubes to nanophase ceramics to form dense nanocomposite improves the diametral strength and fracture toughness. However, the real improvements occur when the nanotubes are purified and well dispersed in the matrix, so that large aggregates do not create macrodefects in the structures, leading to easy fracture and lower strength. Vacuum hot pressing also removes entrapped gases in the composite powder mixture, preventing formation of residual stresses and reduction of strength. These processing improvements show the great promise of nanophase alumina/MWNT composites for light-weight, high-strength, high-toughness materials and in applications such as impact-resistant body armor.

It is widely perceived that carbon nanotubes will allow the construction of composites with extraordinary properties. Metal-matrix composites, as discussed before, are a new range of advanced materials and normally, the liquid-phase fabrication method is an efficient process because of its simple processing. If carbon nanotubes can remain stable within some suitable high-strength metal matrix, outstanding nanocomposites may be obtained. The rapid solidification technique allows the extension of alloying levels and more refined microstructures, which can lead to enhanced mechanical and physical properties. In addition, rapid solidification processing may help carbon nanotubes to survive the process because of the controllable melting step, which is the most important issue to be solved in fabricating nanotube-reinforced composites. Rapid solidification processing has achieved the successful synthesis of nanotube/$Fe_{80}P_{20}$ metallic glass nanocomposites [104]. Their properties show that the addition of nanotubes greatly enhances the thermal stability of the glass matrix and increases

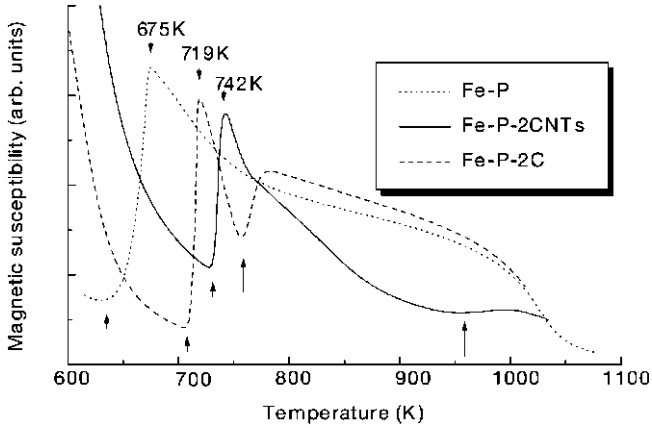

Fig. 1.16 Magnetic susceptibility vs. temperature for various amorphous alloys in nonisothermal heat treatments. The temperatures at the end of the first transition are indicated. The first peak in the plots corresponds to the first crystallization process. The onset temperature of crystallization for amorphous Fe/P/2% CNTs is about 100 K higher than that for amorphous Fe/P alloy at the same heating rate. (Source [105] used with permission)

the low-temperature electrical resistivity by 70% (Figure 1.16; Table 1.2). The activation energy of crystallization for the nanotube composite is higher than those of both the $Fe_{80}P_{20}$ metallic glass and the metallic glass containing 2% carbon. The onset temperature of crystallization for the nanotube composite is almost 100 K higher than for the original glass, according to magnetothermal analysis (MTA).

Tab. 1.2 The onset temperatures at a heating rate of 5 K min^{-1} and activation energy of crystallization for various amorphous metallic glass nanocomposite materials containing carbon (C) and Carbon Nanotubes (CNTs) [105].

Materials	Activation energy (kJ mol^{-1})	Onset T (MTA, K)
Fe/P	354.0 ± 0	630
Fe/P/2C	460.9 ± 29.8	709
Fe/P/2CNTs	574.1 ± 35.4	729

1.8
Functional Low-Dimensional Nanocomposites

Recent years have seen a drive towards creating heterogeneous nanostructures, which could serve as multifunctional materials and essentially satisfy the definition of functional nanocomposites. These stand out from the bulk nanocomposites that are the main subject of this book, but will have important applications as nanoscale sensors, electronic and optical nanodevices, nanoprobes, nanoelectromechanical systems, unique reinforcements, and drug-delivery media. These are particularly interesting for layered material systems in which atomic layers of different material compositions (e.g., graphite, dichalcogenides, clays, etc.) can be assembled into different geometries on the nanoscale. Some excellent examples, which are described below, are endohedral fullerenes (metal/carbon systems), filled carbon nanotubes, boron/carbon/nitrogen nanostructures, and nanosize coaxial cables from a wide range of layered materials.

What are the various synthetic strategies for creating such composite nanoscale structures? One simple, elegant idea is to use infiltration of nanoporous structures, commonly used in bulk composites for creating heterogeneous materials. At the nanoscale, this problem is not trivial, especially if the process occurs through the infiltration of a liquid or molten phase in which the viscosity of the infiltrating phase is high. A very useful example of such a nanocomposite structure is nanotubes and nanowires built into porous alumina templates. The alumina template can be prepared by anodization of Al metal in acidic solvents, and it is possible to create templates with straight, random pores that have diameters of 20–50 nm and are several micrometers long, running through the thickness of the alumina template [106]. Once the templates with pores are prepared, they can be filled (via electrochemical deposition) with nanowires (such as Au, Co, etc.; Figure 1.17) by changing the electrochemical conditions and introducing metal-containing solvents into the electrolyte [107]. The structure of the metal wires can be tailored (amorphous or crystalline) by changing the electrochemical deposition conditions. The distinct difference between nanowires created by other techniques and by template-based synthesis is that the latter technique offers the possibility of creating well-separated individual nanowires with adjustable diameters. Structures such as carbon nanotubes can also be deposited in the pores defined by such templates, by infiltration of gaseous hydrocarbon precursors (e.g., acetylene, benzene) and subsequent annealing [108]. Electrochemical techniques for materials processing (from highly anisotropic wires inside porous templates to particle-dispersed thin-film nanocomposites) provide a powerful alternative technique to vapor phase deposition and solid state reaction for the synthesis of nanomaterials and nanocomposites [109]. Their main advantage is control of the process so as to modulate dimensions and compositions. Their disadvantages are mainly poor crystallinity (being a low-temperature deposition process) and contamination with impurities from the electrochemical baths.

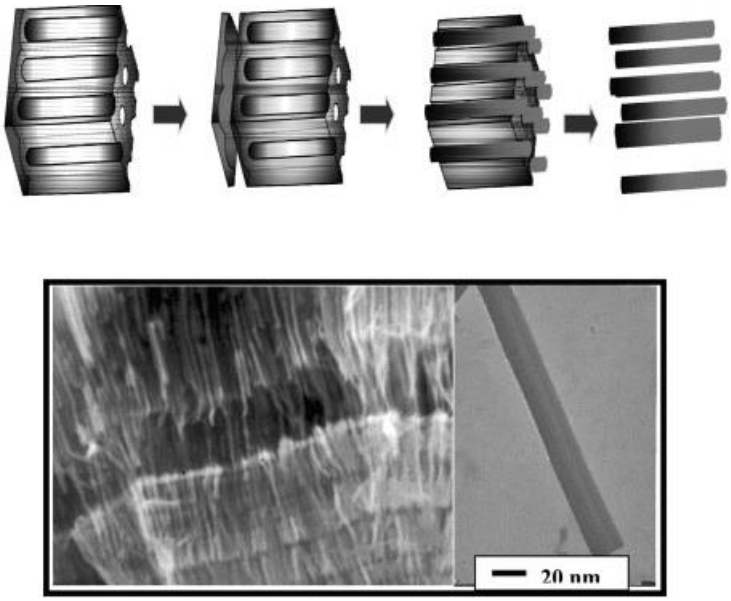

Fig. 1.17 Nanowires grown in alumina templates. Top schematic shows how pores in a straight-pore anodic alumina template are filled with metal by electrodeposition. Scanning electron micrograph of Co nanowire-filled template is shown in lower image; an individual nanowire removed from the template is shown (right). (Courtesy Prof. Mamoun Muhammed, The Royal Institute of Technology Stockholm, Sweden)

1.8.1 Encapsulated Composite Nanosystems

Here, we describe the creation and characterization of composite carbon/metal-based nanostructures (systems consisting of combinations of a layered material and a solid phase, which have been studied by several groups in recent years). These are unique nanocomposite systems with promise for many interesting applications.

Graphite-encapsulated metal/ceramic structures are interesting systems, and the generation of metal/carbon nanosystems requires knowledge of the interactions of metal atoms and the graphite lattice. The experimental study of the behavior of individual metal atoms in a graphitic environment is difficult and has been successful in only a few cases. In 1993, Ruoff et al. [110] performed carbon-arc discharge experiments using C anodes filled with metals and metal carbides and obtained carbon nanotubes and polyhedral carbon nanoparticles that contained both encapsulated metals and metal carbides. Polyhedral graphitic particles generally contain a hollow core, which is given shape by the outer faceting of the particle, and metal nanoparticles can easily fill these cores during formation (Figure 1.18). Metal surfaces are expected to act as nucleation sites for graphitic carbon to surround. The expected tendency of preexisting graphitic filaments is to wrap around metallic nanocrystallites and close by

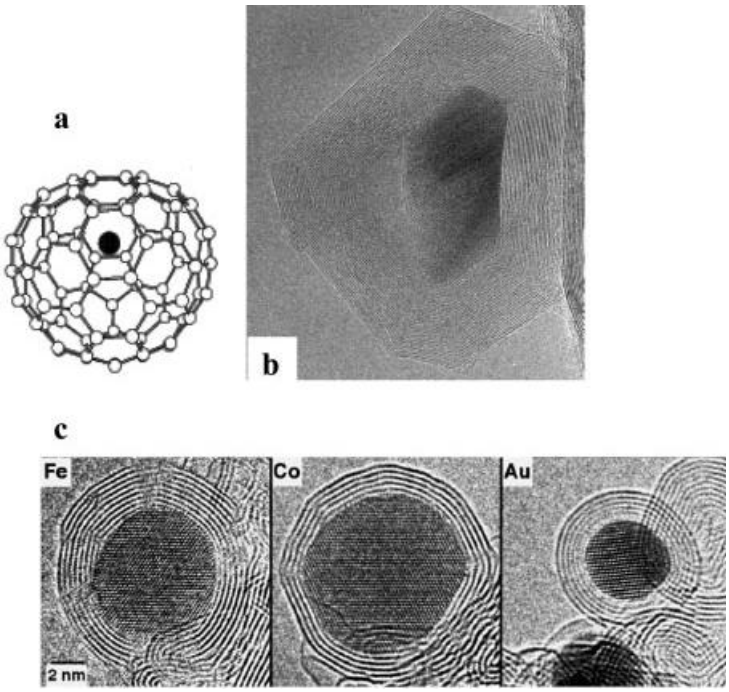

Fig. 1.18 (a) Schematic of an endohedral fullerene. Structural model of a La atom in C_{82} fullerene (b) Encapsulated nanoparticle of lanthanum carbide inside a carbon polyhedral particle (approximately 50 nm in diameter) produced in an arc discharge with a composite carbon/La electrode. (c) Encapsulated nanoparticles of metals (Fe, Co, Au) in spherical graphitic layers (carbon onions). These structures were produced by electron irradiation of carbon soot containing the metal species

saturating all carbon dangling bonds. The properties of encapsulated metal crystals have been the subject of many experimental studies [111]. Graphite-coated ferromagnetic metal crystals should show a reduced magnetic coupling that depends on the thickness of the graphite shell [112], with potential applications in magnetic recording media. Guerret-Piecourt et al. [113] sought general principles relating to the nature and structure of the filling materials, for efficient filling of nanotubes made via the electric-arc method (Figure 1.19). Several metals and/or their compounds have been encapsulated in carbon cages and studied; e.g., Ti, Cr, Fe, Co, Ni, Cu, Zn, Mo, Pd, Sn, Ta, W, Gd, Dy, and Yb. In later experiments, the authors also managed to fill hollow carbon nanostructures with semiconducting structures such as Se, S, Sb, and Ge by similar processes [114]. S, present as impurity in the carbon, was later reported to play a major role in the effective formation of the filled carbon nanotube/nanoparticle structures. The above technique has made it possible to encapsulate a large number of carbides nanocystallites [115, 116] (LaC_2, YC_2, CeC_2, Gd_2C_3, TiC, V_4C_3, ZrC, TaC, MoC, NbC, HfC). With pure metals such as Fe, Ni, or Co, which strongly interact with carbon, encapsulating nanowires inside nanotubes is challenging. However, experiments have

shown that onion-like nanoparticles of metal-containing carbon clusters can be produced relatively easily with the arc method. Here, the metal or metal carbide encapsulate is protected by the C layer coating, which effectively insulates the magnetic metal particles from oxidization upon exposure to the environment and retains its magnetic properties. It is noteworthy that high melting point refractory metal carbides such as TaC, NbC, and MoC, which exhibit superconducting transitions at low temperatures, have been inserted into nanotubes and graphitic nanoparticles [117]. Bulk magnetic susceptibility measurements of encapsulated TaC, MoC, and NbC revealed diamagnetic responses and superconducting transitions between 10 K and 14 K, respectively. The structure and state of these encapsulated nanostructures affects their physical properties; for example, a shrinkage in the lattice parameters for the (fcc) MoC encapsulated structure appears to decrease the Tc by 3.8 K.

Magnetic alloy (e.g., FeCo) nanoparticles encapsulated in carbon layers can also be made in radio frequency (RF) torch reactors, and acetylene was used to generate a large number of carbon-coated particles [118]. The carbon lamination provides several functions for these nanoparticles that have low magnetocrystalline anisotropy and large saturation magnetization (making them valuable as soft magnetic materials). These functions include oxidation protection, prevention of coarsening and particle coalescence during growth, shielding interparticle magnetic interactions, and even reducing eddy current losses in high frequency environments. This technique can readily produce particle sizes anywhere from 5 to 50 nm. Other techniques, such as the tungsten arc, blown arc, or electric arc generation, can be used to create encapsulated nanostructures of similar dimensions.

The first experiments on filling of nanotubes date to 1993, where the filling was done via capillary forces, which pushed molten metals and compounds into the cavities of nanotubes during oxidative opening of their tips (Figure 1.20) [119]. Since then, the most efficient filling of hollow nanostructures to create heterogeneous nanomaterial systems has been achieved by chemical treatment. Tsang et al. [120] filled larger

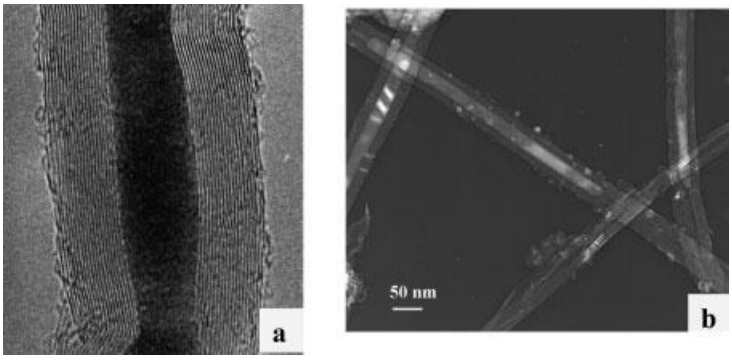

Fig. 1.19 (a) High-resolution transmission electron micrograph of a Mn metal-filled carbon nanotube made by electric arc discharge with electrodes of carbon filled with Mn (b) Encapsulated nanotubes with Fe carbides, formed during a chemical vapor deposition process involving hydrocarbon and metalorganic precursors

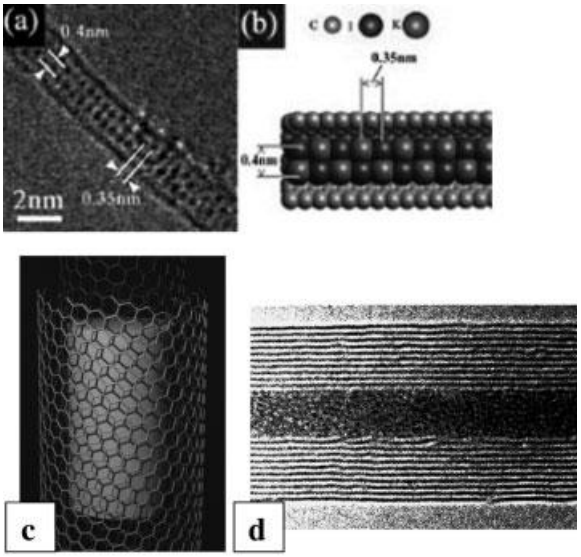

Fig. 1.20 Top: (a) High-resolution transmission electron micrograph of a KI crystal in a 1.4-nm diameter SWNT, (b) its structural representation. Encapsulation of halides and other materials within SWNTs enables the study of 1D crystal structures formed on the smallest scale possible. Bottom: (c, d) Schematic of a filled MWNT and a corresponding transmission electron micrograph of Pb oxide nanowire-filled nanotube, formed by capillary filling of the molten material inside nanotube cavities. In (d) the horizontal lines indicate graphite planes which have a separation of 0.34 nm. (Source, top image and schematic [233] used with permission)

multi-walled carbon nanotubes oxidatively by opening the ends in nitric acid and then filling with solutions containing metal oxides (e.g., oxides of Ni, Co, Fe, U, Mo, Sn, Nd, Sm, Eu, La, Ce, Pr, Y, Zr, Cd) using capillary force. They were then dried to form encapsulated solid materials inside the nanotube cavities. Several other material systems such as Pd, Ag, Au, AuCl, proteins, and enzymes have been introduced into nanotubes with this method. Recently it was reported that single-walled nanotubes (SWNTs) can be opened selectively and filled by wet-chemistry techniques [121]. Treatment with concentrated HCl leads to the selective opening of SWNTs at their tips, and foreign materials may be drawn in, in a similar fashion as MWNTs; the much smaller ($\sim$1 nm) cavities in SWNT make the filling more challenging. Usually, the nanowires formed inside the nanotubes are single crystals. Alternative strategies to fill nanotube cavities with materials have been explored. For example, exposing SWNT nanotubes filled with AgCl/AgBr to light or an electron beam can reduce the encapsulated compounds, resulting in extremely small Ag nanowires [122]. Similarly, constrained chemical reactions within narrow channels can be used to create and characterize nanowire structures of many materials. These promise to be ideal structures for studying 1D properties (electrical, thermal, optical) in materials for applications such as quantum wires and magnetic storage arrays. Characterization of these structures is often challenging, but recent progress in highly spatially resolved microscopy and spectroscopy techniques have enabled researchers to carefully study the structure–property relationships in confined nanocomposite wires. SWNTs containing fullerenes in their inner hollow are another unique form of nanocomposite structure with interesting electronic properties. C_{60} insertion into SWNT could occur during their formation in the arc or laser process. Very recently, researchers have managed to introduce C_{60} inside SWNTs in high yield (Figure 1.21) by thermally annealing C_{60} powders

over SWNTs above 600 °C under vacuum [123]. This class of hybrid materials may form the basis of functional devices for applications in electronics, biomedicine, and microelectromechanical systems. Similarly, endohedral fullerenes [124] (or fullerenes containing single or multiple metal atoms, which in their own right can be considered novel nanocomposite systems; e.g., $La_2@C_{80}$, $Gd@C_{82}$, etc.) have been introduced into SWNTs through the vapor phase. These structures are breaking new ground because creation of nanocomposite structures with discrete atomic species in their cores are resulting in the discovery of novel properties of 1D nanoscale materials.

Recent theoretical studies suggest that the presence of a metal nanowire inside a nanotube greatly alters the mechanical properties of the nanotube, for example, suppressing tube-buckling instability. Increasing tube diameter increases the bending strength; however, in contrast to hollow tubes, there is no decrease in the maximum deflection before buckling. Analysis of the principal bending vibrational mode shows a lowering of the frequency, associated with increased tube inertia. Remarkably, metal-filled tubes exhibit strong damping, whereas unfilled single-walled and multi-walled tubes show no damping of oscillations (Figure 1.22). Simulations of multi-walled nanotubes revealed the lack of damping behavior; the dissipation of the mechanical energy is intrinsically associated with tube filling by a dissimilar material [125]. These studies demonstrated the benefits of filling tubes with solids for modifying the bending strength and flexibility, suggesting implications for nanotube-based elements in micromechanical devices or nanoprobes. Experimental studies on these unique 1D nanocomposite systems are eagerly awaited, since a variety of them have already been fabricated.

Condensed-phase electrolytic processing provides an alternative way to fabricate nanotubes with or without encapsulated metals. The technique involves passage of an electric current through graphite electrodes immersed in molten mixtures of ionic salts (e.g., LiCl, $SnCl_2$) under inert gas atmospheres [126]. The graphite crucible anode

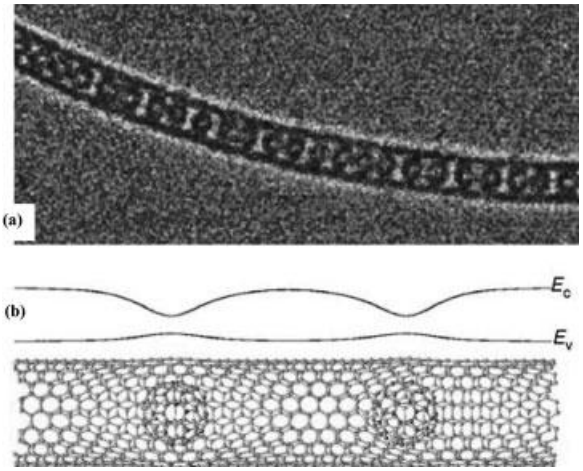

Fig. 1.21 (a) Transmission electron micrograph of a $La_2@C_{80}@SWNT$ assembly. Each C_{80} molecule appears as a dark circle, and the SWNT (1.4 nm diameter) itself appears as two parallel lines. (b) Effect of inserted Gd metallofullerenes (GdMFs) on the topography and band structure of a single-walled nanotube (SWNT). The illustration of a (11,9) GdMF-SWNT. Schematic representation of estimated modulation of conduction (Ec) and valence (Ev) band edges is also shown. (Source: top image [234], bottom part [235] used with permission)

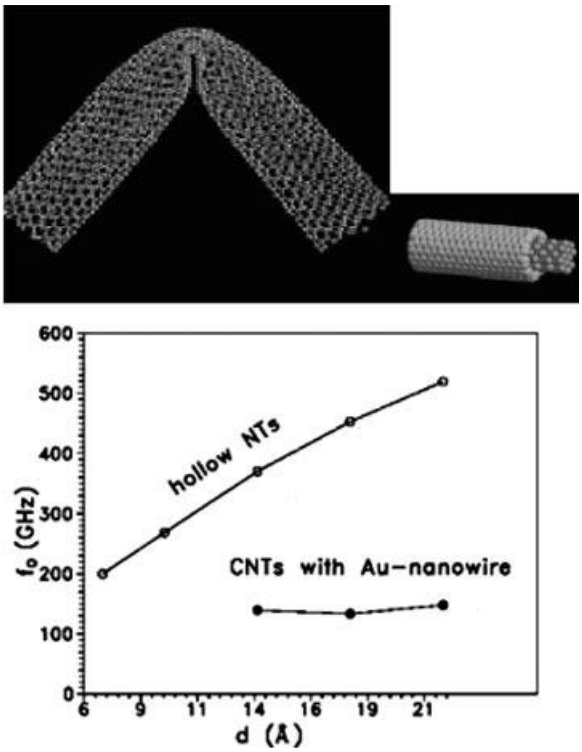

Fig. 1.22 Damping in pure vs. metal-filled nanotubes, simulation results. Top: bending of filled nanotubes; filling makes the nanotubes stiffer to bending and buckling. Oscillatory frequency (f_o) of vibration, as a function of tube diameter for filled and hollow tubes as function of tube diameter. The filled nanotube composite structures show high damping during vibrations. (Source [125])

contains the electrolyte salt, which is heated by an external furnace. When the salt mixture melts, the cathode (graphite rod) is immersed in the electrolyte. During electrolysis, the graphite electrode interacts with the molten electrolyte, forming nanostructures. If pure LiCl is used as the electrolyte, the carbonaceous material formed consists of tangled carbon nanotubes, some of which contain the carbide of the salt (i.e., LiC). Adding small amounts of low-melting metals such as Sn, Pb, and Bi to the electrolyte forms nanowires of the respective metals. The formation of carbide nanowires is based on the reduction of metal ions on the graphite cathode surface and intercalation of the Li between the graphite layers, followed by the formation of Li_2C_2. Carbon then precipitates in the form of nanotubes. When Sn, Pb, and Bi are added to the electrolyte, the cations derived from these metals are discharged at the electrode surfaces by the electrons provided by oxidation of the carbide. This ultimately forms metallic nanowires surrounded by graphitic sheets in the nanotube form. This technique has also generated carbon-encapsulated Sn/Pb nanowires [127].

Pyrolysis of hydrocarbons over metal catalysts at elevated temperatures also produces filamentous structures containing metal and carbon [128]. If the catalyst concentrations are high (>10–20%), encapsulation of the metal catalysts can produce nanowire composites. Pyrolysis of organic compounds or other carbon sources such as C_{60} in the presence of transition metal species (e.g., metallorganics such

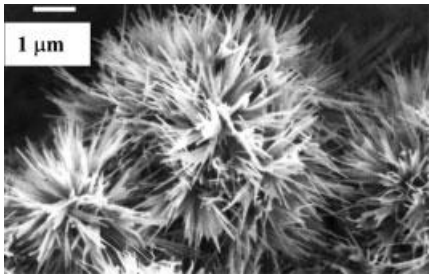

Fig. 1.23 Scanning electron micrograph showing the fibrous structure of carbon nanotube/V_2O_5 nanocomposite. The individual nanotubes (seen as tiny filaments) are finely coated with subnanometer layers of the oxide, uniformly on the surface, modifying the nanotube surface properties. The structure was made by mixing nanotubes and oxide powder and annealing.

as ferrocene) leads to nanotubes containing these metals or their alloys [129]. Metal nanowires over carbon structures can also be prepared via substitution. Recent work suggests that suspending SWNTs and exposing them to metal vapor can be used to fabricate nanowires of Pt, Au, Ti, etc. Hollow nanotubes of the metal are formed around nanotube templates [130]. Composite nanotube-based nanocomposites consisting of nanotubes and other materials can also be created by coating nanotube templates by capillary effects. Nanoscale skins of layered oxides such as V_2O_5 can be uniformly coated onto nanotube surfaces [131] (Figure 1.23). It is also possible to create composite nanowire systems by CVD techniques, in which individual layers of laminated materials such as MoS_2 and WS_2 are coated onto multi-walled carbon nanotubes [132]. The electronic properties of these coated tubes are dominated by their outermost shells (oxides or sulfides, which are generally semiconducting or insulating). However, the inner tube structure (carbon nanotubes) may dominate the mechanical properties. In this way, it will be possible to tailor both the mechanical and electronic properties of these 1D systems. Physical property characterization of these nanocomposite systems is challenging, but much excitement exists about uncovering a rich range of properties inherent to these nanoscale multiphase systems.

Multiple-phase nanowires, constituting different structures along the wire length, may also become important in future nanotechnology. The advantage here will be the ability to form controlled junctions, which could have semiconducting properties (metal–semiconductor junctions), novel deformation behavior (whereby toughness may be increased when they are used as reinforcements), photoluminescence (if

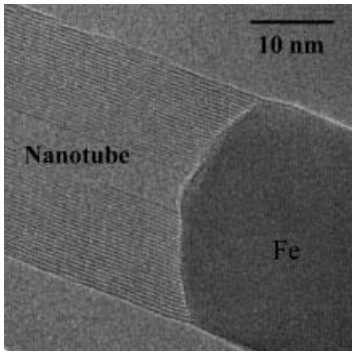

Fig. 1.24 High resolution transmission electron micrograph of a heterojunction formed between an Fe nanowire and a multiwalled carbon nanotube. The structure was formed in the vapor phase during pyrolysis of hydrocarbon and ferrocene. Similar structures can also be made by stepwise electrodeposition inside alumina nanoporous membranes.

phases are semiconducting with distinct n- or p- character), or thermoelectric-junction properties. Carbon nanotube–metal junctions have been made by using excess catalyst (Fe) in the chemical vapor deposition process or by electrochemical deposition in porous alumina templates (Figure 1.24) [133, 134], but the properties of these multiple-phase nanowires have not been evaluated. Controlled solid-state reactions have been used to form heteronanowires of single-walled carbon nanotubes and nanorods of silicon carbide and transition-metal carbides (TiC) [135]. The reactions are carried out via contact annealing with a metal (or Si) solid surface and nanostructures such as nanotubes. The structures created are some of the smallest heterojunctions that have ever been made and will play a large role in the fabrication of future hybrid nanodevices. Similarly, techniques such as laser ablation have been used to form coaxial cables containing heterocompositional layers. For example, high resolution transmission electron microscopy and spatially resolved electron energy loss spectroscopy have characterized wires that consist of β-silicon carbide sheathed inside amorphous silicon oxide surrounded by graphitic shells made of C or h-BN [136] (Figure 1.25). These coaxial nanocables of semiconductor-insulator-metal/semiconductor structures could find applications in nanoscale electronics. The formation of such multiple-layer nanocable structures is challenging and has to be controlled through the self-assembly of various elemental and molecular species in the vapor phase during relatively short growth times, and the directed assembly of such complex structures is one of the most crucial steps in the creation of useful low-dimensional functional nanocomposite structures.

Recent work has also demonstrated that semiconductor nanowires can be controllably grown in cross-bar array architectures, and, if the crossing nanowires can be doped into n- or p- type, then light emission can result at the crossing junctions when a voltage is applied across the wires. High-temperature laser-assisted deposition

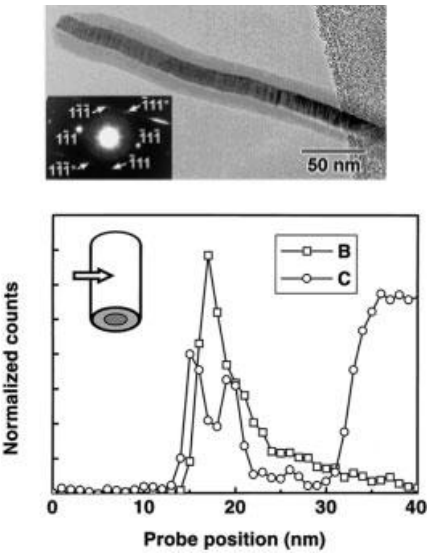

Fig. 1.25 Transmission electron micrograph of nanocable structure ($SiC/SiO_2/BN/C$) showing a crystalline core and an amorphous layer. Inset: the selected area diffraction pattern indicates that the crystalline core is β-phase SiC with the <110> axis parallel to the electron beam. Bottom: profiles of B and C across half a nanocable from EELS measurements, showing a phase separation of graphite and BN layers. (Source [136] used with permission)

has been used to grow single-crystal indium phosphide (InP) nanowires using catalytic gold particles [137], either in p-doped or n-doped form. Superlattice nanowires can also be made with alternating blocks of different semiconducting materials (e.g., Si and SiGe) on a single wire [138]. A hybrid pulsed-laser ablation/chemical vapor deposition method can be used to custom-create various heterostructures on individual nanowires. These structures systematically contain junctions and interfaces between the multiple blocks present in the same wire, enabling them to be useful in miniaturized transistors, LEDs, and lasers.

1.8.2 Applications of Nanocomposite Wires

Of several applications proposed for composite nanowire structures, only one is discussed here. Magnetic recording exploits the hysteresis behavior of ferromagnetic materials: the residual magnetization of a tape or magnetic disc is a record of the maximum field intensity the material experienced with respect to the magnitude and direction of the applied field. For long-term storage, usable magnetic materials should have a reasonably high coercivity, because external magnetic fields should not alter the magnetization. However, the coercive force should not be too large if the medium is to be reusable, since the magnetic fields used during recording should be capable of remagnetizing the material for new data recording. Recently, feature sizes on magnetic disks made using complicated e-beam lithography protocols have shrunk to the sub-100 nm range [139]. Ferromagnetic Fe nanowires could provide an ideal system for recording, but the tendency to oxidize is strong in nanoscale metallic systems. The encapsulation of Fe nanowires within carbon nanotubes will assure that the metal is maintained in the reduced state, due to the protective C coating. These encapsulated nanowires exhibit magnetic coercivities larger than those associated with pure Ni and Co nanowires [140]. The coercive field decreases linearly with increasing temperature, revealing the presence of anisotropy. The small size, anisotropy, and the single (isolated) domain nature of the encapsulated Fe crystals appear to be responsible for this enhanced coercivity. The magnetic properties of encapsulated Fe nanowires do not degrade with time, because they are sealed within the graphitic tubes. These nanowire arrays may have significant potential in magnetic data storage device applications (e.g., quantized magnetic disks) due to their size and anisotropic behavior, with the possibility of drastically increasing the attainable recording density. Film structures of this kind, based on single-domain elements, exhibit the best available storage densities (e.g., 65 Gb in^{-2}) [141]. The type of magnetic nanocomposite particles should also find applications in the fabrication of fine-particle magnets for use in magnetic inks and as toners in xerography.

1.8.3 Applications of Nanocomposite Particles

Several strategies are being pursued for creating nanoparticles containing multiple shell structures (for multifunctionality), with each shell composed of different materials. Template-based approaches are effective in this situation, for which an inner removable template particle (silica, polymer beads) can be used to coat shells of other materials (e.g., a metal) via multi-step colloidal or vapor-phase assembly and can later be easily removed to create empty shells. These could even be filled with different materials to produce multiple-shell composites [142]. Creating uniform coatings on particle templates by colloidal self-assembly is based on the concept of self-assembled organic molecular species. The two ends of the molecules to be joined have specific functional groups (e.g.. thiols, amines, carboxylic groups) that can be targeted for specific interactions with the template and the clusters that are used to make the coatings. Uniform, dense packing of the molecules around the templates leads to close packing

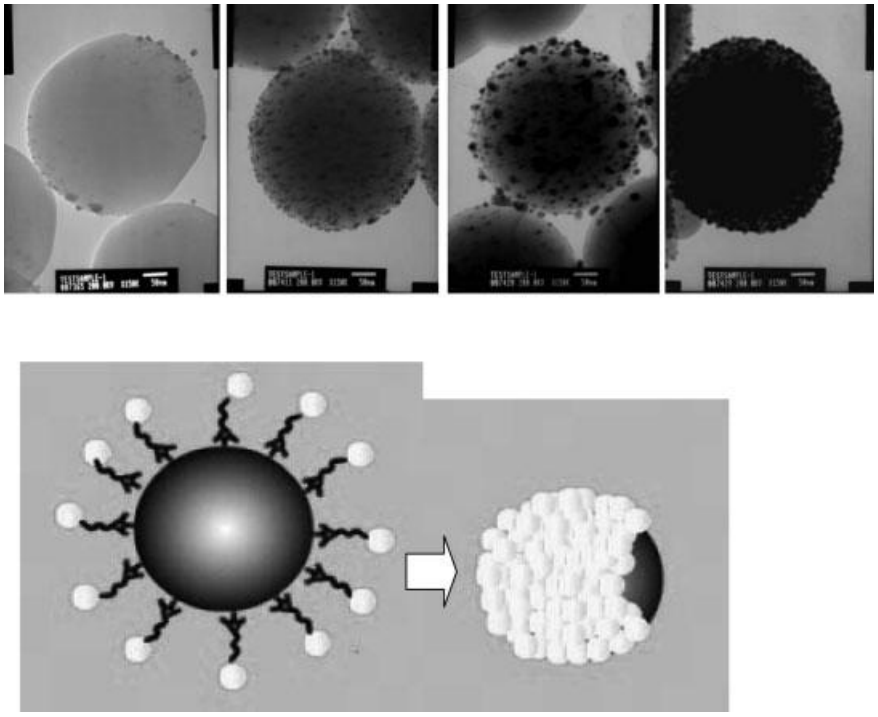

Fig. 1.26 Fabrication of multilayer nanoparticle structures by colloidal synthesis. Top: micrograph of silica spheres being continually coated with gold nanoparticles until a uniform coating is produced. The process of attachment of gold particles (shown in the schematic below) occurs via connectors of self-assembled monolayers of bifunctional organic molecules (e.g., mercaptopropyltrimethoxysilane). Multiple-layer structures can be fabricated by colloidal assembly techniques. (Courtesy Prof. Mamoun Muhammed)

of the clusters that form a porous but space-filled shell around the template (Figure 1.26). Noninteracting metal-coated magnetic particles (SiO_2/Au, Fe_3O_4/Au, NiO/Co, etc.) or coated semiconducting particles (PbS/CdS) are examples of such composite particle structures. These structures can have applications in magnetic recording, as multilayered catalyst materials, or in drug delivery. In such applications of drug delivery systems [143], for which a biocompatible outer layer and a drug-containing inner core are necessary, the multilayered particle approach will be crucial. As an alternative to colloidal templating, structures such as PbS-coated CdS nanocomposite particles (a few nanometers in diameter) may be synthesized by ion displacement in inverse microemulsions and could be useful in nonlinear optical applications. The observed large refractive nonlinearity in these nanocomposite particles may be attributed to the optical Stark effect and to strong interfacial and internanoparticle interactions.

1.9 Inorganic Nanocomposites for Optical Applications

Nonlinear optical effects, such as nonlinear optical absorption and second- and third-order optical nonlinearities, can be used to make optical limiters, optical modulators, etc. Although many organic materials have high optical absorption and nonlinearity, their thermal and optical stabilities are poor. Often, it helps to create hybrids or composites (organic/inorganic, inorganic/inorganic) that have acceptable optical properties and stability. Quantum-confined nanoparticles have been extensively used in the fabrication of such composites because of their novel optical and electronic properties. The organic-matrix nanocomposites for optical applications are described in chapter 2, which briefly discusses some of the organic materials that contain dispersed nanoparticles in various hosts.

Recent advances in controlling the fabrication and dispersion of semiconductor nanoparticles in polymer and ceramic matrices have suggested possible uses for such nanocomposites in optical applications. A good example of an optically functional ceramic nanocomposite is GaAs nanocrystals embedded in SiO_2 matrix. The interest in the novel optical properties of semiconductor nanocrystals [144] has resulted in strategies to package them as nanocomposites. A variety of techniques, such as colloidal synthesis, self-assembly, and electrochemistry, can be used to produce the semiconductor nanoparticles; however, ion coimplantation (Ga+, As+) is an efficient way of creating well-dispersed nanocomposite materials (e.g., GaAs/SiO_2) [145]. Typically, the ions are implanted at fluxes of $\sim 10^{16}$ cm^{-2} into 100 nm silica films on Si substrates and annealed at appropriate temperatures to create nanocrystals of GaAs (several nanometers in size) in the matrix (Figure 1.27). Photoluminescence studies show an efficient, broad luminescence band in the visible and near-infrared spectral regions due to quantum confinement in GaAs nanocrystals and defect states in SiO_2.

Nanoparticles in matrices have interesting photoluminescence properties, due to the effects of quantum confinement on their optical properties. Indirect band semiconductors such as Si and Ge have very poor luminescence efficiency (hence, efficient

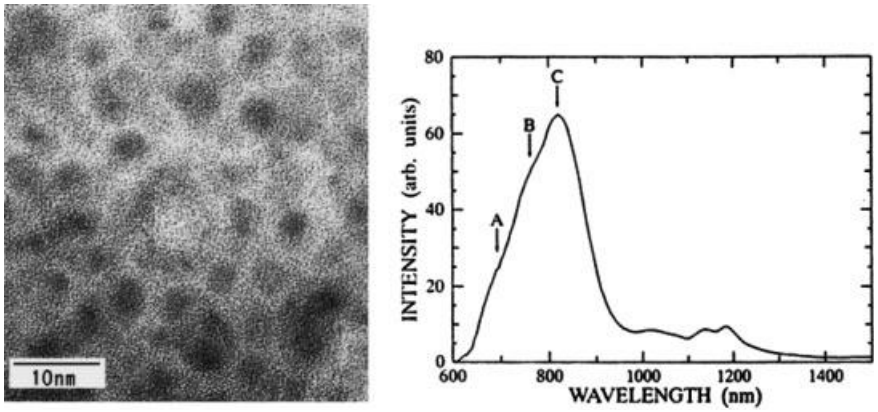

Fig. 1.27 Transmission electron micrograph, left, GaAs nanocrystals embedded inside SiO_2 glass matrix. Sequential ion implantation followed by thermal annealing was used to form GaAs nanocrystals in SiO_2 films. Right, efficient, broad photoluminescence band observed in the red and near infrared spectral regions. The efficient luminescence is attributed to both quantum confinement states in GaAs nanocrystals and defects in SiO_2. (Source [145] used with permission)

light emitters cannot be fabricated directly from them), because the band center transition is optically forbidden. But, by making the particle sizes smaller than the exciton Bohr radius (4.9 nm for Si, 24.3 nm for Ge), the resulting confinement produces an increase in oscillator strength, shifting the luminescence to higher energies; this allows tailoring novel optical materials, which are otherwise impossible. To take full advantage of the particle size effect, the particles must be separated, and the best possible way of accomplishing this is to disperse the particles in a matrix. Understanding and minimizing the interaction of the host matrix and the particles that create interface states are crucial to many of the optical applications. Embedding nanoparticles in different matrices and studying the optical properties provides a way to decipher interface effects. Ge quantum dots have been studied in various hosts, and one way to minimize host interaction is to embed them in oxygen-free environments, such as AlN; AlN/Ge multilayer structures deposited by pulsed-laser deposition show a blue-shifted photoluminescence peak [146]. Similarly, indium oxide (InO) nanoparticles dispersed (by solvent-phase impregnation) within the pores of mesoporous silica (prepared by sol–gel technique) show multiple photoluminescence peaks related to the size and structure of the particles [147]. Amorphous InO particles ($<$6 nm) show a photoluminescence peak that is down-shifted compared to slightly larger crystalline particles. For larger aggregates of InO particles, no photoluminescence is observed. Si nanoparticles themselves are interesting from the point of view of photoluminescence, and porous Si, which contains small particle domains, has been studied in great detail. The problem with porous Si is the structural nonuniformity, lack of reproducibility in emission and aging, and environmental degradation problems. Incorporating light-emitting Si structures in a matrix that is chemically inert and has a wide band gap suitable for quantum confinement can overcome this problem. Nanocomposites of Si nanoparticles ($\sim$5 nm) embedded in polycrystalline diamond matrix have been prepared

and studied. The room temperature photoluminescence behavior of such materials in the 1.6–2.5 eV range shows a strong increase in emission efficiency from the Si nanostructures. The studies conducted on this nanocomposite reveal that selecting the size of the embedded Si particles makes it possible to tune the luminescence frequency in the yellow–green spectral region.

Nanocomposites of nanosized metal particles in transparent dielectrics can also be applied as nonlinear optical materials in photonic devices. These materials are characterized by large third-order optical nonlinearity (χ^3) and fast response times, which are important for device applications such as optical computing, real time holography, and phase conjugators. To incorporate metal nanoparticles into dielectrics, several techniques such as ion implantation, sol–gel techniques, and sputtering can be employed. It is even possible to prepare graded layers of metal nanoparticle distributions (with different particle sizes and interparticle separations) by implantation, and these structures can be carefully tailored to produce interacting and noninteracting nanoparticle layers that produce different optical response in the plasma resonance frequencies. Several of these composite systems have been studied, for example, Au/SiO_2, Ag/SiO_2, Au/Al_2O_3, Au/TiO_2 with metal concentrations varying from 15%–60%, for nonlinearity and plasma resonance frequency shifts. High values of susceptibilities ($\chi^3 \sim 6 \times 10^{-7}$ esu, compared to low values of $\sim 10^{-12}$–10^{-11} esu for glass) have been reported for composites containing an optimized fraction of the metal component [148, 149]. Groups II–VI semiconducting nanocrystals (e.g., CdS) prepared in glass hosts have been studied in great detail, because of their large optical nonlinear response and small carrier lifetimes. Enhancement of carrier recombination rates is observed in nanocrystals with large surface-to-volume ratios, and the enhancement results from increases in the density of surface states and fast surface recombination and capture due to multiphoton emission. Surface recombination in nanocrystals embedded in glass matrices exhibits thermally activated nonradiative recombination, which is enhanced at reduced particle size. The semiconductor/glass interfaces in the composites may give rise to deep traps responsible for photoactive phenomena.

In recent years, nanoparticles have been used to make transparent nanocomposite structures having high refractive indices. Polymers containing inorganic particles in a range of 1–100 nm (nanocomposites) are interesting in this regard. In contrast to composites having particles in the micron size range, nanocomposites do not scatter light and are interesting for optical applications. Preparation of nanocomposites with refractive indices over the entire range of <1 to >3, which is by far the lowest and highest ever achieved for a polymer composite, has been possible. Transparent polymeric materials can be coated with surface layers ($\sim$100 nm thick) of UV-absorbing nanocomposites to inhibit degradation of the polymer by UV light [150]. High-refractive-index transparent materials are mainly used for improving the optical coupling efficiencies in photonic devices. The refractive indices of polymers vary between 1.3 and 1.7, those for inorganic semiconductors vary between 2 and 5, and for high bandgap semiconductors this value is <3. The technological challenge in creating near-transparent high-refractive-index organic/inorganic nanocomposites lies in the creation of nanoparticles in the size range 20–40 nm, to produce high-refractive-index nanoparticles with low absorption coefficients in the visible range. Exam-

ples of such composites are PbS, InP, GaP, Ge, and Si particles in a gelatin matrix. The particle sizes, as well as the loading fraction of the particles, affect the refractive index and absorption coefficient. Very small particles show reduced refractive index. But typically there is a critical size above which the value of refractive index reaches the bulk value (for PbS this is ~25 nm). Hence, to obtain predictable values of refractive index, it is important to have good dispersion of particles. The particles useful for creating these nanocomposites can be produced through a variety of techniques, ranging from mechanical attrition [151] (followed by centrifugation to obtain near-uniform Si particles) to colloidal processing. Nanocomposites can then be prepared by mixing and spin coating (or casting) aqueous solutions of gelatin with suspension of nanoparticles in appropriate organic solvents.

1.10
Inorganic Nanocomposites for Electrical Applications

The incorporation of particles of a nonpiezoelectric phase into a piezo material is unlikely to improve properties such as the strain per unit field or the charge per unit force, but the dielectric loss of the nanocomposite material under high alternating electric fields is an interesting issue. High-drive electrical applications are often restricted by reduced efficiency, due to heating caused by the large dielectric loss at high fields. A clear distinction has been shown between *weak* and *strong* field behavior in materials such as $BaTiO_3$. Above a critical field level, the dielectric constant and dielectric loss increase dramatically, due to hysteretic domain wall motion and the resultant reorientation by spontaneous polarization. It is possible that incorporating nanosized particles (SiC of small volume percentages, ~2.5 %) into an electroceramic matrix ($BaTiO_3$) may hinder domain wall motion sufficiently to reduce dielectric losses at high fields [152]. Accordingly, the microstructure requires the particles to be situated intragranularly. This concept is similar to that used in the development of hard ferromagnetic materials, for which heat treatment is used to produce a fine dispersion of particles within the microstructure, which increases the resistance to domain wall motion. In addition to the possible effect of the particles on piezoelectric properties, additional issues that require examination include the influence of any secondary phases produced by solid-state reactions between the matrix and nanoparticles; in a $BaTiO_3$/SiC system, heat treatment and hot pressing can form new phases such as $Ba_2TiSi_2O_8$. When such reaction phases are present in the composite, the permittivity of the system is lowered. Addition of silicon carbide leads to a change in the microstructure of the material and a decrease in grain size. This outcome has been reported in structural systems, which show corresponding improvements in mechanical properties. In addition, the fracture mode was transformed from transgranular for monolithic $BaTiO_3$ to intergranular for the nanocomposite. Many studies have been undertaken to fabricate piezoelectric particle-dispersed ceramic nanocomposites from other materials: Pb(Zr, Ti)O_3 nanocomposites have been prepared from high-purity PZT powder and small amounts of oxides (Al_2O_3, MgO, etc.) [153]. Small additions of a second phase improve the mechanical properties, such as hardness and

fracture toughness, of the PZT. The nanocomposite's reduced grain size during processing with the second phase is responsible for the improved mechanical properties. The piezoelectric properties of these composites remain essentially unchanged, although for the MgO composites, the electromechanical coupling factor (which is important for actuator applications) becomes larger.

Nanocomposites can also be useful for such applications as electrical contact materials, particularly to replace the toxic Ag/CdO contacts being used now. The reactive milling process has been used for manufacturing Ag/SnO_2 nanocomposites. A high-energy ball mill controls the reaction to obtain nanosized SnO_2 particles in an Ag matrix [154]. Then this powder is hot pressed into electrical contacts with superior erosion resistance and good thermal and electrical conductivity. Such cermet-like nanocomposites (in different configurations) have applications in other areas, like sensors. Many reports have appeared on gas-sensing technologies based on the measurement of changes in the electrical resistances of metal oxides (such as SnO_2, TiO_2) as the environment is changed. The sensitivity and selectivity of these metal oxide sensors can be affected by deposition of discontinuous metal films on their surface. Metals such as Pd, Pt, etc. have been used as surface activators. Similarly, incorporating metal clusters into bulk oxides to form nanocomposites also makes it possible to tailor the effective bulk electrical response of sensor materials. This incorporation allows the range of resistivity changes caused by changes in the carrier concentration at the surface or bulk of the metal oxide sensor material to be altered.

Although ceramic/metal composites are exciting mostly due to improved mechanical properties, the temperature-dependent electrical behavior of metal in ceramic nanocomposites is quite interesting [155]. As examples, Ag and Pb particles have been prepared in silica gels by electrochemical methods. DC electrical characterization of these materials shows surprising changes from semiconducting to metallic behavior as a function of temperature and depending on particle size. The electron conduction mechanism in these nanocomposites is complicated but, in general, occurs via two conduction mechanisms: electron tunneling between metal particles and metallic conduction due to the presence of metal percolated paths. The particle size and microstructure of the composite can be changed to adjust these properties [156]. The variable conductivity of these composites can be used in applications, such as electromagnetic induction shielding.

Percolation Effects and Transport Phenomena in Composite Systems

To understand nanocomposites in terms of conduction processes, we need a basic understanding of the bulk materials as well as of the composite filler. This is where certain issues arise. When dealing with organic or inorganic insulators and semiconductors, we may rely on a form of charge transport through the medium in terms of variable range-hopping conductivity when we add fillers to the system [157]. However, the conductivity is determined by the dominant charge carrier, because the carrier's mobility in hopping from one site to the next is the dominating feature of the conduction mechanism. A detailed study of hopping and its effect on conductivity has been summarized earlier [158, 159].

For metal filler systems in insulating matrices, the dominating feature is the type of filler, with particular regard for its size and shape [160]. Changing the electrical transport properties of these insulators with nanosize fillers is necessary, because we want to retain the innate properties that make the insulators useful. We also want to induce electronic properties that allow us to make quantitative determinations without altering the chemical and/or physical nature of the dominant medium (insulator). For the simple percolative effect, we must look at the insulating/metallic mix. In general, for bulk transport properties, the conductivity follows a power law behavior:

$$\sigma = \sigma_0 (p - p_c)^t \quad (\text{for } t = 2) \tag{1}$$

where σ denotes the conductivity and p represents the mass fraction [161]. In the past, this behavior has been shown to agree with 3D behavior, by Monte-Carlo simulations for thick films [162]. We do not deal with this behavior in detail here, except to note that the study of superconductivity in percolating films is relevant for the interpretation of critical temperature and heat capacity data [163]. A more detailed application of percolation theory deals with the effect of varying the number of interconnections present in a random system [164]. Fourier et al. [165] proposed a model in bulk materials, based on the Fermi–Dirac distribution, that describes the critical insulator-to-conductor transition:

$$\log(\sigma_c) = \log(\sigma_{nc}) + \frac{\log(\sigma_f) - \log(\sigma_{nc})}{1 + \exp[b(p - p_c)]} \tag{2}$$

where σ_c is the composite conductivity, σ_f is the filler conductivity, σ_{nc} is the nanocrystalline conductivity, p is the mass fraction, and b is an empirical parameter that leads to the change in conductivity at the percolation threshold p_c.

On a macro scale, we look at transport properties in terms of 3D processes. The dimensionality of the charge responds to its environment in the x, y, and z directions, as well as to the field that affects it. The simple phrase 'the path of least resistance' is very true for 3D transport. For years, many organic and inorganic materials were examined for their conduction dimensionality on the nanoscale.

In examining composites for their electrical (and electronic) properties, consideration of the volume or mass fraction addition (where we add a metallic component to our insulator) is crucial. However, where this volume addition occurs, the structural phenomena have a large bearing on the composite's transport properties. Alternatively, the metal particles can be distributed randomly, but their proximity (path length) and size can be varied, depending on the technique for adding them. Some clusters will aggregate and therefore nucleate to form larger grain sizes, but other deposition techniques result in islands of metallic clusters. This heterogenity has a dramatic effect on the conduction process as well as on the dimensionality of the conduction pathway. Variable ranges for the critical mass fraction of added filler (5%–50%) required to reach the percolative threshold have been reported. Why should we care about these values and how are they important? The reason

is both complex and simple. To influence transport phenomena, both the shape and size of the filler are crucial. In addition, the manner of deposition and the resulting pathway and mean distance between islands of particles or colloids also directly influence the dimensionality of the charge carriers. We should be aware of certain effects of various fillers. The electrical conductivity of very thin metal films can be much lower than in a bulk material. Closer examination of the thin films reveals a discontinuous structure, where the metal appears as clusters or islands. Detailed examinations have been made of the transition of materials from metallic ballistic transport to insulating, indicating that it is percolative in effect.

As mentioned above, in recent years, the size-dependent properties of nanocrystalline solids have attracted much attention. By gaining an in-depth knowledge of these materials, we can start to use nanocrystalline fillers as components in emerging complex composites. Small changes in the physical size of a simple nanocrystalline material can lead to large changes in its physical properties [166]. In general, to understand such fillers, we must examine many complexities before expanding the investigations into macro- or even nanoscale composites. Work in this field is still inadequate for a complete understanding of percolation effects and dimensionality when nanofillers are used in composites (Figure 1.28) [167]. However, recent studies of carbon nanotubes as a filler in a conjugated polymer have led to some interesting results. Carbon nanotubes were used as fillers in thin-film nanocomposites, and altered conductivity was measured. What makes this effect interesting is that a reasonably well characterized material (the carbon nanotube) was used as a filler in a semiconducting polymer – one whose low conductivity despite conjugation falls in the insulating range [168]. The effect at percolation was to change the conductivity of the composite by 10 orders of magnitude.

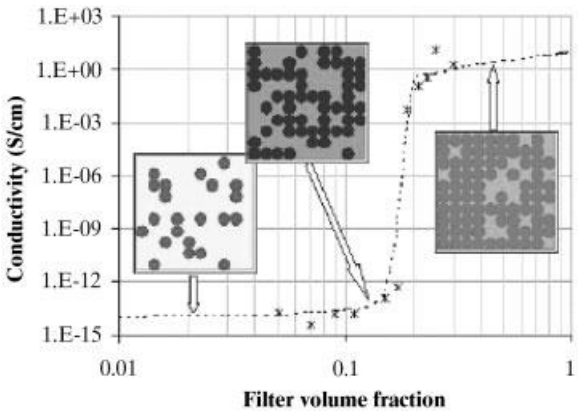

Fig. 1.28 Filler fraction dependence of the conductivity of particle/polymer matrix composites, demonstrating the percolation transition. Insets are schematic microstructures reflecting the extent of particle clustering, at and above the transition. (Source [167] used with permission)

1.11
Nanoporous Structures and Membranes: Other Nanocomposites

Nanoporous materials are materials with pores that have dimensions in the nanoscale. In many ways, these materials can be considered nanocomposites, because they have one phase (empty space) that is either randomly dispersed or ordered within a solid matrix. We have already discussed examples of some of these structures, such as hollow carbon nanotubes with straight hollow channels or porous alumina templates made by electrolytic methods. Examples of random pore distribution are zeolites, mesoporous silica, and porous silicon, all of which have important applications. In this section, we discuss in a little more detail the importance of a few select structures in the realm of nanocomposites. An exhaustive treatise of porous materials and membranes is beyond the scope of this book but has been dealt with elsewhere [169].

The transformation of a chemically homogeneous material into a porous structure by some form of chemical reaction controlling pore size is challenging, because chemical homogeneity and selectivity during such processes do not appear to go hand in hand. However, several strategies can be used (Figure 1.29). Examples include zeolites (pore diameter $\sim$0.3 – 0.4 nm), Al foils converted to alumina having straight pores (diameter $\sim$7 – 250 nm) via an electrochemical self-organization, compact polymeric membranes and also mica plates and glassy metals treated by irradiation or particle (e.g., ion) beams that also develop straight pores ('chemical drilling'), porous carbon structures generated by carbonization of appropriate polymeric precursors and subsequently subjected to an activation reaction (diameter 0.3 – 4 nm), and cyclodextrin polymers [170] (diameter $\sim$0.8 nm).

The pore sizes in porous structures and membranes range from 0.3 nm to 10 μm. Pore dimensions below 0.3 – 0.4 nm may also be considered, but these are nearly the dimensions of ordered or disordered interstices in solids. However, the upper limit of 10 μm covers the pores of most membranes. Pore size uniformity (and distribution) is obviously important for applications such as separations on any size scale [171]. In addition, the physical and chemical character of the pore surfaces can play a significant role at smaller pore sizes, especially when gases or vapors are to be separated. In general, the fabrication of a defect-free porous membrane addresses two problems: one is the creation of pores of the desired local geometry (size, void fraction, and pore coordination number); the other is the achievement of mechanical robustness while repeating the local arrangement over macroscopic distances.

Polymeric membranes useful at lower temperature (20 – 100 °C) and for large-scale routine applications are an important class of porous materials [172]. Ceramic membranes, compared with their polymeric counterparts, are usually more fragile, more expensive, and harder to fabricate. On the other hand, ceramic membranes tend to withstand harsher separation conditions (e.g., high temperatures, solvents, and corrosive or fouling-favoring environments) and can often be cleaned easily. Carbon membranes are based on appropriate polymeric or pitch precursors, and they are intermediate (in character and properties) between polymeric and ceramic membranes [173]. The properties of carbon membranes are closer to the properties of their ceramic counterparts: high temperature and chemical stability (except in oxidative environ-

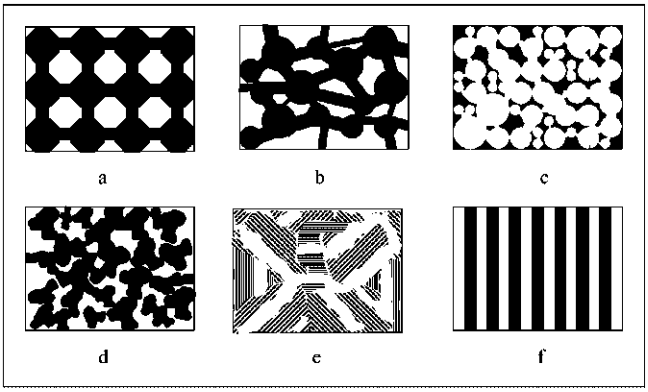

Fig. 1.29 2D schematics of a selection of 3D bicontinuous structures commonly encountered in nanoporous materials. Except for structure (e), the void part in indicated by black. (a) Fully ordered pore network, as in zeolites (pore size 0.4–1 nm). (b) Generic nanoporous material with an imprecisely tailored porous network. (c) Structure generated by compression/mild sintering of solid, nearly round nanoparticles. Pores down to a few nanometers are achievable. (d) Structure typically generated by spinodal decomposition (a Corning silica-based product with 4 nm pores) (e) Nanoporous carbon with a reference nanodomained graphitic structure. Black lines represent graphitic planes and slit-shaped pores correspond to missing graphitic material. (f) Nanoporous material with tubular pores in a parallel semiordered arrangement, anodic alumina (with a minimum pore size in the 10-nm range), and various mesoporous zeolites (pore size in the range of several nanometers). (Courtesy Dr. Konstantinos Beltsios, Institute of Physical Chemistry, NCSR, Demokritos, Greece)

ments at temperatures $>350-400\,^{\circ}C$). Current interest in carbon membranes focuses mostly on those appropriate for gas separations; at least for air separation, these membranes exhibit a combination of permeability and selectivity superior to those known so far for polymeric materials. Examples of applications include separation of CO_2 from CH_4 in landfill gas, production of oxygen-enriched air, and separation of propylene from propane. As a consequence of some of the routes for their preparation and/or their final structure, BN and SiC membranes constitute a bridge between carbon and generic ceramic membranes. Because BN is superior to C in terms of oxidative resistance, developing BN versions of C membranes is potentially interesting. In analogy to the fabrication of porous carbon structures from pitch and other precursors, appropriate organic precursors can be found for BN fibers. Deposition of a precursor organosilicon polymer or oligomer [174] (e.g., polycarbosilane) on porous ceramic substrates, followed by pyrolysis, can be used to fabricate silicon carbide or Si-O-C containing ceramic top layers of composite membranes. Pores from <1 nm to mesopores can be generated, depending on the precursor and the processing. In very recent years, self-assembled single-walled carbon nanotube-based arrays have been proposed for membranes (Figure 1.30). The membrane action is based on quantized transport of water through nanotubes [175] (<1 nm pore size), mimicking water transport in physiological structures through tubules of similar dimensions.

Several forms of well-defined nanostructured carbons (Figure 1.31) exist, and these forms have important practical applications, such as development of electronic, catalytic, and hydrogen storage systems. These materials can be synthesized by thermal chlorination of various carbides. It has so far been possible to synthesize nanoporous carbon, nanoparticles with multi-walled, band-like lamellar graphitic carbon, and turbostratic carbon. The nanoporous amorphous carbon consists of very high-surface-area carbon with a tunable, very narrow, pore size distribution and is suitable in applications such as supercapacitors and specific adsorbents. Template-based (e.g., quartz, silicates) synthesis techniques can also be used to prepare such materials. Structures such as mesoporous aluminum silicate or nanoporous silica have well-ordered arrays of open structures randomly connected by pores (pore size <3.5 nm). The pores can be filled with organic solvents, heated, then pyrolyzed at high temperature; finally, the template is etched off to produce nanoporous carbons [176].

Semiconductor and metal porous membranes have specialized applications [177]. The most important example of metal membranes is hydrogen-separating palladium-based membranes [178], which work on the basis of selective diffusion of gaseous species through the metal lattice. Composite membranes also exist, in which one or more top or buried layers are added to a bulk membrane material. At least one of the layers plays an active role in separation or provides defect healing. Composite materials, consisting of a matrix material (most often a polymer) and a dispersion of a

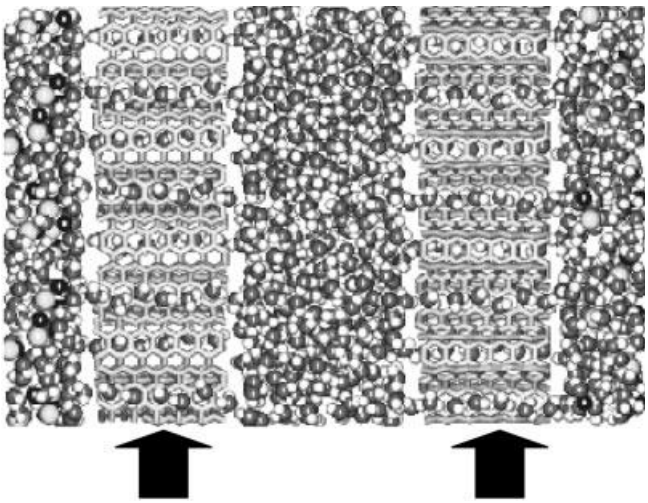

Fig. 1.30 Above: schematic of a possible multiple layer membrane consisting of self-assembled nanotubes (along the arrows), packed together densely. Between the membrane layers is a water-salt mixture. Simulation suggests that osmotic pressure can drive selective transport of species across the membranes, as shown by molecules moving through the nanotubes. Such porous architectures can find use in many applications ranging from bioseparations to drug delivery. (Courtesy Prof. Shekhar Garde, Department of Chemical Engineering, Rensseloer Polytechnic Institute, Troy, New York, USA)

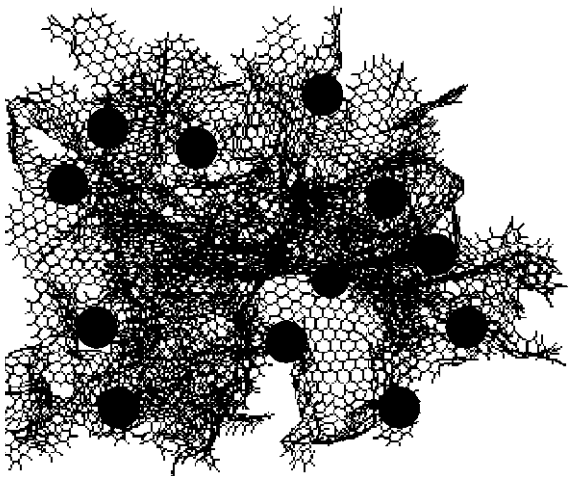

Fig. 1.31 Atomic-level schematic of nanoporous carbon structure with loaded metal particles. High surface area of porous carbon materials are ideal for holding dispersed metal catalyst particles for use in heterogeneous catalysis. (Source: [236] used with permission)

standard nanoporous material (such as zeolites or microporous carbon), can also be useful in catalysis and separation applications.

Straight-pore alumina membranes (which were briefly described above, in the section on preparation of templates for the growth of nanowires and nanotubes) are prepared by anodic oxidation of thin aluminum foils, in the electrolysis of a solution of oxalic, phosphoric, chromic, or sulfuric acid [179]. The electrolyte is chosen among those having some capacity for dissolving alumina. As electrolysis progresses, self-organization occurs; the aluminum oxide formed in the anode undergoes spatial redistribution, resulting in a honeycomb-like structure, with straight pores distributed in a nearly hexagonal arrangement. Pore sizes in the 10 – 250 nm range, porosities on the order of 0.2 – 0.3, and film thickness in the 10 – 100 μm range are usually obtained. For separation applications requiring small pores, it is preferable to develop asymmetric versions of anodic alumina membranes. In addition to asymmetry achievable by depositions, changing the conditions during growth, especially through voltage changes, makes asymmetry possible. In addition to the anodic porous alumina structures created, novel approaches being tested include, for example, the use of a master pattern (made of, e.g., SiC) with nanosize features to imprint well-defined surface textures that guide the formation of nearly defect-free pore channels with high aspect ratio over a wide area [180]. Long-range ordered channel arrays with dimensions on the order of millimeters and a channel density of 10^{10} cm^{-2} can be obtained, with aspect ratios of over 150 for individual channels.

Although the limited thickness achievable by the aluminum anodization approach makes the membranes produced unlikely candidates for extensive use as gas-separation membranes, a substantial amount of research has been dedicated to generating model asymmetric ceramic structures with additional functional layers deposited for specific functions; oriented microcrystals of porous phosphate structures and zeolite-like solids (which have tailorable pore sizes of 2 – 20 nm) can be grown on the surface of straight-pore alumina membranes to provide added functionality in separation ap-

plications [181, 182]. Straight-pore alumina membranes have been used as templates for generating a porous metal membrane by electroless plating [183]. Dissolution can remove the original and intermediate templates.

Polymeric nanoporous materials and nanocomposite materials have improved the technology of polymeric membranes drastically. In a complete reversal of roles for organic and ceramic matter in the building of organized gas- or vapor-selective materials, it has been possible to infiltrate the channels of zeolite-like materials with dimensionally constrained active organic (and metal-containing organic) phases. The architecture of the inorganic zeolite can be used to build other porous structures, including porous carbons. For example, a zeolite structure exposed to propylene gas at a high temperature, after carbonization and acid washing, yields a microporous/nanoporous carbon material [184].

1.12
Nanocomposites for Magnetic Applications

1.12.1
Particle-Dispersed Magnetic Nanocomposites

Magnetic nanocomposites in which magnetic species are dispersed within nonmagnetic or magnetic matrices are practically useful. Magnetic recording, giant-magneto resistance, and magnetic refrigeration are some important areas in which magnetic nanocomposites have relevance. Nanocomposite magnets with both particle/matrix systems being magnetic have received much attention, because they may have high remanence (associated with exchange coupling at interfaces separating hard and soft magnetic phases) and large energy product, $(BH)_{max}$, relative to conventional magnetic materials [185]. The remanence enhancement can be as high as 0.8 M_s, the saturation magnetization, compared to the isotropic value of 0.5 M_s. Many reports have appeared on the enhanced magnetic properties of nanocomposite magnets made of hard magnetic phases such as $Nd_2Fe_{14}B$ and $Sm_2Fe_{17}N_3$ within soft magnetic matrices (e.g., $\alpha-$Fe) [186]. The effect of the strength of intergrain exchange interaction is important in these materials and influences properties of nanocomposite magnets such as coercivity and maximum energy product [187]. Decreasing the grain size of the material and reducing the intergrain exchange interaction can increase the maximum energy product to as high as 200 kJ m^{-3} [188]. In general, the coercivity also increases (and peaks at some value) with a decrease of the exchange constant compared to the intragrain exchange interaction. Nanosize magnetic particles typically have grain sizes smaller than the critical single domain particle size. Also typically in magnetic nanocomposite films, the coercivity increases with grain size if the grains are isolated (no interaction), but when the grains start contacting and exchange interaction kicks in, the coercivity falls rapidly with grain size. The coercivity is highest at percolation, where the grains just start touching each other. In a very recent study, exchange-coupled nanocomposites were fabricated by nanoparticle self-assembly. Here, both

FePt and Fe_3O_4 particles were incorporated as nanometer-scale building blocks into binary assemblies, which were subsequently annealed to obtain $FePt/Fe_3Pt$ nanocomposites, in which FePt is a magnetically hard phase and Fe_3Pt a soft phase. An optimum exchange coupling, and therefore an optimum energy product, is obtained by independently tuning the size and composition of the individual building blocks [189].

The improvements in magnetic properties in nanocomposites can be explained as follows. A nanocomposite magnet can be considered as hard and soft magnetic grains connected by magnetically interacting springs. The intergrain interaction has a tendency to align the magnetization in each grain in the same direction. When a magnetic field is applied in the opposite direction, reversal of magnetization occurs only in the soft grain (until a critical field value is reached). The magnetization in these grains is reversed when the field is removed, resulting in high values of reversible susceptibility. However, for high applied fields, which reverse the magnetization even in the hard grains, the magnetization in the soft grains does not reverse upon removal of the field. This effect is most notable in magnets (Nd/Fe/B) having grain sizes smaller than 50 nm. The strength of interaction between the grains is crucial in determining the properties of the nanocomposite magnets; in addition, the magnetic properties also depend on the grain size, the fraction of soft and hard phases present, and the shape of the grains.

Different synthesis routes can be used to produce magnetic composites. Melt spinning/splat cooling of alloys accompanied by heat treatments such as fast annealing have been used to prepare alloy ribbons of nanocrystalline and nanocomposite magnets (e.g., containing $Nd_2Fe_{14}B$, Fe_3B, and α-Fe). The most successful technique has been mechanical alloying of two-phase mixtures (e.g., α-$Fe/Sm_2Fe_{17}N_3$), which typically results in two-phase mixtures consisting of a nanocrystalline soft magnetic matrix and an amorphous hard magnetic phase. Annealing and crystallization at higher temperatures lead to nanocomposite magnets that show superior magnetic behavior. The evolution of the microstructure and grain morphology during mechanical milling and subsequent heat treatments affects the magnetic properties and has to be controlled precisely. Cosputtering from multiple targets is another method capable of fabricating uniform nanocomposite structures. Uniform thin-film nanocrystalline cobalt grains (10–20 nm) surrounded by graphitic layers have been prepared by this technique followed by post-annealing treatments [190–192]. The Co/C system is immiscible, with a negative interdiffusion coefficient, and because the carbides in this system are metastable, they decompose into the elemental forms. Hence, uniform films of segregated magnetic and encapsulant layers can be fabricated for controlling the magnetic interaction between the different Co grains present in the films. Such films may prove useful for high-density magnetic recording, because carbon provides good isolation, so as to reduce the intergrain exchange interaction. The thickness of the film deposited also needs to be controlled for preparing optimal recording media, and this thickness should be comparable to the grain size ($\sim$10–15 nm) within the films for best performance.

1.12.2 Magnetic Multilayer Nanocomposites

The increase in storage density of hard disk drives and the parallel decline in cost per megabyte (MB) of storage is happening rapidly [193]. Along with disk performance and price, sputter equipment is evolving in both design and efficiency. Current standard processing modules involve heating, dc or RF sputter deposition, and cooling. Further improvements and required modifications of these modules, as well as new processing steps such as substrate cleaning, multilayer deposition, and plasma chemical vapor deposition of carbon are necessary in the future. Magnetic nanocomposites are the end result of many of those improvements.

1.12.2.1 Microstructure and Thermal Stability of Layered Magnetic Nanocomposites

Granular solids consist of small metal granules embedded in an immiscible medium, which may be insulating or, less frequently, metallic [194]. Like other artificially structured solids, granular solids have intricate structure on the nanometer scale and extra degrees of freedom within which the physical properties can be manipulated to achieve tailored materials for applications and for explorations of physical phenomena. The relevant extra degree of freedom for granular solids is the granule size. In magnetic granular solids, all such granules are single domains exhibiting 'hard' magnetic properties. On the other hand, for samples with large metal volume fractions, the metal granules form an infinite network, exhibiting metallic conductivity and 'soft' magnetic properties, because the conducting paths and magnetic closure structure are readily facilitated. For most common metals (e.g., Fe, Au, Co, Cu), the ultrafine solid granules can be made as small as 10 to 100 nanometers. This is the size range in which finite-size effects, single-domain magnetic properties, and other phenomena are observed. Work on this type of nanostructured film began with the pioneering studies of Abeles et al. [195]. These films have attracted considerable attention in recent years because of theoretical suggestions dealing with their physical properties and also because of practical applications, among which the use of ferromagnetic nanocomposites as data recording media stands out. For this application, superior magnetic performance can be tailored by manipulating the size and volume fraction of the particles. Other advantages also derive from the structure of the film, in that the insulating portion of the film provides chemical and mechanical protection to the metal particles.

A variety of deposition methods can be used to produce granular, layered magnetic solids. Of these, sputtering is the most versatile. Sputtering is most often applied via a single homogenous target, or by cosputtering. Sequential deposition is also applicable if layer formation can be avoided. Generally, because the nanostructures of granular metal solids are strongly influenced by the processing conditions, deposition parameters such as deposition rate, sputtering pressure, and substrate temperature must be tightly controlled. Multilayer thin films with an under layer and a cover layer (total film thicknesses are usually in the range of several micrometers) have been prepared with multiple-gun dc and RF sputtering systems. The multilayers were de-

posited onto glass or silicon substrates. Flowing high-purity gas (Ar, N_2, etc.) was used in sputtering. The sputtering parameters, including gas pressure, the power rates of the sputtering guns, and the target-to-substrate distance, were chosen to produce films with maximum coercivity. Heat treating the as-deposited films in a furnace or rapid thermal annealing yielded nanocomposite films with random nanostructure. Generally, high coercivity is obtained only after heat treatment.

As an example, cobalt nitride films, CoN, in pure form and also as a nanocomposite in a boron nitride or silicon nitride matrix were generated by reactive sputtering of cobalt metal, cobalt boride, or cobalt silicide as targets, respectively, in nitrogen plasma [196]. Cobalt nitride decomposes into the elements when heated under vacuum at 500 °C. The nanostructure of the composites was preserved in the heat treatment, thus creating a fine dispersion (<10 nm) of cobalt particles in a ceramic matrix. The magnetic properties of the nanocomposites were studied in detail; the precursor cobalt nitride is paramagnetic but the cobalt dispersions, having dimensions smaller than single magnetic domain size, show characteristics typical of systems such as superparamagnetism and, at temperatures lower than the blocking temperature, marked hysteresis. The coercive fields at 5 K for the BN and Si_3N_4 nanocomposites are 3250 and 850 Oe, respectively.

The problem of long-term stability of written bits in magnetic data storage devices places a fundamental limit on the possible increase in area density for conventional magnetic recording. Because decreased magnetic grain size is required for the improved media signal-to-noise ratio that is needed to support higher area densities, thermal energy becomes significant relative to the switching energy, and the playback signal amplitude decays over time. Thermal stability will ultimately limit the maximum area density achievable with conventional longitudinal recording. The key aspects of the media microstructure contributing to thermal stability are the grain size and grain size distribution, alloy composition, alloy segregation, lattice defects, and strain. Random nucleation processes occurring during media deposition create grain size distributions. Continued increases in area density will require tighter grain size distributions and improved microstructural control of very thin magnetic layers [197].

Controlling the media grain size and tightening the grain size distribution are probably the most difficult, yet most important, aspects of media processing. Due to the exponential dependence of the decay on $K_\mu V/kT$, ($K_\mu V$ is the product of the uniaxial anisotropy energy density and the switching volume), small changes in V determine the difference between stable and unstable bits, with the smallest grains in the distribution decaying first. Thermal decay experiments have shown that the data cannot be well explained without taking the contribution of the grain size distribution into account. Slow lateral grain growth rates or high nucleation rates favor smaller average grain sizes. Materials or growth conditions that limit surface mobility reduce the grain size. Because a minimum number of atoms are needed to form a critical nucleus, a narrower grain size distribution is expected as the grain size approaches the size of the critical nucleus. To significantly improve the grain size distribution, one needs a regular array of nucleation sites or a new type of media in which the magnetic grains do not grow together to form a fully dense film. Although research on so-called self-as-

sembled quantum dot arrays for media is ongoing, these approaches are still far from being implemented for production media.

1.12.2.2 Media Materials

Area densities in longitudinal magnetic recording have reached 36 Gbits in^{-2} in laboratory demonstrations [198] and 10 Gbits in^{-2} in media designs already in use (12 ± 4 nm grains) [199]. Roadmaps toward 40–100 Gbits in^{-2} have been proposed [200]. At such densities, tight control of the media microstructure, especially grain size, grain size dispersion, and chemical isolation to break exchange are necessary, in order to keep the media noise within acceptable bounds [201]. Continued grain size scaling to diameters considerably below 11–12 nm should be possible, allowing for densities well beyond the currently perceived 40–100 Gbits in^{-2} limit. This prospect has been the driving force behind industrial and academic research in the area of thin-film hard magnet materials, which promise minimal thermally stable grain sizes down to 2–3 nm and a more than 10-fold potential density gain. However, for extremely high density recording media, typically defined as >100 Gbits in^{-2}, the critical values of relevant magnetic properties will be stringent for achieving low media noise: coercivities of 4 kOe and weak exchange coupling in grains <10 nm are estimates.

High-K_μ (uniaxial magnetocrystalline anisotropy) materials are attractive for ultrahigh-density magnetic recording applications (e.g., audio tapes, video cassettes, magnetic memory devices) because they allow smaller, thermally stable media grains (Figure 1.32). Particle-dispersed recording systems are also possible targets for future magneto-optical data storage. For the particulates, high magnetization is crucial, because it determines the strength of the field to be detected during read/write. Metals such as Fe and Co have high magnetization, but one drawback is that they oxidize easily when particle sizes are small. Alloys have advantages in this regard and encapsulation in a medium (matrix) can solve several problems associated with chemical stability of the particulates. The search for higher magnetic recording densities pur-

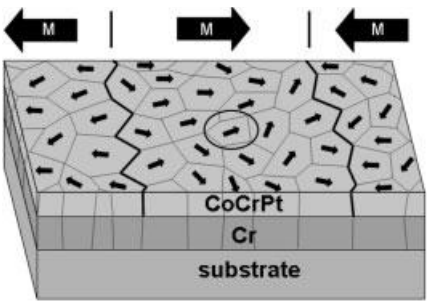

Fig. 1.32 Schematic of multilayer microstructures of typical nanocomposites used in magnetic recording media. The area bound by the thick jagged lines corresponds to the transition between bits (dimension of each bit ~80 × 400 nm). Within each bit, the grains of the magnetic layer, CoCrPt, have uniaxial anisotropy due to the random orientation of magnetic moments. The total magnetic moment is the vector sum of all magnetic orientations (shown by arrows M). The orientation of the Cr layers can induce magnetization in the plane of the film by their epitaxial relationship. The thickness of the films correspond to 20 nm for the CoCrPt layer and ~40 nm for the Cr layer. (Courtesy Prof. M. Shima, Department of Materials Science & Engineering, Rensselaer Polytechnik Institute, Troy, New York 12180, USA.)

sues particle sizes that are <10 nm. With such small particle sizes, high magnetocrystalline anisotropy is needed to avoid thermal and field fluctuations that can destroy the magnetization in recorded locations. When particle sizes become that small, in many material systems the magnetization can become inherently unstable, due to effects such as superparamagnetism. Intrinsic magnetic properties of several potential alternative media alloys can be found in reference [202]. Recent studies have emphasized rare earth intermetallic compounds with high magnetic anisotropy and small grain sizes in the search for the best magnetic properties for high-density recording media.

Nanocomposites, e.g., metal/carbon, metal/oxide, or immiscible metal/metal mixtures, are prospective routes toward generating <10-nm granular structures, needed for ultrahigh density recording. Much work has been reported on nanocrystalline rare-earth transition-metal films, most prominently Co_5Sm- and $Co_{17}Sm_2$-based films. High-density recording studies have been reported on CoSm/Cr structures with coercivities in the 2000–4000 Oe range. Another example is nanocrystalline high coercivity CoPr/Cr films, for which coercivities of about 8000 Oe and grain sizes of 10 nm have been obtained.

Face-centered tetragonal (fct) structures of near-equiatomic composition, CoPt and FePt, have been studied extensively. Both compositions result in large coercivities, close to the theoretical maximum obtained for 12–15-nm-thick epitaxial Fe/Pt (001) films with perpendicular orientation grown on MgO substrates. 'Nanometer-size' CoPt particles (100–300 nm) obtained by dc-magnetron sputtered, and post-annealed CoPt films exhibited coercivities of about 30–37 kOe. Annealed nanocomposite CoPt/C films may be tailored for magnetic recording media applications. Some of the common problems with hard magnet nanomaterials are unfavorably high processing temperatures during annealing or growth, which may adversely affect grain growth. As a consequence, the noise performance is compromised, as was recently found in perpendicular recording studies of polycrystalline ordered Fe/Pt (001) thin films. Codeposited nanophase materials, e.g., CoPt/Ag and CoPt/C, may alleviate some of these problems. CoPt alloys undergo phase transition from fcc to the more anisotropic face-centered tetragonal (fct) phase at higher temperature (835 °C), which makes this material magnetically hard. RF magnetron sputtering from targets containing CoPt alloys and Ag can be used to prepare nanocomposite (CoPt/Ag), and post-annealing treatment embeds the hard magnetic phase. Large coercivities, which can be tailored over the whole range by changing the processing route and hence the microstructure, were achieved for these multilayer films of CoPt fct phases in a fcc Ag matrix, with average grain sizes in the range of 7–100 nm [203]. Different matrix materials (other than Ag) can also be used, serving as the isolation material between the hard magnetic grains, for example, silica and carbon. Carbon should be an ideal isolation material, because it does not react with Co or Pt to form carbides. CoPt/C nanocomposite films have been prepared that show the high coercivity and chemical stability required for high density recording media. Exciting new developments in high density recording media may further derive from chemical synthesis routes, self-assembly of magnetic nanoparticles, and template-based growth of magnetic nanowire arrays; these options are currently being explored for generating monodisperse, ordered nanoparticle arrays.

In addition to the common applications outlined above, magnetic nanocomposite materials also have applications in ferrofluids, imaging, and separation technologies and as magnetic carriers for drug delivery. The challenge here is to make the magnetic nanocomposite particles (e.g., silica-coated iron oxide) resistant to agglomeration and chemical attack. The magnetic particles are often coated with protective and functional materials such as silica, which can be done effectively and easily by sol–gel synthesis or liquid phase coating processes (Figure 1.33). The silica coating provides protection against chemical attack and also provides a shell that can be modified chemically to make functional nanocomposites [204]. The sol–gel process (performed in organic solvent via hydrolysis of tetraethoxysilane) is good for making thin inorganic films with tailored porosity; however, because the coating is porous, chemical protection is not necessarily achieved. Supersaturated monosilicic acid can be used to achieve homogeneous thick coatings on particles. Often, a combination of the two processes is used to obtain uniform coatings of silica on magnetic particles. The key in this technology is to provide a protective coating without any reduction in magnetic properties such as saturation magnetization (important for magnetic carrier technology) and to provide an outer surface for additional easy modification. Thin silica films also ensure the stability of the magnetic nanocomposites against aggregation and metal (Fe) release to the environment, which may contaminate the systems during use. Isotropic ferrofluid dispersion can be obtained for these silica-coated magnetic particles (due to electrostatic repulsion and strong hydration forces between the outer silica surfaces) in the absence of a magnetic field, and the dispersion can be easily switched

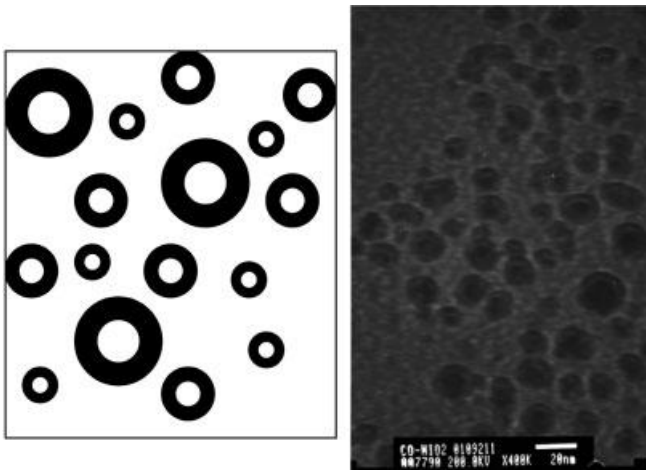

Fig. 1.33 Schematic and micrograph showing the fabrication of core shell structures. Several possible routes can be used to make such structures, for example, vapor phase coating or multi-step precipitation via nanoemulsion processing. The micrograph shows cobalt (core)-nickel oxide shell magnetic nanocomposite particles in the 20 nm size range. Such structures could find applications in magnetic xerography and as ferrofluids. (Micrograph courtesy Prof. Mamoun Muhammed)

to an anisotropic structure in external magnetic fields. These nanocomposites have applications as stable ferrofluids and in magnetic carrier applications. Magnetic particles embedded in polymer matrices (e.g., iron oxides inside a conductive polyaniline matrix) have also been synthesized for the fabrication of conductive, superparamagnetic plastic films [205]. Deposition of conductive polymer chains and magnetic nanoparticles in a layer-by-layer fashion may lead to new properties such as giant magnetoresistance (GMR) and novel organic-based nanostructured GMR materials.

1.13 Nanocomposite Structures having Miscellaneous Properties

Photoelectrochemical properties are inherent to semiconducting nanostructures. Electrochemical deposition from baths loaded with colloidal nanoparticles of the semiconductor (e.g., Ni films incorporating TiO_2, CdS, etc.) can produce metal films containing photoactive semiconducting particles. Much larger photocurrents are produced from these nanocomposite electrodes compared to conventional semiconductor electrodes and contiguous nanocrystalline semiconductor electrodes [206]. Separating the semiconductor nanostructures within a matrix in a nanocomposite system and creating intimate contacts between the particles and the molecular redox media can improve quantum yields in the photoexcitation processes. Controlling the local environments of the semiconductor species in the nanocomposite can modulate electron transfer and carrier mobility at the electrodes. Such photoelectrodes provide an interesting context for studying charge transfer processes at semiconductor–molecular contacts. As noted here, electrochemical deposition to fabricate nanocomposites is a powerful synthetic approach that has been used in several other instances to create nanocomposites with enhanced properties. One example is the formation of Ni/Al_2O_3 films [207], where $\sim$50 nm Al_2O_3 particles are uniformly distributed in a Ni matrix. The only requirement for this synthesis process is a stable inclusion phase (ceramic or semiconductor) and its well-dispersed suspension in the electrochemical solution. The Ni/Al_2O_3 nanocomposite shows enhanced mechanical properties due to reinforcement of the ductile metal matrix by the hard ceramic nanoparticles (dispersion hardening). These can be used as coatings that retain most of the properties of the metal.

Applications of TiO_2 colloids and thin films extend from photovoltaics to catalytic devices and sensors. Nanocrystalline TiO_2 and ordered structures have been synthesized by the sol–gel method. Processing conditions can be controlled to produce various interesting (isotropic to anisotropic) morphologies and structures in the microstructure of the films that can be deposited. Rod-like or truncated pyramidal morphologies are formed at the anatase phase as the temperature is varied during processing [208]. Controlling the base used in the colloidal synthesis can make aligned rod-like structures self-organize into regular arrays. The ordering occurs due to surface charges and forces that can be altered by controlling the basicity and the dielectric constant of the colloidal medium. Thin-film optoelectronic devices with semiconductor and metal nanoparticles are hot candidates for research these days [209]. Alternating layers of

TiO_2 thin films and modified nanoparticles (semiconductor–metal layers) have been prepared for nonlinear optical applications [210]. Layer-by-layer assembly and surface sol–gel processing are used to fabricate these nanocomposites. Surface-stabilized (with organic monolayers such as thiols) gold nanoparticles (4–5 nm) can, in addition, be assembled into layers forming close-packed monoparticulate layers; multilayer films of TiO_2/Au can be prepared this way. The surface hydroxyl groups present on the Au particles act as an active component in the surface sol–gel process [211], which can be used to make metal oxide thin films with nanometer-scale control of film thickness.

The optical properties of small semiconductor particles are interesting, showing quantum confinement effects and shifts in their absorption spectra. Also, dielectric/nanocrystalline semiconductor interfaces enhance carrier recombination to picoseconds, with the possibility of ultrafast optical applications. Applications of semiconductor polymer nanocomposites in optics are discussed briefly in the next chapter. Similarly, metal/semiconductor hybrid nanoparticles produce novel effects such as enhanced optical nonlinearity [212] and shifted plasmon resonances for the metal particles [213]. Such hybrid nanocomposite particles (CdS/Ag) have been prepared in glass matrices by a modified melt–quench process [214]. The hybrid CdS-coated Ag nanoparticles exhibit red-shifted plasmon resonance absorption spectra, which can be tuned by the heat treatment that controls the particle size and other interfacial effects (Figure 1.34). Arrays of nanometer-sized CdSe clusters have been fabricated inside the pores of porous silicon matrices. The purpose here is to increase photoluminescence by enhancing the light-emitting centers by chemical infiltration [215] (using first an aqueous $Cd(COO)_2$ solution, resulting in the formation of CdO, and subsequently selenidation by passage of H_2Se). The nanosize semiconducting clusters (3–5 nm) provide the high-density light-emitting centers in this nanocomposite on top of the intense photoluminescence spectra in the visible range from the porous silicon. Electrochemically depositing metal (Au) within pores of optically transparent nanoporous alumina templates can be used to prepare interesting optical nanocomposites. The plasmon resonance absorption band of the metal nanoparticles as a function of particle size and aspect ratio (nanoparticle vs. nanowires in the channels of the alumina) was studied in such composites [216]. As the particle size decreased, the λ_{max} (wavelength of maximum absorption intensity) approached theoretical values and reached a quasi-static lower limit for particles of ~16 nm, irrespective of the aspect ratio.

Functional nanocomposites in which nanoparticles are deposited inside appropriate substrates can be used as sensors that react by changing optical properties in response to gas exposure. CdO-doped SiO_2 nanocomposites have been prepared by RF cosputtering, and show gas-sensing capabilities [217]. This nanocomposite showed a change in optical transmittance during exposure to nitrogen oxide gas. For such nanocomposites to function, the embedded nanoparticles should change optical transmittance upon exposure to gases, the matrix should have porosity for the gas molecules to diffuse and interact with the particles, and the matrix should be transparent to allow detection of the changing optical signals.

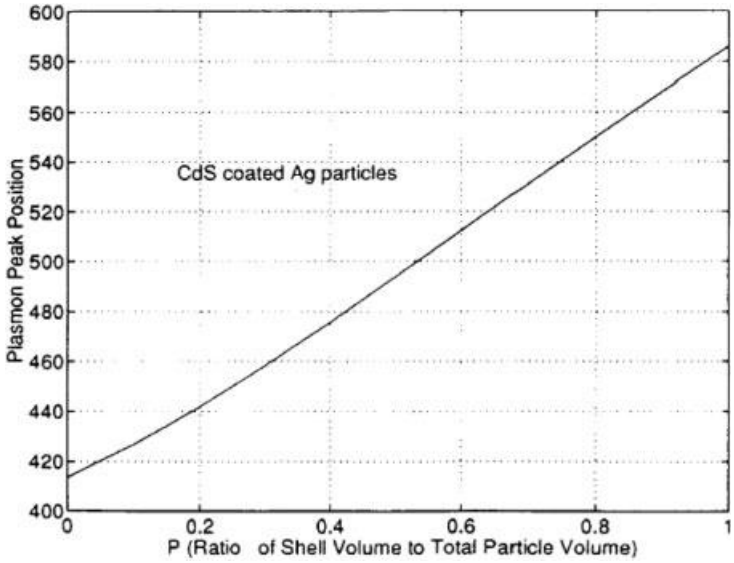

Fig. 1.34 Optical (luminescence) property of CdS-coated Ag particles embedded in a glass matrix nanocomposite. Plot shows the plasmon peak position as a function of the ratio of the CdS shell volume to the total particle volume in the nanocomposite particle. Semiconductor/metal hybrid nanoparticle composites were prepared in a glass host by a modified melt/quench process and examined with respect to their optical properties. The coated hybrid nanoparticles exhibit surface plasmon resonance absorption spectra that are red-shifted relative to that of a dispersion of homogeneous Ag nanoparticles in the same host. (Source [214] used with permission)

Many nanocomposite systems derive their usefulness from the fact that value-added functions can be advantageous, in addition to the primary function of the nanostructured phase. For example, we already discussed the dispersion-induced toughening and strengthening of ceramic nanocomposites (Al_2O_3/SiC, Si_3N_4/SiC, etc.), and, if the dispersoid phase acquire add new functions, such as piezoelectricity and ferroelectricity, then new applications can result. Conventional powder metallurgy techniques (milling, mixing, and hot pressing) can be used to prepare barium titanate-dispersed MgO nanocomposites [218]. The criteria for the formation of well-dispersed nanocomposites are that the dispersoids do not react with the matrix phase during sintering. In these perovskite-dispersed composites, the mechanical properties were not degraded, but new piezoelectric properties were added, enabling possible applications as sensors. Such materials have sensing ability for crack propagation by using electromotive forces or by introducing internal strains via electrical impulses, resulting in increased fracture toughness. The introduction of piezo- and ferro-electricity into structural ceramic nanocomposites will create new materials that exhibit 'intelligent' functions [219]. For transition-metal dispersed-oxide ceramic composites, ferromagnetism is also compatible with its excellent mechanical properties. In addition, good magnetic response to applied stress was found in these ceramic/fer-

romagnetic-metal nanocomposites, showing the possibility of remote sensing of fracture or deformation of ceramic materials.

Nanocomposites can also be effective as catalytically active membranes (e.g., catalytic converters in automobiles), in which a catalytically active phase is uniformly distributed in a matrix of high porosity. The operating conditions for such materials are quite demanding, because they are used over a wide range of temperatures and chemical environments. Nanostructured γ-Al_2O_3 catalyst supports with a dispersed cerium oxide phase and supporting noble-metal nanoparticle (Pt, Pd, etc.) heterogeneous catalysts are commonly used in automotive exhaust streams. The ceria phase serves as an oxygen-storage component, to buffer sudden changes in the fuel/air ratio; it also stabilizes the alumina structure and the noble metal particle dispersion. Calcination of sol–gels (prepared from Al and Ce chlorides and nitrides), followed by microwave or autoclave heating, have been used to prepare such nanocomposites [220]. The microwave-generated powder contains nanocrystalline ceria and alumina phases, suitable for catalytic applications. Note that, in nanocomposite structures, microstructure evolution and the final dispersion structure and its relation to the matrix decide the functionality of the composite. For example, if the final product in the above alumina/ceria composite is autoclaved instead of microwaved, a coarse microstructure that has no catalytic ability results. Silica/copper oxide nanocomposites have been prepared by a sol–gel process (controlled hydrolysis/polymerization of sodium metasilicate and copper nitrate via a microemulsion technique with anionic surfactants) and show promise in catalytic applications [221]. These nanocomposites have specific surface areas ranging from 200 to 400 $m^2 g^{-1}$ and are mesoporous, with pore sizes in the range 3–6 nm. Nanocomposites are also being considered for use as photocatalysts to decompose environmental pollutants and harmful microorganisms. As an example of such materials, transparent nanocomposite anatase films have been deposited at low temperatures on various substrates by a sol–gel method [222]. For the substrate, materials such as porous SiO_2 work well because, for such applications, a high surface area, transparency to light (including UV), and durability for the photocatalytic activity are required.

Low-dimensional catalytic nanocomposites can also be envisioned. For example, molybdenum carbide has been considered as a substitute catalyst for metals like Ru in several heterogeneous catalysis systems. Sonochemically prepared nanocomposites of molybdenum oxide and carbide dispersed as discontinuous surface coatings on microspheres of silica are being considered as nanocomposite catalysts and fit the profile of the optimal catalyst material, considering that the composites retain the nanoscale dimensions of the active phases, provide effective interaction between the catalyst and the solid support, and have a uniform distribution of the active phase on the support surface [223]. The formation of strong interfacial Si-O-Mo bonds is observed in this material. The use of sonochemical activation is yet another approach to breaking down and dispersing precursor materials into nanocrystalline forms and simultaneously activating surfaces onto which the dispersed phase can be uniformly coated.

Oxidation-resistant coating systems have been developed, based on nanocomposite technology, for applications such as resistive heating elements for industrial melting.

Materials such as Mo, which has several excellent electromechanothermal properties, are used for such applications, but suffer from severe oxidation problems. $MoSi_2$ is a substitute material for such applications, due to its excellent resistance to oxidation at high temperatures. The high temperature strength of this material is a problem, and incorporation of SiC into the $MoSi_2$ matrix provides a compromise. The best solution is to put $MoSi_2$/SiC coatings onto Mo substrates, by techniques such as RF magnetron sputtering of composite targets [224]. As deposited films, they are usually amorphous but can be converted into nanocrystalline form by annealing under vacuum at $>1000\,^{\circ}C$. The high interdiffusion of Si and C in these films can be minimized if the sputtered films are made in a nitrogen atmosphere. Pyrolysis of $MoSi_2$ particles coated with polycarbosilane and subsequent hot-pressing can also be used to prepare bulk $MoSi_2$/SiC nanocomposite materials for high-temperature applications [225]. Uniform dispersions of SiC particles are obtained in the $MoSi_2$ matrix after densification. The room-temperature and high-temperature flexural strengths of this nanocomposite are several times those of unreinforced matrix.

DLC-based nanocomposites possess very interesting properties and hence can be targeted for several applications (a high-profile application being the DLC coating on the Gillette Mach 3 razor blade). Amorphous diamond-like/quartz-like (C:H/Si:O) composites and metals containing such materials constitute a class of DLC-based nanocomposites with unique bulk and surface properties. These nanocomposite materials have excellent diffusion barrier properties, high wear resistance, and low coefficient of friction, in addition to good adhesion to most substrates, variable electrical resistivity, thermal shock resistance, and controllable optical properties. Films of diamond-like nanocomposites can be deposited by plasma-assisted vapor deposition of organosilane precursors and involves C- and Si-containing free radicals and, optionally, transition-metal atoms [226]. These nanocomposites can find applications in tribology, especially in magnetic recording read/write heads. DLC/SiO_2 nanocomposites have been prepared with better optical clarity as thin films [227]. The films of the nanocomposite (Figure 1.35) were deposited at room temperature by RF plasma, from tetraethoxysilane (TEOS) as the precursor. The advantage of this precursor is that it serves as the source for both the DLC and the SiO_2 during a simultaneous deposition process. By introducing O_2 into the plasma, the surface of the deposited film can be made more hydrophilic, changing its wetting characteristics.

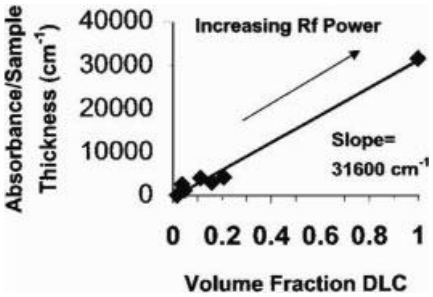

Fig. 1.35 Beer–Lambert plot of normalized absorbance of DLS/SiO_2 nanocomposites as a function of volume fraction of DLC. With increasing RF power the normalized absorbance increases linearly with the volume fraction of DLC in the nanocomposite thin films. The slope is the optical absorption, and the value obtained for the nanocomposite is similar to typical polar absorptions found for organic compounds. (Source [227] used with permission)

1.14
Concluding Remarks on Metal/Ceramic Nanocomposites

This chapter includes examples of how ceramic and metal-based nanocomposite materials can be useful in several applications and how they can be superior to conventional composites and to the separate, independent constituent phases. Thischapter in no way provides an exhaustive list, and the field is still evolving, providing new directions for applications of nanocomposites. Some of the synthesis techniques were discussed, as were challenges involved in fabricating nanocomposites with optimized properties. Synthesis parameters, which determine the microstructure, greatly affect the final properties of the nanocomposite, particularly with respect to tailoring the interface between the constituent phases. In the next chapter we discuss another important class of nanocomposites based on polymer matrices.

Acknowledgements

I greatly appreciate the help of Dr. Bing Qing Wei in putting together parts of this chapter and several of the figures. I also thank Dr. Seamus Curran and Dr. Robert Vajtai for their help in preparing this chapter. I thank the National Science Foundation (in particular the Nanoscale Science and Engineering Center at RPI) for funding support.

References

1 M. Jose-Yacaman, L. Rendon, J. Arenas, M. C. Serra Puche, Science, 273, 223 (1996).
2 K. Niihara , Metal Powder Report, 54(3), 37 (1999).
3 Y. H. Choa, A. Nakahira, K. Niihara, J. Mater. Sci., 35, 3143 (2000).
4 K. Niihara, Y. K. Jeong, T. Sekino, Y.-H. Choa, Ceram. Trans., Adv. Ceram. Matrix Composites IV, Am. Ceram. Soc., Westerville, OH, USA, 96, 185 (1999),
5 J.-F. Yang, T. Sekino, Y.-H. Choa, K. Niihara, T. Ohji, J. Am. Ceram. Soc., 84, 406 (2001).
6 M. Yoshimura, T. Ohji, M. Sando, K. Niihara , Mater. Res. Innovations, 1, 16 (1997).
7 T. Nakayama, T.A. Yamamoto, Y.H. Choa, K. Niihara, Ceram. Trans., 108, 257 (2000).
8 T. Nakayama, Y. Choa, T. Sekino, K. Niihara , J. Ceram. Soc. Jpn, 108, 781 (2000).
9 H. J. Hwang, S. Ueda, K. Niihara, Ceram. Trans., 44, 399 (1994).
10 R. Riedel, H. J. Kleebe, H. Schonfelder, F. Aldinger, Nature, 374, 526 (1995).
11 H. K. D. H. Bhadeshia, Proc. R. Microsc. Soc., London, 35(2), 95 (2000).
12 L. Takacs, Mater. Lett., 13, 119 (1992).
13 M. Pardavi-Horvath, L. Takacs, Scripta Met. Mater., 33, 1731 (1995).
14 L. Takacs, Nanostruct. Mater., 2, 241 (1993).
15 L. Takacs, in *Nanophase and Nanocomposite Materials*, eds. S. Komarnemi, J. C. Parker, G. J. Thomas, MRS Symp. Proc., 286, 413 (1993).
16 K. Niihara, A. Nakahira, T. Sekino, MRS Symp. Proc., 286, 405 (1993).
17 D. Osso, O. Tillement, G. Le Caer, A. Mocellin, J. Mater. Sci., 33, 3109 (1998).
18 M. Pardavi-Horvath, L. Takacs, IEEE Trans. Magn., 28, 3186 (1992).
19 L. Takacs, M. Pardavi-Horvath, in *Nanophases and Nanocrystalline Structures*, eds. R.

D. Shull, J. M. Sanchez, The Minerals, Metals & Materials Society, Warrendale, PA, USA, 1994, p. 135.
20 M. Pardavi-Horvath, L. Takacs, J. Appl. Phys., 73, 6958 (1993).
21 J. S. C. Jang, C. C. Koch, J. Mater. Res., 5, 498 (1990).
22 G. Picaluga (ed), Sol–Gel Preparation and Characterization of Metal–Silica and Metal Oxide–Silica Nanocomposites, Trans Tech Publications, Zurich, Switzerland (2001).
23 J. D. Wright, N.A.J.M. Sommerdijk, *Sol–Gel Materials: Chemistry and Applications*, Taylor & Francis, New York, NY, USA (2001).
24 L. W. Hrubesh, J. F. Poco, J. Non-Cryst. Solids, 188, 46 (1995).
25 A. J. Hunt, M. R. Ayers, W. Q. Cao, J. Non-Cryst. Solids, 185 227 (1995).
26 N. Wang, Z. K. Tang, G. D. Li, J. S. Chen, Nature, 408, 51 (2000).
27 X. Y. Song, W. Q. Cao, M. R. Ayers, A. J. Hunt, J. Mater. Res., 10, 251 (1995).
28 W. Q. Cao, A. J. Hunt, Appl. Phys. Lett., 64, 2376 (1994).
29 M. R. Ayers, X. Y. Song, A. J. Hunt, J. Mater. Sci., 31, 6251 (1996).
30 M. R. Ayers, A. J. Hunt, J. Non-Cryst. Solids, 225, 343 (1998).
31 H. Jiang, M. Lau, V.L. Tellkamp, E.J. Lavernia, Synthesis of nanostructured coatings by high velocity oxygen-fuel thermal spraying, Chapter 3 in *Handbook of Nanostructured Materials and Nanotechnology*, ed. H.S. Nalwa, Academic Press, San Diego, CA, USA, 2000.
32 E. Petrovicova, L. S. Schadler Int. J. Mater. Rev., In press.
33 M.L. Luton, C.S. Jayanth, M.M. Disko, S. Matras, J. Vallone, in *Materials Research Society Symposium Proceedings*, L.D. McCandlish et al., eds, Pittsburgh PA, 1989, p. 79.
34 B. Huang, J. Vallone, M.J. Luton, Nanostruct. Mater., 5, 631 (1995).
35 J. He, M. Ice, S. Dallek, E. J. Lavernia, Metall. Mater. Trans. A, 31, 541 (2000).
36 B. Huang, R.J. Perez, E.J. Lavernia, Mater. Sci. Eng., A 255, 124 (1998).
37 J. He, M. Ice, E. J. Lavernia, Metall. Mater. Trans. A, 31, 555 (2000).
38 J. He, M. Ice, J. M. Schoenung, D. H. Shin, E. J. Lavernia, J. Therm. Spray Technol., 10, 293 (2001).
39 M.L. Lau, E.J. Lavernia, Mater. Sci. Eng., A, 272, 222 (1999).
40 T.R. Malow, C.C. Koch, in Synthesis and processing of Nanocrystalline powder, D.L Bourrell, ed., The Minerals, Metals & Materials Society, Warrendale, PA, USA, 1996, p. 33.
41 M.L. Luton, C.S. Jayanth, M.M. Disko, S. Matras, J. Vallone, in *Multicomponent Ultrafine Microstructures* (L.D. McCandlish et al., eds) MRS Symp. Proc., Pittsburgh PA, USA, 1989, p. 79.
42 B. Fultz, L.B. Hong, Z.Q. Gao, C. *Bansal, in Synthesis and Processing of Nanocrystalline Powder*, D.L Bourrell, ed., The Minerals, Metals & Materials Society, Warrendale, PA, USA, 1996, p. 233.
43 G.J. Fan, W.N. Gao, M.X. Quan, Z.Q. Hu, Mater. Lett., 23, 33 (1995).
44 D.A. Stewart, P.H. Shipway, D.G. McCartney, Wear, 225–229, 789 (1999).
45 Y. Zhu, K. Yukimura, C. Ding, P. Zhang, Thin Solid Films, 388, 277 (2001).
46 E.H. Jordan, M. Gell, Y.H. Sohn, D. Goberman, L. Shaw, S. Jiang, M. Wang, T.D. Xiao, Y. Wang, P. Strutt., Mater. Sci. Eng., A, 301, 80 (2001).
47 R.S. Lima, A. Kucuk, C.C. Berndt, Surf. Coat. Technol., 135, 166 (2001).
48 S.C. Tjong, Z.Y. Ma, Mater. Sci. Engin., 29, 49 (2000).
49 W.O. Soboyejo, R.J. Lederich, S.M.L. Sastry, in *High Performance Composites for the 1990s*, S.K. Das, C.P. Ballard, F. Marikar, eds.), The Minerals, Metals & Materials Society, Warrendale, PA, USA, 1991, p. 127.
50 X.C. Tong, H.S. Fang, Metall. Mater. Trans. A, 29, 893 (1998).
51 K. Lu, Mater. Sci. Eng., 16, 161 (1996).
52 Y. Yoshizawa, S. Oguma, K. Yamauchi, J. Appl. Phys., 64, 6044 (1988).
53 J. Eckert, A. Reger-Leonhard, B. Weiss, M. Heimaier, Mat. Sci. Eng., A, 301, 1 (2001).
54 A.W. Weimer, R. K. Bordia, Composites B, 30, 647 (1999).
55 M. Herrmann, C. Schuber, A. Rendtel, H. Hubner, J. Am. Ceram. Soc., 81, 1095 (1998).

56 Y. Wang, M. Sasaki, T. Goto, T. Hirai, J. Mate. Sci., 25, 4607 (1990).
57 A. A. Voevodin, S. V. Prasad, J. S. Zabinski, J. Appl. Phys, 82, 855 (1997).
58 K. Niihara, J. Ceram. Soc. Jpn., 99, 945 (1991).
59 X. H. Jin, L. Gao L. H. Gui, J. K. Guo J. Mater. Res., 17, 1024 (2002).
60 A. Sawaguchi, K. Toda, K. Niihara, J. Ceram. Soc. Jpn., 99, 510 (1991).
61 Y. Xu, A. Zangvil, A. Kerber, J. Eur. Ceram. Soc., 17, 921 (1997).
62 J. Dusza, M. Steen, Int. Mater. Rev., 44, 165 (1999).
63 M. Sternitzke, B. Derby, R. J. Brook, J. Am. Ceram. Soc., 81, 41 (1998).
64 Y. Sakka, D. D. Bidinger, I. A. Aksay, J. Am. Ceram. Soc., 78, 479 (1995).
65 H.J. Choi, K.S. Cho, J.G. Lee, J. Am. Ceram. Soc., 80, 2681 (1997).
66 K. Niihara, K. Izaki, A. Nakahira, J. Mater. Sci. Lett., 9, 598 (1990).
67 J. Dusza, P. Sajgalik, M. Steen, Key Eng. Mate., 175, 311 (1999).
68 P. Descamps, D. O'Sullivan, M. Poorteman, J. C. Descamps, A. Leriche, F. Cambier, J. Eur. Ceram. Soc., 19, 2475 (1999).
69 T. Ohji, Y.-K. Jeong, Y.-H. Choa, K. Niihara, J. Am. Ceram. Soc., 81, 1453 (1998).
70 J. Perez-Riguero, J. Y. Pastor, J. Llorca, M. Elices, P. Miranzo, J. S. Moya, Acta Mater., 46, 5399 (1998).
71 M. R. Scanlon, R. C. Cammarata, J. Appl. Phys., 76, 3387 (1994).
72 B. Abeles, P. Sheng, M. D. Coutts, Y. Arie, Adv. Phys., 24, 407 (1975).
73 W. M. C. Yang, T. Tsakalakos, J. E. Hilliard, J. Appl. Phys., 48, 876 (1977).
74 R. C. Cammarata, K. Sieradzki, Phys. Rev. Lett., 62, 2005 (1989).
75 J. S. Koehler, Phys. Rev. B, 2, 547 (1970).
76 M. Yu et al., Appl. Phys. Lett., 75, 3992 (1999).
77 Y. J. Liu, H. J. Kim, Y. Egashira, H. Kimura, H. Komiyama, J. Am. Ceram. Soc., 79, 1335 (1996).
78 R. Hauert, J. Patscheider, Adv. Eng. Mater., 2, 247 (2000).
79 W. D. Sproul, Science, 273, 889 (1996).
80 C. Subramanian, K. N. Strafford, Wear, 165, 85 (1993).
81 U. Helmersson, S. Todorova, S. A. Barnett, J. Sundgren, L. C. Markert, J. E. Greene, J. Appl. Phys., 62, 481 (1987).
82 M. Shinn, L. Hultman, S. A. Barnett, J. Mater. Res., 7, 901 (1992).
83 X. Chu, S. A. Barnett, J. Appl. Phys., 77, 4403 (1995).
84 I. Wadsworth, I. J. Smith, L. A. Donahue, W. D. Munz, Surf. Coat. Technol., 94/95, 315 (1997).
85 H. Holleck, V. Schier, Surf. Coat. Technol., 76/77, 328 (1995).
86 M. Shinn, S. A. Barnett, Appl. Phys. Lett., 64, 61 (1994).
87 S. Veprek, S. Reiprich, L. Shizhi, Appl. Phys. Lett., 66, 2640 (1995).
88 A. A. Voevodin, J. S. Zabinski, J. Mater. Sci., 33, 319 (1998).
89 A. A. Voevodin, M. A. Capano, A. J. Safriet, M. S. Donely, J. S. Zabinski, Appl. Phys. Lett., 69, 188 (1996).
90 S. Zabinski, A. A. Voevodin, J. Vac. Sci. Technol., A, 16, 1890 (1998).
91 J. E. Sundgren, B., O. Johansson, S. E. Karlsson, Thin Solid Films, 105, 353 (1983).
92 H. Dimigen, C. P. Klages, Surf. Coat. Technol., 49, 543 (1991).
93 W. J. Meng, B. A. Gillispie, J. Appl. Phys., 84, 4314 (1998).
94 R. Gampp, P. Gantenbein, Y. Kuster, P. Reimann, R. Steiner, P. Oelhafen, S. Brunold, U. Frei, A. Gombert, R. Joerger, W. Graf, M. Kohl, *Optical Materials Technology for Energy Efficiency and Solar Cell Conversion*, SPIE Proc. Series, vol. 2255, 92 (1994).
95 R. Gilmore, M. A. Baker, P. N. Gibson, W. Giassler, Surf. Coat. Technol., 105, 45 (1998).
96 L. E. McCandlish, B. H. Kear, B. K. Kim, Mater. Sci. Tech., 6, 953 (1990).
97 Y. T. Zhu, A. Manthiram, J. Am. Ceram. Soc., 77, 2777 (1994).
98 J. R. Wilde, A. L. Greer, Mater. Sci. Eng., A, 304, 932 (2001).
99 H.J. Choi, K.S. Cho, J.G. Lee, J. Am. Ceram. Soc., 80, 2681 (1997).
100 R. Andrews, D. Jacques, A. M. Rao, T. Rantell, F. Derbyshire, Y. Chen, J. Chen, R. C. Haddon, Appl. Phys. Lett., 75, 1329 (1999).
101 P. M. Ajayan, Chem. Rev., 99, 1787 (1999).

102 R. Z. Ma, J. Wu, B. Q. Wei, J. Liang, D. H. Wu, J. Mater. Sci., 33, 5243 (1998).

103 S. Chang, R. H. Doremus, P. M. Ajayan, R. W. Siegel, Ceram. Eng. Sci. Proc., 21, 653 (2000).

104 Y.B. Li, B.Q. Wei, C.L. Xu, J. Liang, D.H. Wu, J. Mater. Sci., 34, 5281 (1999).

105 B.Q. Wei, Y. Li, Ph. Kohler-Redlich, R. Lück, S. Xie, J. Appl. Phys., In press.

106 H. Masuda, M. Satoh, Jpn. J. Appl. Phys., 35, 126 (1996).

107 X. Y. Zhang, L. D. Zhang, G. W. Meng, F. Philipp, Chem. Mater., 13, 2511 (2001).

108 G. L. Che, B. B. Lakshmi, E. R. Fischer, C. R. Martin, Nature, 393, 346 (1998).

109 P. C. Searson, R. C. Cammarata, C. L. Chien, J. Electron. Mater., 24, 955 (1995).

110 R. S. Ruo, D. C. Lorents, B. C. Chan, R. Malhotra, S. Subramoney, Science, 259, 346 (1993).

111 S. A. Majetich, J. O. Artman, M. E. McHenry, N. T. Nuhfer, S. W. Staley, Phys. Rev. B, 48, 16845 (1993).

112 T. Hayashi, S. Hirono, M. Tomita, S. Umemura, Nature, 381, 772 (1996).

113 C. Guerret-Piecourt, Y. Le Bouar, A. Loiseau, H. Pascard, Nature, 372, 761 (1994).

114 A. Loiseau, H. Pascard, Chem. Phys. Lett., 256, 246 (1996).

115 S. Subramoney, Adv. Mater., 10, 1157 (1998).

116 Y. Saito and T. Yoshikawa, J. Cryst. Growth, 134, 154 (1993).

117 M. Tomita, Y. Saito, T. Hayashi, Jpn. J. Appl. Phys., 32, L280 (1993).

118 J. H. J. Scott, A. A. Majetich, Z. Turgut, M. E. McHenry, M. Boulos, MRS Symp. Proc., 457, 219 (1997).

119 P. M. Ajayan, S. Iijima, Nature, 361, 333 (1993).

120 S. C. Tsang, Y. K. Chen, P. J. F. Harris, M. L. H. Green, Nature, 372, 159 (1994).

121 R. R. Meyer, J. Sloan, R. E. Dunin-Borkowski, A. I. Kirkland, M. C. Novotny, S. R. Bailey, J. L. Hutchison, M. L. H. Green, Science, 289, 1324 (2000).

122 J. Sloan, D. M. Wright, H. G. Woo, S. Bailey, G. Brown, A. P. E. York, K. S. Coleman, J. L. Hutchison, M. L. H. Green, Chem. Commun., 8, 699 (1999).

123 B. W. Smith, M. Monthioux, D. E. Luzzi, Nature, 396, 323 (1998).

124 J. Lee, H. Kim, S.-J. Kahng, G. Kim, Y.-W. Son, J. Ihm, H. Kato, Z. W. Wang, T. Okazaki, H. Shinohara, Y. Kuk, Nature, 415, 1005 (2002).

125 D. Danailov, P. Keblinski, P. M. Ajayan, J. Nanosci. Nanotechn., In press.

126 W. K. Hsu, H. Terrones, M. Terrones, N. Grobert, A. I. Kirkland, J. P. Hare, K. Prassides, P. D. Townsend, H. W. Kroto, D. R. M. Walton, Chem. Phys. Lett., 284, 177 (1998).

127 W. K. Hsu, S. Trasobares, H. Terrones, M. Terrones, N. Grobert, Y. Q. Zhu, W. Z. Li, J. P. Hare, R. Escudero, H. W. Kroto, D. R. M. Walton, Chem. Mater., 11, 1747 (1999).

128 M. S. Dresselhaus, G. Dresselhaus, K. Sugihara, I. L. Spain, H. A. Goldberg, *Graphite Fibers and Filaments*, vol. 3, Springer, Berlin, Germany (1988).

129 C. N. R. Rao, R. Sen, B. C. Satishkumar, A. Govindaraj, J. Chem. Soc. Chem. Commun., 15, 1525 (1998).

130 Y. Zhang, H. J. Dai, Appl. Phys. Lett., 77, 3015 (2000).

131 P. M. Ajayan, O. Stephan, P. Redlich, C. Colliex, Nature, 375, 564 (1995).

132 W. K. Hsu, Y. Q. Zhu, H. W. Kroto, D. R. M. Walton, R. Kamalakaran, M. Terrones, Appl. Phys. Lett., 77, 4130 (2000).

133 M. Terrones, P. M. Ajayan, Unpublished.

134 J. Luo, L. Zhang, Y. Zhang, J. Zhu, Adv. Mater., 14, 1414 (2002).

135 Y. Zhang, T. Ichihashi, E. Landree, F. Nihey, S. Iijima, Science, 285, 1719 (1999).

136 Y. Zhang, K. Suenaga, C. Colliex, S. Iijima, Science, 281, 973 (1998).

137 Lieber Group, Nature, 409, 66, (2001).

138 Y. Wu, R. Fan, P. Yang, Nanoletters, 2, 83 (2002).

139 S. Y. Chou, M. S. Wei, P. R.Krauss, P. B. Fischer, J. Appl Phys., 76, 6673 (1994).

140 T. M. Whitney, J. S. Jiang, P. C. Searson, C. L. Chien, Science, 261, 1316 (1993).

141 S. Y. Chou, Proc. IEEE, 85, 652 (1997).

142 D. K. Kim, M. Mikhaylova, M. Toprak, Y. Zhang, M. Muhammed, *Nanoparticulate Materials*; MRS Proc., 704 (2001).

143 D. K. Kim, Yu Zhang, M. Muhammed, W. Voit, K. V. Rao, J. Kehr, B. Bjelke, Scripta Mater., 44, 1713, (2001).

144 T. Ogawa, Y. Kanemitsu, *Optical Properties of Low-Dimensional Materials*, World Scientific, Singapore (1995).

145 Y. Kanemitsu, H. Tanaka, S. Mimura, S. Okamoto, T. Kushida, K. S. Min, H. A. Atwater, MRS Symp. Proc., 536, 223 (1999).

146 K. M. Hassan, A. K. Sharma, J. Narayan, J. F. Muth, C. W. Teng, R. M. Kolbas, Appl. Phys. Lett., 75, 1222 (1999).

147 H. Zhou, W. Cai, L. Zhang, Appl. Phys. Lett., 75, 495 (1999).

148 H. B. Liao, R. F. Xiao, H. Wang, K. S. Wong, G. K. L. Wong, Appl. Phys. Lett., 72, 1817 (1998).

149 Z. Li, H. Wang, H. Li, X. Wang, Appl. Phys. Lett., 72, 1823 (1998).

150 T. Kyprianidou-Leodidou, W. Caseri, U. W. Suter, J. Phys. Chem., 98, 8992 (1994).

151 F. Papadimitrakopoulos, P. Wisniecki, D. E. Bhagwagar, Chem. Mater., 9, 2928 (1997).

152 S. R. Panteny, R.Stevens, C. R.Bowen, Ferroelectrics 2000 UK (Editors N. McN. Alford & E. Yeatman), ISBN 1-86125-135-1, P75.

153 K. Tajima, H. J. Hwang, M. Sando, K. Niihara, J. Eur. Ceram. Soc., 19, 1179 (1999).

154 D. Hoppe, D. Ernst, H. Weiß, Proc. Eur. Conf.: Junior – Euromat '96, Lausanne, Switzerland, 26–30 August (1996), S. 18f.

155 S. Banerjee, D. Chakravorty, J. Appl. Phys., 85, 3623 (1999).

156 M. D. Jaeger, R. E. Soltis, J. A. Thomas, J. Hangas, A. E. Chen, E. M. Logothetis, MRS Symp. Proc., 549, 173 (1999).

157 A. Miller, E. Abrahams, Phys. Rev. B, 120, 745 (1960).

158 A. Aldea, M. Dulea, Phys. Rev. Lett., 60, 1672 (1988).

159 M. E. J. Newman, R. B. Stinchcombe, Phys. Rev. B, 43, 1183 (1991).

160 X.H.Yan, J.W.Ding, Q.B.Yang, Eur. Phys. J., B, 20, 157 (2001).

161 B. Abeles, Adv. Phys., 24, 407 (1975).

162 G. Deutscher, A. Kapitulnik, M. Rappaport, *Percolation Structures and Processes*, Adam Hilger, Bristol, UK (1983), Chapter 10.

163 G. Deutscher, O. Entin-Wohlman, S. Fishman, Y. Shapira, Phys. Rev. B, 21, 5041 (1980).

164 R. Zallen, *Physics of Amorphous Solids*, Wiley, New York, NY, USA (1983) Chapter 4.

165 H. Baessler, N. Herrmann, N. Riehl, G. Vaubel, J. Phys. Chem. Solids, 30, 1579 (1969).

166 H. Gleiter, Prog. Mater. Sci., 33, 223 (1989).

167 I. J. Youngs, J. Phys. D: Appl. Phys., 35, 3127 (2002).

168 J.N. Coleman, S. Curran, A.B. Dalton, A.P. Davey, B.M. McCarthy, W. Blau, R.C. Barklie, Phys Rev B, 58, 7492 (1998).

169 K. Beltsios, T. Steriotis, K. Stephanopoulos, N. Kanellopoulos, in *Handbook of Porous Solids*, ed. F. Schueth, K. Sing, J. Weitkamp, Wiley, New York, NY, USA, p. 2281 (2002).

170 E. Wilson, Chem. Eng. News, 77(5), 32 (1999).

171 K. Keizer, A.J. Burggraaf, J. Membr. Sci., 66, 259 (1992).

172 R.W. Baker, *Membrane Technology and Applications*, McGraw-Hill, New York, NY, USA, (1999).

173 S. Sircar, M. B. Rao, in *Recent Advances in Gas Separation by Microporous Membranes*, ed. N. Kanellopoulos, Membrane Science and Technology Series, vol. 6, Elsevier, Amsterdam, Netherlands, p. 473 (2000).

174 K. Kusakabe, Z.Y. Li, H. Maeda, S. Morooka, J. Membr. Sci., 103, 175 (1995).

175 Shekhar Garde, personal communication.

176 website: http://www.etis.net/balpyo/envi/envilz.pdf

177 B. Hamilton, Semicond. Sci. Technol., 10, 1187 (1995).

178 J.B. Hunter, US Patent 2, 773, 561 (1956).

179 J.P. O'Sullivan, G.C. Woods, Proc. R. Soc., London, A, 317, 511 (1970).

180 H. Masuda, H. Yamada, M. Satoh, H. Asoh, M. Nakao, T. Tamamura, Appl. Phys. Lett., 71, 2772 (1997).

181 C.N. Wu, K.J. Chao, T-G. Tsai Y.-H. Chiou, H.-C. Shih, Adv. Mater., 8, 1008 (1996).

182 P. Behrens, Adv. Mater., 5, 127 (1993).

183 H. Masuda, K. Nishio, N. Baba, Thin Solid Films, 223, 1 (1993).

184 T. Kyotani, T. Nagai, S. Inoue, A. Tomita, Chem. Mater., 9, 609 (1997).

185 R. Skomski, J. M. D. Coey, Phys. Rev. B, 48, 15812 (1993).

186 K. O'Donnel, C. Kuhrt, J. M. D. Coey, J. Appl. Phys., 76, 7068 (1994).

187 H. Fukunaga, J. Kuma, Y. Kanai, IEEE Trans. Magn., 35, 3235 (1999).

188 P. G. McCormick, W. F. Miao, A. A. I. Smith, J. Ding, R. Street, J. Appl. Phys., 83, 6256 (1998).

189 H. Zeng, J. Li, J. P. Liu, Z. L. Wang, S. Sun, Nature, 420, 395 (2002).

190 T. Hayashi, S. Hirono, M. Tomita, S. Umemura, Nature, 38, 772 (1996).

191 M. Yu, Y. Liu, D. J. Sellmyer, J. Appl. Phys., 85, 4319 (1999).

192 M. Yu, Y. Liu, A. Moser, D. Weller, D. J. Sellmyer, Appl. Phys. Lett., 75, 3992 (1999).

193 B. Cord, J. Scherer, IEEE Trans. Magn., 36, 67 (2000).

194 C.L. Chien, J. Appl. Phys., 69, 5267 (1991).

195 B. Abeles, P. Shoeing, M. D. Coutts, Y. Arie, Adv. Phys., 24, 407 (1975).

196 L. Maya, M. Paranthaman, J.R. Thompson, T. Thundat, R. J. Stevenson, J. Appl. Phys., 79, 7905 (1996).

197 M. F. Doerner, K. Tang, T. Arnoldussen, H. Zeng, M. F. Toney, D. Weller, IEEE Trans. Magn., 36, 43 (2000).

198 "Seagate announced 23.8 Gbits/in2, Read-Rite 26.5 and 36 Gbits/in2, and IBM 35.3 Gbits/in2 demos in recent press releases," Data Storage Magazine, p. 8, July 1999.

199 J. Li, M. Mirzamaani, X. Bian, M. Doerner, S. Duan, K. Tang, M. Toney, T. Arnoldussen, M. Madison, J. Appl. Phys., 85, 4286 (1999).

200 H. N. Bertram, H. Zhou, R. Gustafson, IEEE Trans. Magn., 34, 1845 (1998).

201 M. F. Doerner, K. Tang, T. Arnoldussen, H. Zeng, M. F. Toney, D. Weller, IEEE Trans. Magn., 36, (2000).

202 D. Weller, A. Moser, L. Folks, M. E. Best, W. Lee, M. F. Toney, M. Schwickert, J.-U. Thiele, M. F. Doerner, IEEE Trans. Magn., 36, 10 (2000).

203 S. Stavroyiannis, I. Panagiotopoulos, D. Niarchos, J. A. Christodoulides, Y. Zhang, G. C. Hadjipanayis, Appl. Phys. Lett., 73, 3453 (1998).

204 Q. Liu, Z. Xu, J. A. Finch, R. Egerton, Chem. Mater., 10, 3936 (1998).

205 B. Z. Tang, Chemtech, page 9, November 1999.

206 N. R. de Tacconi, J. Carmona, K. Rajeshwar, J. Phys. Chem. B, 101, 10151 (1997).

207 R. R. Oberle, M. R. Scanlon, R. C. Cammarata, P. C. Searson, Appl. Phys. Lett., 66, 19 (1995).

208 S. D. Burnside, V. Shklover, C. Barbe, P. Comte, F. Arendse, K. Brooks, M. Gratzel, Chem. Mater., 10, 2419 (1998).

209 G. Schmid, Chem. Rev., 92, 1709 (1992).

210 H. Yonezawa, T. Matsune, T. Kunitake, Chem. Mater., 11, 33 (1999).

211 I. Ichinose, H. Senzu, H. Kunitake, Chem. Mater., 9, 1296 (1997).

212 J. W. Haus, N. Kalyaniwalla, R. Inguava, C. W. Bowden, J. Appl. Phys., 65, 1420 (1989).

213 A. P. Alivisatos, Science, 271, 932 (1996).

214 M. J. Ko, Adv. Mater. Opt. Electron., 8, 173 (1998).

215 A. I. Belogorokov, L. I. Belogorokhova, A. Perez-Rodriguez, J. R. Morante, S. Gavrilov, Appl. Phys. Lett., 73, 2766 (1998).

216 G. L. Hornyak, C. J. Patrissi, C. R. Martin, J. Phys. Chem., 101, 1548 (1997).

217 K. Yasumoto, N. Koshizaki, J. Mater. Sci. Lett., 16, 215 (1997).

218 T. Nagai, H. J. Hwang, M. Yasuoka, M. Sando, K. Niihara, J. Am. Ceram. Soc., 81, 425 (1998).

219 T. Takagi, Bull. Ceram. Soc. Jpn., 28, 539 (1993).

220 B. Djuricac, S. Pickering, D. McGarry, P. Tambuyser, P. Thomas, J. Mater. Sci., 34, 1911 (1999).

221 K. Zhang, C. H. Chew, G. Q. Xu, J. Wang, L. M. Gan, Langmuir, 15, 3056 (1999).

222 A. Matsuda, Y. Kotani, T. Kogure, M. Tatsumisago, T. Minami, J. Am. Ceram. Soc., 83, 229 (2000).

223 N. A. Dhas, A. Gedanken, Chem. Mater., 9, 3144 (1997).

224 D. J. Aldrich, K. M. Jones, S. Govindarajan, J. J. Moore, T. R. Ohno, J. Am. Ceram. Soc., 81, 1471 (1998).

225 J. I. Lee, N. L. Hecht, T. Mah, J. Am. Ceram. Soc., 81, 421 (1998).

226 F. Ruiz, W. D. Sun, F. H. Pollak, C. Venkatraman, Appl. Phys. Lett., 73, 1802 (1998).

227 J. J. Senkavitch, D. E. Leber, M. J. Tutor, N. A. Heiks, G. A. Ten Eyck, D. W. Scherrer II, J. Vac. Sci. Technol., B, 17, 2129 (1999).

228 http://www.sanken.osaka-u.ac.jp/labs/scm/about_resE.html

229 http://aldix.mpi-stuttgart.mpg.de/E_head.html

230 http://www.msm.cam.ac.uk/phase-trans/2000/RMS.pdf

231 http://eande.lbl.gov/ECS/aerogels/sapho-to.htm
232 http://eande.lbl.gov/ECS/aerogels/sapho-to.htm
233 http://www.chem.ox.ac.uk/researchguide/jsloan.html
234 http://www.seas.upenn.edu/~luzzi/re-search.html
235 J. Lee, H. Kim, S.-J. Kahng, G. Kim, Y.-W. Son, J. Ihm, H. Kato, Z. W. Wang, T. Okazaki, H. Shinohara & Young Kuk, Na-ture, 415, 1005 (2002).
236 http://www.che.udel.edu/~strano/structu-re.html